SUB-PHASE DESIGN FOR ELECTROSPUN NANOFIBROUS INTERLAYER TOUGHENING IN HIERARCHICAL COMPOSITES
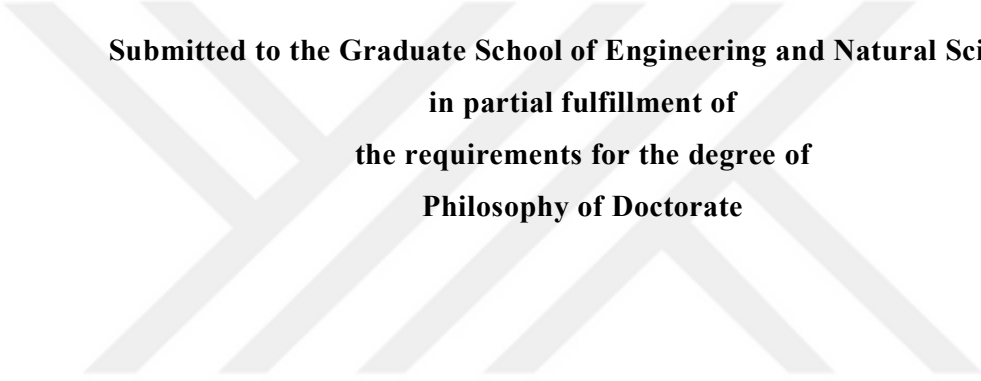
by

KAAN BİLGE

**Submitted to the Graduate School of Engineering and Natural Sciences
in partial fulfillment of
the requirements for the degree of
Philosophy of Doctorate**
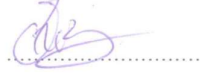
Sabancı University

January, 2017

SUB-PHASE DESIGN FOR ELECTROSPUN NANOFIBROUS INTERLAYER
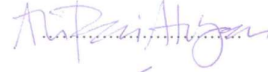TOUGHENING IN HIERARCHICAL COMPOSITES

APPROVED BY:

Assoc. Prof. Dr. Melih Papila
(Thesis Advisor)

Assoc Prof. Dr. Güllü Kızıltaş Şendur

Prof. Dr. Ali Rana Atılgan

Assoc.Prof.Dr. Nuri Ersoy

Assist.Prof.Dr. Elif Özden Yenigün

DATE OF APPROVAL:06/01/2017

Everything should be as simple as it is, but not simpler.

Albert Einstein

To my family and my çiçek

SUB-PHASE DESIGN FOR ELECTROSPUN NANOFIBROUS INTERLAYER TOUGHENING IN HIERARCHICAL COMPOSITES

Kaan BILGE

PhD, Doctor of Philosophy Thesis, 2017

Thesis Supervisor: Assoc. Prof. Dr. Melih Papila

Keywords: composite materials, hybrid composites, nanofiber, interlayer, toughening mechanisms, crosslinking

Abstract

Interlayer toughening of composite materials forms the basis of this thesis work. Two out of the box application oriented case studies present incorporation of polystyrene-co-glycidyl methacrylate (P(St-co-GMA)) based nanofibers to carbon/epoxy prepreg surfaces as interlayers. The effect of nanofibrous interlayer toughening approach on the in-plane strength of composites with/without stress raisers (such as holes) is initially evaluated. Performance of interlayer toughened thick laminated composites under high strain load conditions is then exemplified. While elaborating potential material limits for thermoplastic nanofibrous interlayers, novel heat stimuli in-situ crosslinking methodology and its integration into composite curing are discussed. Continously electrospinnable P(St-co-GMA)/Phtalic Anhydride(PA)- Tributyl Amine(TBA) nanofibers are able to crosslink inside the epoxy matrix upon reaching certain initiation temperature. The novel concept of self-same nanocomposites formed only through electrospinning and its stand-alone thermal processing is also presented. Enhanced curing associated with the epoxy-P(St-co-GMA)/PA-TBA nanofiber interaction is demonstrated through cure kinetics study. Superior mechanical properties in each case study are extensively elaborated through fracture surface analyses.

ELEKTRODOKUNMUŞ NANOLİF ARAKATMAN DESTEKLİ YAPISAL KOMPOZİTLER İÇİN MALZEME TASARIMI

Kaan BILGE

PhD, Doktora Tezi, 2017

Tez Danışmanı: Assoc. Prof. Dr. Melih Papila

Anahtar Kelimeler: kompozit malzemeler, hybrid kompozitler, nanolifler, arayüz güçlendirme, çapraz bağlanma

Özet

Bu tez çalışması yapısal kompozit malzemelerde elektrodokunmuş nanoliflerle elde edilen arayüz güçlendirme metodunu temel almaktadır. Polistiren-kopolimer glisidilmetakrilat (P(St-co-GMA)) bazlı epoksi uyumlu nanofibelerin yapısal kompozitler içindeki çalışma prensibi anlatıldıktan sonra, bu prensibin işlediği iki orjinal uygulama problemi göz önüne alınmıştır. Arayüzleri güçlendirilmiş kompozit malzemelerin performansı eksenel yüklemeler ve yapı içinde gerilim arttırıcıların (örnek:delik) varlığında değerlendirilmiştir. İkinci örnekte ise arayüzü güçlendirilmiş kalın kompozit laminatlar yüksek gerinim koşullarına tabii tutulmuştur. Çalışmanın ikinci kısmında ise, termoplastik temelli nanolifler için sıcaklık temelli malzeme limitler değerlendirilmiştir. Buada öncelik sürerli elektrodokunabilen ve sıcaklık etkisiyle kompozit kürlenme sürecinde yapı içi çapraz bağlananilen P(St-co-GMA)/Ftalik Anhidrit(FA)-Tribütilamin(TBA) nanoliflerine verilmiştir. Bu fiberlerin çapraz bağlı ve çapraz bağsız hallerinin sadece ısıl işlem ile birlikte kendinden destekli nanokompozit yapılara dönüşümü açıklanmıştır. Son olarak P(St-co-GMA)/TBA-PA nanoliflerinin yapı içi kürlenme kinetiği prepreg malzemeler üzerinde çalışılmıştır. Çalışma boyunca tüm mekanik veriler kırılma yüzey analizleriyle desteklenmiş ve elde edilen yüksek mekanik performans bu yüzeylerdeki morfolojik oluşumlarla ilişkilendirilmiştir.

Acknowledgments

I would like to express my special thanks and gratitude to Assoc.Dr.Prof.Dr. Melih Papila who has always been a source of guidance and insipiration for me with his continuous support and endless enthousiasm. I sincerely think most of the works we produced are definitey fruits of his personality and never ending patient. I will always value our academic and casual chit-chats that have shaped my professional self. As a result of 10 years of working, I would also like to thank him for his impenetrable trust on me.

I would also want to thank to my committee members Doç. Dr. Güllü Kızıltaş, Prof. Dr. Ali Rana Atılgan, Assist.Prof. Dr. Elif Ozden Yenigün and Assoc. Prof. Nuri Ersoy. I am grateful for their willingness for both helping and supporting me in my research activites and for enriching my PhD thesis with their valuable comments and reviews.

A very special thank goes to my fiancée İpek for her love, caring presence and endless positivism. Neither me , nor my works wouldn't be the same if it wasn't for her.

I would also like to thank to Ayça Ürkmez, Bengisu Yılmaz, Yelda Yorulmaz and Farzin Javanshour who have trusted me on their research, who have spent countless hours with me for discovering new boundaries and who have had patient on me. Most of the works that are reported herein would not exist without them.

I feel happy to thank to Mustafa Baysal, Oğuzhan Oğuz and Melike Mercan Yıldızhan as my dearest science bros and sister. Thanks to them, I tasted the elegance of human academic sharing, saw how valuable are the different point of views and how they can be made real.

Furthermore, I am thankful to TUBITAK for providing me scholarship and project funding (TUBITAK 213M542) during my thesis.

Finally, my deepest gratitude goes to my family for their love and support throughout my whole life.

TABLE OF CONTENTS

LIST OF FIGURES

Chapter 2 Figures

Chapter 3 Figures

3.1 Global and Local Nanofibrous Interlayer Toughened Composites for

Higher In-Plane Strength

3.2 High Strain Rate Response of Nanofiber Interlayered Structural Composites

Chapter 4 Figures

4.1 Stabilized Electrospinning of Heat Stimuli/In-situ Cross-linkable Nanofibers and Their Self Same Nano-composites

4.2 Synergistic role of In-Situ Crosslinkable Electrospun Nanofibrous Interlayers for Superior Laminated composites

LIST OF TABLES

Chapter 4 Tables

CHAPTER 1 GENERAL INTRODUCTION

1.1 Introduction

1.1.1 Overview

By definition, composite materials are composition of two or more distinct constituents/phases. Their mix at any length scale except molecular level, form interface between one another. 'Inclusion' phases are typically called reinforcement when they are responsible from principal load bearing function. Common type of reinforcement is in form fibers (aspect ratio ~1000), made out of different material choices such as glass, carbon, aramid, boron, graphite. 'Binder' phase also called as matrix phase is responsible from the load transfer between relatively stiffer/stronger inclusions and from keeping inclusions together to guarantee the structural integrity of resulting composite material. Depending on the functioning and expected final performance, the matrix phase can be polymeric, metallic or ceramic materials.

In terms of their high strength to weight ratio and tailorable characteristics fiber reinforced polymeric composite materials (FRPC) are types of composite materials which allow competitive engineering designs in structural applications.

1.1.2 Issue to address

While uses of laminated composites is significantly growing in sophisticated engineering fields, the weakest links/issues hindering much superior mechanical performance have been subject of numerous studies for many years. Understanding and suppression of the complicated failure modes in composite structures is one of the keys for road map towards creating better composites.

Among several failure modes, the resistance to progression of transverse cracking and delamination specifically relies on the interlaminar region (defined as the matrix dominated zone between two subsequent plies). This region in composite materials, is relatively weak initially due to its resin based composition and due to the fact it is responsible from load transfer between twomuch stronger/stiffer composite plies which are not necessarily expands or contracts equally due to associated fiber orientations. The weakness and susceptibility of that region to cracking may cause the appearance of pre-mature damages (due to un-expected failure modes) in composite materials. Although transverse cracking is considered as relatively minor failure mode meaning not causing the direct ultimate failure, their progression at multiple zones may trigger and lead to more severe damage modes including delamination and ply-splitting. That is, unless they are suppressed the matrix cracking weaken the overall laminated structures and form potential failure spots for most severe failure events.

Suppression of the matrix cracking and increasing delamination resistance requires focus on the strengthening of interlaminar reigon, and various alternatives of different nature are present in the literature. For instance, with a design perspective, the ply angles can be optimized to minimize potential interlaminar damage. Or with hybridization idea, introduction of secondary phases, such asperpendicular z-pins, ply stitches and the use of micro-particle reinforced resins are shown to enhance the resistance of composite laminates against delamination and transverse cracking. However, the studies also showed these solutions may also induce drawbacks effecting unintended properties of the composites.

By definition, interlaminar region is a relatively difficult region to interact with and manipulate during composite manufacturing. Both for most advanced prepreg based manufacturing methods and for resin flow based (RTM, VARTM) manufacturing

methods, the nature of that region reveals itself apriori to manufacturing. Again depending on the manufacturing type size of this region is very small when compared with ply thickness. Furthermore the engineering problem in these regions has a multi-scaled insight itself where subsequent ply properties and resin properties can be stated as variables. In that sense, an engineering approachi with less drawbacks requires correct determination of the nature of delamination and transverse cracking and ability to intervene against these failure modes without effecting the already promising abilities of the composite materials and with a very low weight cost. In a matter of fact, the tailorability of this region requires a smaller length scaled approaches.

Interlaminar toughening by electrospun nanofibers (the subject of this thesis) is an approach that offers reasonable solutions to the interlaminar toughening approaches. This methodology aims the implementation of nano/sub-micron sized nanıofibers manufactured by electrospinning to composite interlaminar region. From a very basic point of view, it satisfies certain macro design conditions such as reinforcement scale and applicability to available manufacturing methods. On the otherhand, the addition of a nano-scaled sub-phase to the composite structure enlarges the design problem. Constitutive interactions at nano-scale, their overall effect on micro-scale constituent relations and the overall effect to macro scaled laminate behavior has to be determined for effective implementation. Also the characteristic of newly introduced nano-scaled reinforcements are to be evaluated.

1.1.3 Proposed Approach

This thesis work aims to provide insight to this multi-scaled nature of interlaminar toughening. Initial efforts reported in this work consists of gathering state of art information on interlaminar toughening by electrospun nanofibers and to demonstrate if they were applicable to conventional composite strucutres. Prior knowledge that is at the

basis of this thesis are provided as form of a published book chapter. In terms of design approach, the characteristics of transverse matrix cracking and related severe failure events have been carefully characterized by a sound-assisted failure analysis. Originating from thse characterizations working mechanism behind interlayer toughening strategy is demonstrated.

1.1.4 Out-of-the-box Examples

Proposed approach is then exemplified in two out-of-the box composite problems. The basic hypothesis in that chapter is that with improved matrix compatibility and base polymer choice (polystyrene-co-glycidylmethacrylate) nanofibrous interlayer toughening methodology could improve in-plane strength of he composites which reported to be a major drawback for that kind of approach. Longituıdinal tension and open hole tension of uni-directional and cross-ply laminates are concerned. Furthermore, a new approach called "local nanofiber toughening" showed that time and cost requirement for interlayer toughening can be reduced by focusing on the presence of potential stress raisers in the structures (e.g holes).

In a second example, the application of electrospun nanofibers to thick laminates (~1cm) under high strain rate (2600 ,3500, 4000 $^{s-1}$) conditions is evaluated. Via Split-Hopkinson pressure bar tests, interlayered laminates were compressed in both fiber and through the thickness directions. An important achievement that has been done in that work was to be able to manufacture thick laminates with nanofibrous interlayers and to show that a nano-scaled touch on the structure could be effective in extreme loading conditions. In terms of their characteristics and repoted data these two works mainly focuses on the application of P(St-co-GMA) nanofibers to macro-scaled problems.

1.1.5 Material Limits and Sub-Phase Design

Although "nanofibrous interlayer toughening" methology is proven to be effective under many loading conditions (reported in current state of art) it involves the implementation of a thermoplastic material to the composite structrues whose resin structure is mostly thermoset. Hence, the material limits for the newly added thermoplastic material are now a part of the problem. Different from the thermoset polymers, for thermoplastic polymers severe microstructural changes can take place when material limits are overreached. It is also vital to underline that composite processing conditions may not be suitable for the processing of each thermoplastic material. One of these limits is determined to be glass transition temperature (T_g). The second part of this thesis work focuses on the demonstration of morphological changes that appears on P(St-co-GMA) fibers when processed above their T_g. As a matter of fact, it has been found that the nanofibrous morphology could be totally lost when T_g is overcome. However, this problem was solved with a new chemistry based nanofiber design where P(St-co-GMA) nanofibers are able to self-crosslink before their T_g. Two important problems were addressed in new sub-phase design. Initially the electrospinability of P(St-co-GMA) solutions in the presence of crosslinker agents (which usually causes viscosity of the polymer solution to increase if reacted in room processing temperature and hinders electrospinning.) was investigated and correct amounts crosslinker (Phtalic Anhydride), initiator (Tributylamine) that leads to manufacturing of continuously electrospinnable and self-crosslinkable P(St-co-GMA)/PA-TBA nanofibers. Second problem was to tune crosslinking of the P(St-co-GMA) nanofibers so that they remain in nanofibrous mat morphology after composite processing. Choice of crosslinker PA and initiator TBA guaranteed that a heat stimuli crosslinking process that is applicable to composite curing process and as a result of

5

which in-situ crosslinked nanofibrous interlayers were efficiently manufacture. In a general view, offered P(St-co-GMA)/PA-TBA nanofibers are continuously electrospinnable in room temperature hence they can also be applied to composite structures. P(St-co-GMA)/PA-TBA nanofibers are able to self-crosslink after 60^0C and able to complete their crosslinking reaction before glass transition temperature. Hence they can be introduced to composite laminates without being crosslinked and the crosslinking reaction occurs in-situ. As the result of in-situ crosslinking reaction nanofibrous morphology is perfectly maintained inside of the epoxy and better interfacial nanofiber/epoxy reactions are expected. Furthermore, a novel approach of "self-same nanocomposites" where P(St-co-GMA)/PA-TBA nanofibers embedded in P(St-co-GMA) matrix which can be achieved only by electrospinning and thermal processing is exemplified. In the general picture of interlaminar toughening, this work explained the problems and approaches to overcome these problems in interlayer design.

Although new in-situ crosslinking approach offers improved structural integrity, the interaction of P(St-co-GMA)/PA-TBA nanofibers with epoxy matrix is of crucial importance since the process alters overall chemistry of the curing. For mechanical property imporvements in macro-scale, this chemical alteration should not reduce the curing properties of the epoxy resin. The last effort in this thesis work is done on the curing kinetics and mechanical behavior of P(St-co-GMA)/PA-TBA nanofibers inside of carbon/epoxy composite laminates. A cooperative curing behavior where P(St-co-GMA)/PA-TBA and epoxy matrix were crosslinking together, is reported and finalized the discussion on epoxy compatibility and integrity of P(St-co-GMA)/PA-TBA nanofibers. The mechanical response of this carefully tailored nanofibrous interlayers was even more elevated.

As a general overview, this thesis work aims to demonstrate the efficiency of interlayer toughening of composite materials under various loading conditions and to show various steps towards structural demand directed nanofibrous material design.

1.2 Thesis Structure

This thesis work is divided into 4 inter-connected chapters. The contents of these chapters are formed of 3 published journal articles, 1 published book chapter and 2 un-published journal articles that are under currently revision. For completeness, the references and in-text figure/table numbers are unique to each article. The references for each article is provided in the related thesis sub-section.

Contents of the chapters are as follows:

Chapter 2 : A general introduction to interlayer toughening mechanisms in structural composite materials, current state of art and the previous works which forms the basic knowledge on the subject of this thesis are presented in Chapter 2. The contents of Chapter 2 have been recently published as a book chapter (PAPER A). As a novelty in that chapter, the working mechanisms of electrospun interlayers against transverse matrix cracking and subsequent delaminations is discussed in detail. The working principle was discovered by a sound assisted tensile testing methodology whose details are provided in a journal article (PAPER B) which can be found in 2.10 (Additional info) of chapter 2.

Chapter 3: "Out of the box composite examples for interlayer toughening by electrospun nanofibers"

This chapter focuses on the novel applications of P(St-co-GMA) nanofibers as interlayers in different composite structures that have been tested under various mechanical conditions. In that sense it is formed of 3 published papers of the author named as Paper 3.1 and Paper 3.2 . The contents and the publication information of these are as follows:

(Paper B) "Global and Local Nanofibrous Interlayer Toughened Composites for Higher In-Plane Strength"

In this work the application of nanofibrous interlayers to the potential stress raisers have been studied. In the content of this work global toughening approach for nanofibrous interlayers is novelly demonstrated. Furthermore, different than many works reported in [1] the testing methodology have focused on in-plane strength of the composite laminates. To measure that P(St-co-GMA) nanofibers were either applied globally, as in the case of tensile tests of $(0)_6$ and $(0/90)_{3swoven}$ laminates, or localy, as in the case of $(0/90)_{3s}$ open hole tension tests. In-plane strength improvements achieved with wettability and matrix-compatiblity of P(St-co-GMA) nanofibers are reported.

(PAPER C) "High Strain Rate Response of Nanofiber Interlayered Structural Composites"

Nanofibrous interlayer toughening strategy for laminated composite materials typically demonstrated at quasi-static loading is here evaluated under high strain rate deformation. Carbon fiber reinforced composite laminates of $(0/90)_{25s}$ stacking sequence are interlayered by P(St-co-GMA) nanofibers which are chemically tuned for interfacial compatibility when embedded in epoxy matrix. The cubical composite specimens are cut and subjected to high strain-rate deformation via Split Hopkinson pressure bar testing. Specimens are hit at their through-the-thickness (stacking) and side-to-side (in-plane) directions. The change in the dissipation of energy due to altered interlaminar microstructure is monitored and reported. Enhancement in the capacity of the energy dissipation due to the nanofibrous interlayers is as high as 80% in-plane and 40% through thickness directions, depending on the strain rate. The results overall suggest that

interlayer toughening strategy used in this work prevents the formation of critical matrix cracks that can cause the formation of instantaneous mode II delamination. Incorporation of the nanofibers without causing notable weight penalty effectively toughen the matrix dominant interlaminar zones under high strain rate conditions as well.

Chapter 4:

(Paper D) : "Stabilized Electrospinning of Heat Stimuli/In-situ Cross-linkable Nanofibers and Their Self Same Nano-composites"

We present a strategy for stabilizing the morphological integrity of electrospun polymeric nanofibers by heat stimuli in-situ cross-linking . Amorphous polymer nanofibers, such as polystyrene (PS) and its co-polymers tend to lose their fiber morphology during processing at temperatures above their glass transition temperature (T_g) typically bound to happen in nanocomposite/structural composite applications. As an answer to this problem, incorporation of the cross-linking agents, phtalic anhydride (PA) and tributylamine (TBA), into the electrospinning polymer solution functionalized by glycidylmethacrylate (GMA) copolymerization, namely P(St-co-GMA), is demonstrated. Despite the presence of the cross-linker molecules, the electrospinning polymer solution is stable and its viscosity remains unaffected below 60°C. Cross-linking reaction stands-by and can be thermally stimulated during post-processing of the electrospun P(St-co-GMA)/PA-TBA fiber mat at intermediate temperatures (below the T_g). This strategy enables the preservation of the nanofiber morphology during subsequent high temperature processing. The cross-linking event leads to an increase in T_g of the base polymer by 30°C depending on degree of crosslinking. Cross-linked nanofibers are able to maintain their nanofibrous morphology above the T_g and upon exposure to organic solvents. In-situ crosslinking in epoxy matrix is also reported as an example of high temperature

demanding application/processing. Finally a self-same fibrous nanocomposite is demonstrated by dual electrospinning of P(St-co-GMA) and stabilized P(St-co-GMA)/PA-TBA, forming an intermingled nanofibrous mat, followed by a heating cycle. The product is a composite of cross-linked P(St-co-GMA)/PA-TBA fibers fused by P(St-co-GMA) matrix.

(PAPER E): **"Synergistic role of In-Situ Crosslinkable Electrospun Nanofibrous Interlayers for Superior Laminated composites"**

In a multi-scaled toughening approach, in-situ crosslinkable P(St-co-GMA)/TBA-PA nanofibers are electrospun both onto epoxy adhesive films and carbon/epoxy prepreg plies that have the same epoxy system. Nanofiber/epoxy nanocomposite specimens were manufactured via in-house developed, hot press associated film casting methodology. Nanofiber crosslinking is in-situ, that is triggered and advanced through the epoxy curing cycle. The in-situ crosslinking is monitored by DSC analyses where increased cure enthalpies (ΔH) are reported. Furthermore cure kinetics analysis following Ozawa-Flynn-Wall method shows that P(St-co-GMA)/TBA-PA nanofibers have a significant autocatalytic effect on the epoxy matrix curing. Mechanical behavior-crosslinking chemistry correlation is initially investigated by the tensile test of nanofiber/epoxy nanocomposite samples where tensile strength and elastic modulus are increased by 30% and 8% respectively with respect to un-reinforced specimens. Laminated composites with $(0)_{48}$ lay-up configuration are subjected to end notched flexure. Significant increase as high as 95% in G_{IIC} is also noted due to incorporation of P(St-co-GMA)/TBA-PA nanofiber interlayers. Results suggest the crosslinking manupilated properties of the nanofibers themselves and surrounding epoxy matrix synergistically form mechanically enhanced nanocomposite interlayer zones. Fracture surface analysis is presented to

11

elaborate significant role of the proposed in-situ crosslinked nanofibers on the notable improvements in mechanical behavior of laminated composites.

CHAPTER 2: INTRODUCTION AND PREVIOUS WORKS

Author's Note: In the overall set-up of the thesis structure, this section firstly provides required literature review specifically focused on interlayer toughening methodologies. Following that the experimentation that has been done on previous works are provided in the form case examples to provide basic knowledge to the reader about the problems that have been faced and the methodologies that are commonly applied to manufacture and test interlayer toughened structural composites. The general insight of the chapter is based on initial applications of P(St-co-GMA) nanofibers whose application and modifications are at the core of this thesis work. Furthermore, the working principle of electrospun interlayers is explained with a custom matrix cracking test that has been assisted with sound apmplitude analysis to explore the nature of failure.

Sound assisted failure analysis of cross-ply laminates is a novel concept that has been introduced to the literature as a part of the thesis work. This chcaracterization method has been presented as additional info to that chapter in detail.

2. Interlayer Toughening Mechanisms of Composite Materials

Reference (Paper A) : **K.Bilge**, M.Papila,"Interlayer Toughening Mechanisms of Composite Materials", Toughening Mechanisms in Composite Materials, Edited by Qinghua Qin and Jianqiao Ye, Woodhead Publishing (Elsevier), 2014.

2.1 Abstract

Interlayer toughening in polymer-matrix composite materials can address the usual suspects in regard to the failure of laminated composites. Issues contributing to poor interlaminar strength and toughness can be delayed or eliminated by interleaving, in addition to suppressing matrix cracking, whether the root cause of delamination is isolated or synchronous. The interlayers/interleafs are considered herein as the additional design features enabling tuning of the ply-to-ply interfacial (interlaminar) regions. A comprehensive literature review is presented for different interleaving strategies, with a special focus on nanofibrous electrospun interleafs. A road map and a series of examples are also discussed for effective incorporation of the nanofiber interlayers/interleafs into the laminated composites. Toughening mechanism in the presence of electrospun nanofiber interleafs are shown to be effective under both in-plane and out-of-plane loading. Specifically, epoxy-compatible poly(styrene-co-glycdylmethacrylate), P(St-co-GMA) and P(St-co- GMA)/MWCNT nanofibrous interlayers incorporated into carbon/epoxy laminated composites are exemplified for enhancing mechanical behavior under longitudinal and transverse tension, open hole tension, three point bending and end notched flexural tests. Moreover, the working mechanism of these interlayers under in-plane loads is further elaborated by the custom design tensile tests of $(0_2/90_4)s$ interleaved laminates, backed-up by cracking-sound recording and analysis.

2.2 Introduction

2.2.1 Interlayer Toughening Methods

Tailor-able specific strength and modulus (strength-to-weight and modulus-to-weight ratios respectively) of advanced composite materials is of great advantage in design of light-weight high performance structures. However, there are limitations yet to overcome for making use of the composites at their full potential and capacity. Interlaminar strength is arguably the weakest link for which substantial improvement may be sought by a strategy so called interlayer toughening.

Among several other toughening strategies for composites, the interlayer toughening focuses basically on the interlaminar regions of laminated composites where two subsequent plies are interfaced with each other. Theoretically speaking, the interlaminar regions are very thin resin rich regions with relatively weak mechanical properties. In these terms, the behavior of an interlaminar region depends on the mechanical properties of the matrix phase as well as the interaction of the two subsequent plies affected by the fiber architecture, orientation and lamination sequence (Tsotsis, 2009). Toughening of the interlaminar region may be achieved by enhanced matrix toughness itself. But also by the introduction of a crack deflection/suppression media in which more energy is required for crack growth to continue, that is, the cracks can essentially be stopped. Therefore interlayer toughening strategies typically consider the addition of sub-phases such as dispersed particles, films, secondary fibrous reinforcements or their combinations into interlaminar planes to avoid extensive crack formation (Shivakumar and Panduranga, 2013).

2.2.2 Particle/filler dispersion Based Interlaminar Toughening

Particle/filler based interlaminar toughening strategies for structural composites are implemented by inserting/dispersing particles/nanotubes that have different mechanical behavior than the resin phase. The addition of thermoplastic particles effectively toughens the matrix phase by increasing mode I, mode II fracture toughness (Pham and Burchill, 1995, Huang and Hom, 1998, Matsuda et. al, 2009) as well as specific energy absorption capacities (Sela and Ishai,1989, Wilkinson et.al,1993). Through a well exemplified fractography analysis Stevanovic et al. (2013) showed how a thermoplastic particle (ABS) played role on plastic deformation of interlaminar region and underlined the importance of particle/matrix compatibility. On an application problem, Warrior et.al (2004) investigated the effect of thermoplastic particles on the behavior of composite tubes made of continuous filament random mats and non-crimp fibers (NCF) and showed the effect of fiber architecture.

Particle/filler inclusion based interlaminar toughening of structural composites especially drew attention with the availability of very stiff nanotube structures. Numerous recent studies showing the hierarchical integration of carbon nanotubes into conventional composites have been comprehensively reviewed by Qian et al. (2010). Khan and Kim (2011) collected and presented specific studies which focus on the effect of CNTs to impact and delamination characteristics of polymer composites. Among the similar efforts, Garcia et.al (2008) showed clearly the CNT orientation effect on the out of plane properties by aligning them transversely inside the epoxy matrix. In another study, Veedu et.al (2006) increased the Mode I and Mode II interlaminar toughness of 3D composites by 348% and 54% respectively by growing aligned CNTs on the surface of SiC fibers.

Apart from CNTs, nanoclays (Nuhiji et al., 2011) halloysite nanotubes (Ye et al., 2011) can be stated amongst the recently reported nanoscale fillers/ additives for composite materials. The main focus in these studies was to improve the out-of-plane properties of composite materials by both toughening the matrix phase and introducing stiff crack deflection zones into the interlaminar region. However, the particle based toughening methodology may profoundly suffer from dispersion problems associated with the nano nature of inclusion materials (Coleman, 2006). Any potential inhomogenity due to the agglomerates of stiff nano-fillers can create potential cracking spots inside the composite laminate which will significantly decrease composite performance.

2.2.3 Film Interleaving Approaches

The main idea of film interleaving methods is to introduce a continuous crack deflection media into the interlaminar planes (Tsotsis, 2009). Planar addition of reinforced or non reinforced thermoplastic/thermoset polymer films has been considered extensively since the beginning of 90's till early 2000's (Ishai et al., 1988, Masters, 1989, Carlsson and Aksoy, 1991,1992, Ozdil and Carlsson,1992, Li et al., 1996, Duarte et al.,1999, Sohn et al.,2000, Sohn et. al,2000, Jiang et al.,2001, Xuefeng et al.,2002). The goal of these studies was primarily to enhance out of plane properties such as impact, Mode I and Mode II delamination resistances. Hojo et al, (2006) compared the behavior of mode I delamination fatigue properties of composite materials interleaved with thermoplastic particles and ionomer based continuous resin films. Combining the emerging nanotube technologies and their advantages, Sun et al. (2010) offered the use of partially cured epoxy/SWCNT thin films as reinforcement agents for vacuum assisted resin transfer molded (VARTM) composites. More recently White and Sue (2012) followed this idea

and noted significant increases in mode II crack initiation and propagation onsets for composites manufactured by VARTM method. Yasaee et al (2012a, 2012b) considered the addition of different types of interlayers; thermoplastic film, chopped aramid fibers, pre-impregnated fiber reinforced tape, thermosetting adhesive film, and compared their efficiencies in damage suppression specifically for Mode I and Mode II delaminations. Moreover, Khan and Kim (2012) managed to manufacture bucky-paper interleaves out of carbon nanofibers and showed significant improvements in interlaminar shear properties for CFRP composites.

2.2.4 Nanofibrous Interlayers for Composite Materials

Nanofibrous interlayer toughening strategy is in principal the same as of film-interleaving, but incorporates nano- to sub-micron fibrous interleafs with substantially high surface area instead of the continuous polymeric films. Fibrous interlayers are inserted into the laminates for their potential to increase the resistance against micro-cracking and ensure better bonding of the adjacent plies (Zuchelli et al., 2011). Lee et al., (2002, 2006) demonstrated the use of non-woven mats for interlayer toughening without referring to the manufacturing technique of interest herein, so called electrospining which is commonly used to produce non-woven polymeric nanofibers (Huang et al.,2013). This relatively new concept was first introduced by Kim and Reneker (1999) and Dzenis (Dzenis and Reneker, 2001, Dzenis 2008). Zuchelli et al. (2011) thoroughly reviewed available studies that have followed the traces of this novel idea and demonstrated capabilities of electrospun nanofibers as interlayers in the composite materials. Table I aims to supplement the review also with very recent studies on polymeric nanofiber toughening of composite materials (Dzenis and Reneker, 2001,

Dzenis,2008, Sihn et al.,2008, Liu et al.,2006,2008,2014, Zuchelli et.al,2012, Magniez et al.,2011, Zhang et al.,2010,2012, Bilge et al., 2012,2014, Subagia et al.,2014, Li et al., 2015, Heijden et al.,2014,). It is clear from the available literature that nanofiber interlayer toughening method via polymeric nanofibers is considered as a promising strategy to toughen composite materials both under in-plane and out of plane loading conditions (Sihn et al.2008).

Table 1: Summary of works incorporating polymeric nanofibers as interlayer toughening agents in structual composites

Author/Year	Composite System	Nanofibrous Interlayer	Experiment	Results
Dzenis and Reneker, 2001 Dzenis,2008	Carbon/Epoxy	Polibenzimidazol	DCB	G_{IC} 15%
			ENF	G_{IIC} 130%
Liu et al.,2006	Glass/Epoxy	PA 6	T	Comparison of Three Nanofibers
		Epoxy 609	3PB	
		TPU	SBS	
Sihn et.al,2008	Carbon/Epoxy	Polycarbonate	T	Microcrack initiation 8,5% Delamination 8%
Liu et al.,2008	Glass/Epoxy	Epoxy 609	ENF	G_{IIC} 9%
Zuchelli et.al,2012	Graphite/Epoxy	Nylon 6,6	DCB	G_{Ic} 5% Energy Absorbed 23%
			ENF	Energy Absorbed 8,1% G_{IIc} 6,5%
Magniez et al.,2011	Carbon/epoxy	poly(hidroxyether bisphenoll A)	DCB	G_{IC} %118
Zhang et al.,2010	Carbon/epoxy	Polyetherketon cardo	DCB	Initiation G_{IC} %60 Propagation G_{IC} %81
Zhang et al.,2012	Carbon/epoxy	poly(e-caprolactone)	DCB	Initiation G_{IC} %37 Propagation G_{IC} %92
Bilge et al., 2012	Carbon/epoxy	P(St-co-GMA)	3PB	Flexural Strength 16%
			ENF	G_{IIC} 55%
			Impact	Absorbed energy 8%
			TT	Transverse tensile strength 17%
		P(St-co-GMA)/MWCNT	3PB	Flexural Strength 25%
			ENF	G_{IIC} 70%
			Impact	Absorbed energy 20%
			TT	TransverseTensile strength 27%
Bilge et al., 2014	Carbon/epoxy	P(St-co-GMA)	T	Ultimate Tensile Strength 12%

			OHT	Open Hole Tensile Strength 9%
Subagia et al.,2014	Basalt/Epoxy	Polyurethane/CNT	T	Flexural Strength 17%
			3PB	Tensile Stregth 13%
Liu et al.,2014	Carbon/Epoxy	Polyurethane/CNT	3PB	Tensile strength 8%
			T	Flexural Strength 16%
Li et al., 2015	Carbon/Epoxy	MWCNTs-EP/PSF with different MWCNT loadings	SBS	Interlaminar Shear Strength 12%
			3PB	Flexural Strength 13%
			ENF	G_{IIc} 49%
Heijden et al.,2014	Glass/Epoxy	Polycaprolactane	DCB	20% G_{Ic} Initiaton
				12% G_{Ic} Propagation
			T	Maintained
			OHT	Open Hole Tensile Strength 7,5%

Note: Test name initials in the table represents
DCB: Double Cantilever Beam
ENF: End Notched Flxure
T: Tension
TT: Transverse Tension
OHT: Open Hole Tension
3PB: 3 Point Bennding
SBS: Short Beam Shear

The polymer choice of electrospun interleaf fibers for toughening composites should be made carefully in compliance with the polymer matrix chemistry and cure conditions (Ozden et al 2010, 2012, Zuchelli et al 2011, Bilge et al 2012). Because thermal stability of the polymeric fibrous interleaf morphology, wettability and nanofiber interfacial compatibility with the resin system have impact on the interlayer performance. On the other hand, polymer based nanofibers may be converted into much stiffer carbon nanofibers (CNF) (Zussman et al., 2005, Wang et al., 2003, Gu et al.,2005a,2005b, Zhou

et al., 2009). Chen et al. (2011) showed that the incorporation of CNF interlayers (made from electrospun PAN nanofibers) into composite laminates resulted in significant increases in both in- and out-of-plane plane properties. The capabilities of CNF as efficient interlayers were reported on several other studies in the literature with special attention on the crack bridging characteristics on mode I (Palmeri et al, 2011, Yudin et al., 2008, Sadeghian et al., 2006, Rodriguez et al., 2011, Hossain et al., 2013).

There is a challenge and demand for interlayer materials which can work and provide improvement efficiently both under in-plane and out-of-plane loading conditions. It is also important to adapt the interlayer toughening concept into conventional manufacturing techniques and materials. In this regard, the nanofibrous interleaf/interlayer toughening arguably appears to be more promising for which particular attention is devoted in this chapter.

Therefore, the objective herein is to provide a guideline for incorporating nanofibrous interlayers effectively into laminated composites and discuss their toughening effects.

Key steps for exploring this toughening strategy are elaborated, namely polymer synthesis and characterization, electrospinning, laminate manufacturing, specimen preparation, mechanical testing strategies and mechanical property improvements in accordance with microscopy assisted failure analysis. Supplementary examples and case studies in section four are also provided from our reference studies (Bilge et al., 2012, 2014).

2. 3 Materials, Process and Characterization

Although the nanofibrous interlayer toughening strategy stands rather simple, its interdisciplinary and multi-scale nature asks for a systematic work to demonstrate its potential and establish an effective implementation. Proposed roadmap herein needs to cover three major sections: materials choice/development, processing and characterization. Materials section typically addresses polymer selection and synthesis for the base polymeric nanofiber interlayers. Processing should discuss first the prefered nanofiber manufacturing technique so called electrospining. Plan and description on how the interlayers are incorporated into conventional composite manufacturing techniques should follow next. Specimen preparation is also under this general topic. Characterization content overlaps with both materials and processing sections. Therefore associated details are nested in respective sections. In addition, a separate section covers the ultimate assessments for toughening of the interlayered/interleaved composites via extensive mechanical testing.

2.3.1 Materials (and Characterization)

2.3.1.1 Base Polymeric Material Selection for Nanofibrous Interlayers

The idea of toughening by nanofibrous interlayers begins with the choice of a base polymer (see Table 1 for variety of polymeric materials introduced as interlayer materials). The right choice is the initial and essential step for the success of nanofibers as toughening interleaf, and therefore should take into account the sequel of the processes and materials systems in the targeted composite laminate. In regard to sequence of the whole process, key factors to note are:

i)   Electrospin-ability: this criterion is related to the characteristics of electrospining polymer solution that can enable uniform fiber spinning, preferably without any bead formations.

ii)   Matrix/resin of composite material: It is of paramount importance that the polymeric nanofiber material should enable strong bonding and interface compatibility with the hosting matrix of the composite material. For instance epoxy compatibility is sought as in the majority of the practical cases.

iii)   Resin curing conditions: posterior to the nanofiber formations via electrospinning, composites are formed following the cure cycle of the resin system of the target composite material. Therefore the thermal properties of the nanofibers (such as glass transition or melting temperature) should allow stability/integrity of the fibrous interlayer to be maintained in accordance with the cure cycle which can be at an elevated temperature.

Polymer Choice example: P(St-co-GMA) for Highly Epoxy compatible Nanofibers

Considering the traditional epoxy matrix composite systems, compatibility between the polymeric nanofibrous structure and the epoxy can be incorporated into the choice. The main idea is to create surface modified/reactive nanofibers with epoxide functional groups so that the interfacial bonding with the epoxy based polymer matrix is improved. As a consequence the crosslinking between the epoxy and nanofibers is promoted. In the recent study (Ozden et al.,2010), choice of P(St-co- GMA) for which the chemical structure is given in figure 1 has been demonstrated to be superior to polystyrene that would be also commercially available choice. The custom choice may typically require specific synthesis procedures as exemplified next.
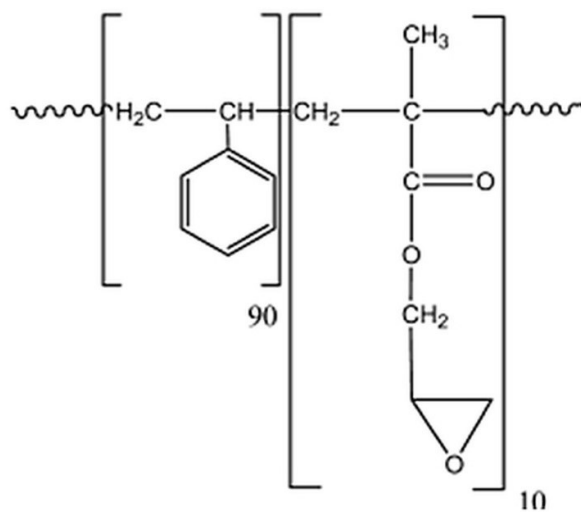
Figure 1: Chemical structure of in-house synthesised P(St-co-GMA) polymer with 10 wt% of GMA.

2.3.1.2 Synthesis and Characterization of a Custom Polymer

In the scope of toughening via electrospun interlayers, the polymer synthesis is a very crucial step in particular for the custom polymer choice as described in the previous section. Because the correct synthesis of the base polymer does not only affect the nanofiber properties, but also determines the electrospinning characteristics in the nanofiber manufacturing. In parallel, another important step is to choose the right synthesis methodology among several conventional polymer synthesis methodologies (Braun et al.,2013) in order to obtain the base polymers with proper molecular weight and polydispersity characteristics required for electrospinning process. These characteristics of the synthesized polymer must be well characterized and reported. Gel Permeation Chromatography (Moore, 1964) is an efficient method to determine molecular weight

distribution and polydispersity index of synthesized polymers. In addition, nuclear magnetic resonance (NMR) (Hatada and Kitayama,2004) and Fourrier Transform Infra Red (FTIR) (Koenig, 2005) analyses determine if the synthesized polymer has the targeted chemical structure.

Synthesis example: P(St-co-GMA) copolymer synthesis

Copolymer poly(St-*co*-GMA) can be synthesized by solution polymerization technique as reported in (Ozden et al.,2010). Purified styrene and GMA (by weight fractions: 0.9 styrene and 0.1 GMA) are mixed in a test tube contained in ice bath. Dimethylformamide (DMF) is then added into St-GMA monomer mix such that volume proportion was 3:2, respectively. The initiator azobisisobutyronitrile (AIBN) is added into the test tube flushed with nitrogen. The tube containing the dissolved monomers is then kept 24 h in the iso-thermal bath at 65 °C for the polymerization reaction. Finally, the polymer solution is poured out into a beaker containing methanol and the methanol/polymer mixture was filtered and dried in an oven at 60 °C for 2 h. The synthesized P(St*co*-GMA) copolymer structure can be determined by H NMR. For instance, molecular weights and polydispersities were recorded as 110000 and 160000 g/mol. (1.35-1.45 PDI).

2.4 Process (and Characterization)

2.4.1 Electrospinning of nanofibers

Electrospinning is widely used for manufacturing nanofibers for a variety of applications including interlayer toughening. Figure 2 represents a typical laboratory set-up for the electrospinning process where polymer solution in a syringe is charged by high voltage and an electric field between the tip of the syringe and an electrically grounded collector is formed. When the magnitude of this electrical field overcomes the surface tension of the polymeric solution on the tip of the pipette/syringe needle the fluid is ejected as a jet from the tip to the grounded collector. During the flight of the
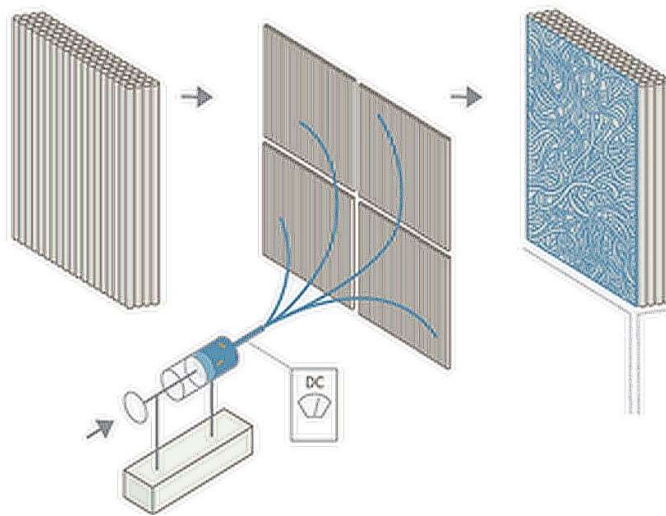
Figure 2: A representative electrospinning setup for nanofiber production

jet the solvent evaporates and the base polymer solidifies forming nanofiber mats at the grounded collector.

Although it is an efficient and easy way to manufacture nanofibers, the optimal electrospinning process is highly dependent on the correct choice of process parameters such as tip to collector distance, voltage applied and the flow rate of polymeric solution as well as the properties of polymeric solutions itself. In terms of electospinning operation parameters the applied voltage, distance between collector and the tip and the flow rate of the solution inside the pump may be considered as major parameters (Yordem et al., 2008). Depending on the nature of the polymeric solution and targeted morphology these parameters must be optimized with the help of assessments on the scanning electron microscopy (SEM) images.

Apart from the electrospinning operation parameters, an important fact for nanofiber manufacturing is the need for an homogenous polymer solution. Therefore it is vital to choose the right solvent for the base polymer to electrospin. The problem of inhomogenity mostly shows itself during the electrospinning as an unstabilized Taylor Cone (Wendorff et al.,2012) or bead occupied structures on the nanofiber morphologies which are arguably undesired in the composite applications. Solution inhomogenity problem especially occurs when the electrospinning is done in the presence inclusions such as carbon nanotubes, silica nanoparticles and numerous other nano to sub-micron nanoparticles (Liut al., 2011). The inclusions can be used to alter/tailor properties of the electrospun nanofibers. However agglomeration problems may occur which hinder the electrospinning process and cause inhomogenous particle distrubution in/on the nanofibers. Hence in order to have a homogenous interlayer, the polymer solutions with the nano-inclusions should be well characterized preferentially with a Dynamic Light Scattering (DLS) method (Schartl, 2007). Also a process optimization effort may be

followed to determine the optimum particle/inclusion percentage and polymer concentration aiming to reduce the fiber diameter and typically avoid bead and/or agglomerate formation.

Example: Electrospinning on Carbon/Epoxy Prepreg Plies

For this specific example P(St-co-GMA)/DMF solutions were prepared by dissolving 30wt% P(St-co-GMA) in DMF solution. The solution was stirred for 3 hours on a magnetic stirrer. MWCNTs at 1wt% was also loaded into another batch of the same copolymer solution to consider an additional case with composite nanofiber interlayers. Note that, the amount to be added to the solution was determined by a preliminary process optimization study (Ozden et al., 2012). Solutions containing MWCNTs were further stirred for another 24 hours to achieve good dispersion. Applied voltage, solution flow rate and tip to ground distance were set at 15 kV, 30 lL/h and 10 cm, respectively during electrospinning. The polymer solution was electrospun directly onto carbon/epoxy prepreg layers such that the overall interlaminar regions will be toughened by a thin homogenous layer of nanofibers, with an additional weight as low as 0.2% of the prepreg ply weight.

2.4.2 Manufacturing of Structural Composites with Nanofibrous Interlayers

For the manufacturing of nano-interlayered structural composites, the conventional composite manufacturing strategies may be employed. Commonly used methods can be noted as Vacuum Assisted Transfer Moulding (Seyhan et al.l,2008) , RTM (Heijden et al, 2014) and prepreg lamination (Bilge et al.,2012, 2014). Among these manufacturing processes the prepreg lamination strategy may be classified arguably as the most efficient

and a superior way to implement nanofibrous interlayers to composite structures. Because it avoids possibility of unstable positioning of the interlayer between the dry reinforcing fibers and the resin flow-front pressure during the liquid-molding type productions (resin infusion/transfer) which can also have detrimental effects of the nanofibers network position and structure.

On the other hand, the prepreg lamination requires certain speed of manufacturing in order to minimize the environmental effects such as moisture on the prepreg plies. Depending on the equipment/set-up used the deposition of nanofibers onto prepreg surfaces through electrospinning may demand a considerable amount of time which can be detrimental to the prepreg plies. Therefore this process is preferably done in working area of controlled temperature and humidity as in a regular prepreg based production.

2.5 Characterization Nanofibers and Composite

2.5.1 Microscopy for Interlayer Morphology

Microscopy is an essential tool in the assessment of the nanofibrous interlayer study and their composites. First part is on the study of morphology of the nanofibers that is relevant to both materials and processing. It is because, the resultant nanofiber formation depends significantly on electrospining process variables, the choice of polymer type, solvent and their solutions along with the operation parameters such as applied electric field. The morphology characterization for nanofibrous materials is typically done by scanning electron microscopy (SEM).   Fiber diameter distributions may be analyzed via SEM images. Transmission electron microscopy (TEM) or high resolution transmission electron microscopy (HR-TEM), on the other

hand, are typically needed to see nano-scaled particle inclusion if they too are incorporated in the electrospining process.

Noting the SEM imaging is also very effective in fractography of composite materials, it is used in the fracture surface and cross section analysis required for understanding the effect/trace of the interlayers on crack propagation and deformation paths along with optical microscopy.

Example: P(St-co-GMA) and P(St-co-GMA)/MWCNT nanofiber morphologies

A systematic study on the electrospinning of P(St-co-GMA)/MWCNT fibers was first carried out and reported by Ozden et al. 2012. Bilge et.al 2012 then implemented the process parameters and material proportion suggested for successful introduction of the MWCNTs and the morphology of the fibrous webs. Figure 3 presents the TEM analysis of P(St-co-GMA) electrospun nanofibers composed of 1 wt.% MWCNTs and demonstrates that MWCNTs were efficiently placed in the polymeric nanofibers as supplementary pin-like reinforcing elements.
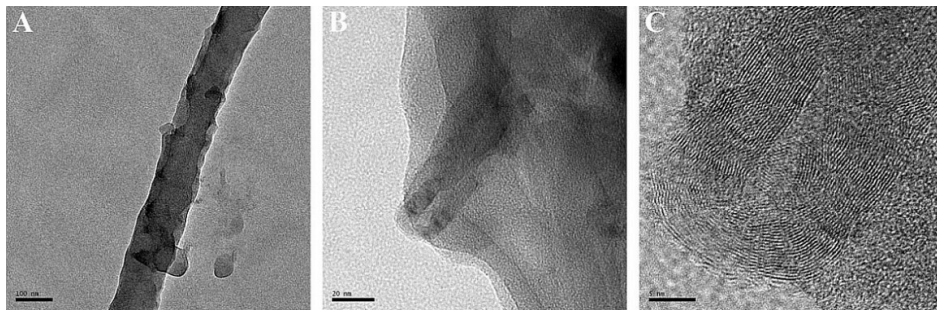
Figure 3: TEM images of MWCNTs on nanofiber surfaces. (a) A single fiber. (b) Slice view of a single fiber. (c) Zoomed view of MWCNTs.

2.5.2 Compatibility via Wettability

Compatibility of interlayer toughening agents with matrix phase forms the main bridge between toughening for both in-plane and out of plane responses. Therefore the interlayer addition specifically asks for a detailed compatibility analysis which can be done interactively with SEM analysis and Drop Shape Analysis (DSA) as exemplified in the following section.

Example: Epoxy compatible Interlayers

Another key aspect in evaluating the properties of polymeric nanofiber morphologies is to determine their in-situ wettability and stability once exposed to resin and associated curing conditions. High performance resin systems typically require elevated temperature and pressure for curing. These conditions should be tested for and tailored in regard to the thermal characteristics and limits of the nanofibrous interlayers, Otherwise the electrospun nanofiber morphologies or network of the nanofibers may not be preserved when integrated into composite laminates.
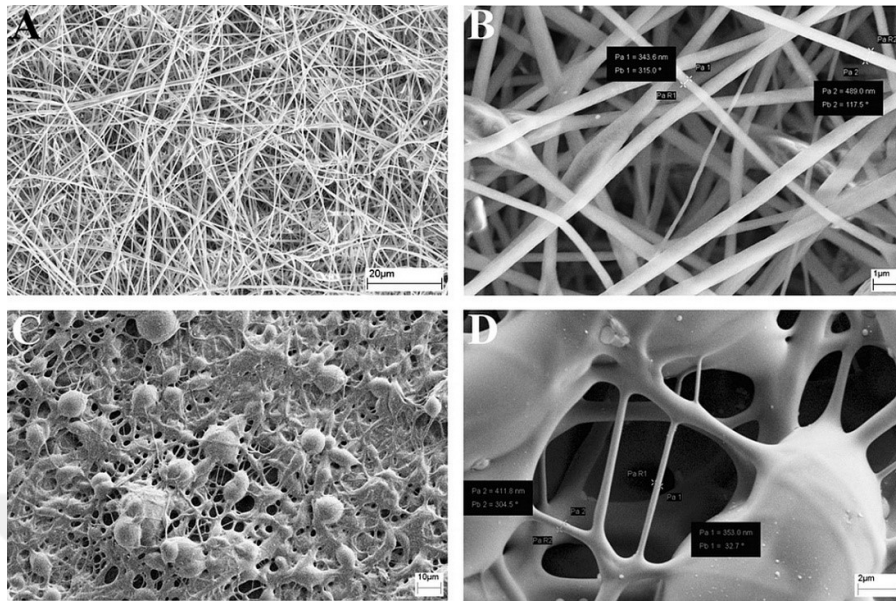
Figure 4: Nanofiber morphologies on the prepreg surfaces: (a and b) at room temperature and (c and d) at 100 °C.

This evaluation is exemplified in figures 4a-4d which were taken for the nanofibers at the prepreg surface. Figure 4a and 4b belongs to electrospun P(St-co-GMA)/MWCNT nanofibers at room temperature whereas figures 4c and 4d belongs to the nanofiber morphology at 100°C (i.e. the curing temperature for the prepreg system). It is clearly visible the non woven fibrous morphology was transformed into a network-like structure composed of fibers covered by epoxy and micron scale epoxy coated bead like nodal points. This change in the microstructure suggests the presence of a good interaction and wetting between nanofibrous interlayers and epoxy matrix phase at the laminate curing temperature. Figure 6 shows image of the electrospun layer-prepreg system kept at curing temperature 100°C (left hand side) and pristine samples at room temperature (right hand side) for comparison. It was quite visible that when the prepreg with the electrospun fibrous layer coat was

heated, the epoxy matrix penetrated into the fibrous layer and wetting of the layer was completed even standing free with no consolidation pressure (i.e. vacuum bagging pressure) (Figure 5b). Recall that the zoomed-in view of the surface of unheated laminate in Figure 5b appeared as shown in Figure 4a. However, when the temperature was increased, those layers of the majority of the nanofibers were no longer visible due to what may be called as progressive self-wetting (Figure 5c and d).
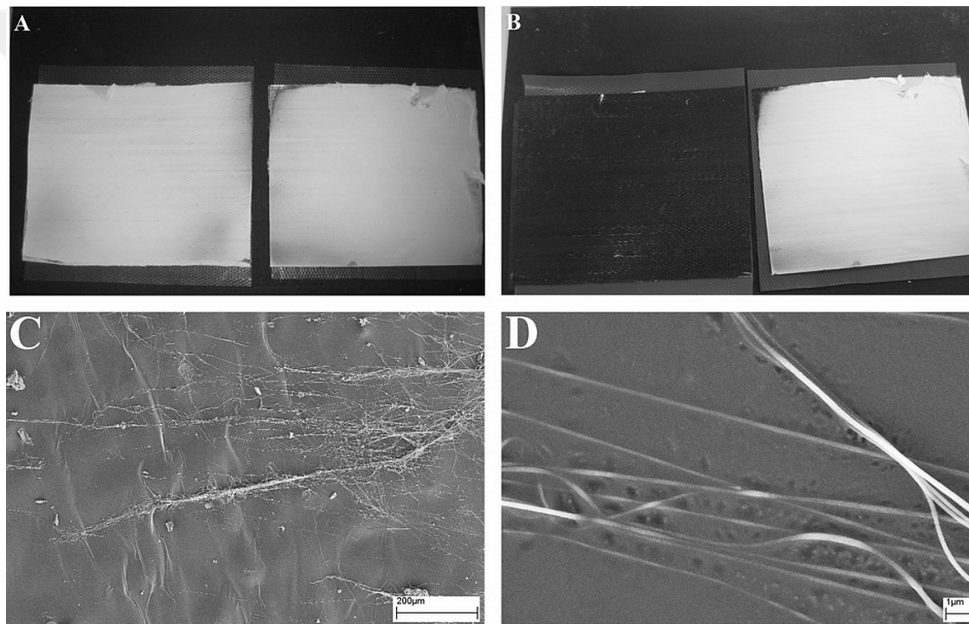
Figure 5: Nanofiber morphologies on the prepreg surfaces: (a and b) at room temperature and (c and d) at 100 °C.

More direct and formal investigation of the wettability was performed via contact angle measurements with epoxy/hardener mixture on the surface of the electrospun mat. When a droplet of epoxy/hardener mixture was put on the electrospun mat, it advanced and wetted the surface by leaving an average contact angle as low as 26.5 ± 6.1, as shown in Fig. 6. This result indicated that the viscous epoxy/hardener mixture could penetrate through the pores in the fibrous surface morphology without challenging a remarkable

capillary pressure due to the attractive forces (Feng and Jiang, 2006) which is another indication of the chemical compatibility between the copolymer and the epoxy system.
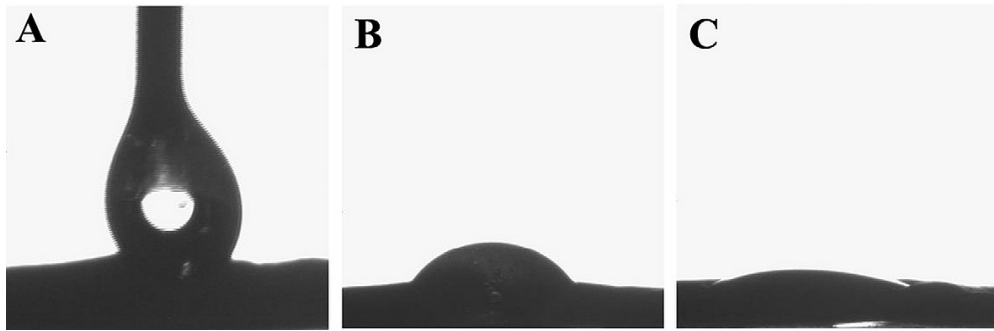
Figure 6: An epoxy/hardener drop on the P(St-co-GMA)/MWCNT surface.

2. 5.3. Mechanical Testing of Nano-Interlayered Structural Composites

Mechanical tests that are included as example in this chapter are summarized in Table 2. All of the tests were carried on both neat and P(St-co-GMA) interlayered carbon/epoxy laminates. Also for some cases composite interlayers of P(St-co-GMA)/MWCNT were considered. In addition to these tests the resistance against delamination can also be measured by Short Beam Shear and 4-point bending tests.

It should be noted that the choice of fiber orientations and stacking sequences of the laminates can be tailored in accordance with the test to be applied and whether for the determination of delamination resistance and/or matrix cracking. Considering (0°) and (90°) fiber orientations in parallel and transverse, respectively, to the major axis (longer side) of rectangular test specimens made by unidirectional composite materials, the use of (0/90) lay-up variations can introduce characteristics for critical failure modes to be toughened about. For instance, presence of (90) plies under tension enables to facilitate

matrix cracking/inter-fiber-failure (IFF) described by Knops (2008). Moreover, inducing the matrix cracking initiation and delamination posterior to matured transverse cracking through the 90 ply thickness can be enforced by the presence of (0/90) ply interface which makes the anisotropic mismatch at the interlayer region maximum. A good example is (90/0/90) configuration for which interleaved version can be represented as (90/I/0/I/90), "I" denoting the nanofibrous interleaf/interlayer. When it is subject to three point bending test the bottom 90° ply is expected to fail under tension due to transverse matrix failure and an opening and/or shear mode failure with stable crack growth from 90/0 interface can progress and lead to the ultimate failure (Bilge et al, 2012).

Table 2: Followed mechanical strategy for example case

Test Name	Standard	Properties	Lay-Up Sequence	Interlayer Region	Comments on Failure+
Three Point Bending	ASTM D790	Flexural Modulus / Flexural Strength	**(0)x**	**All***	Both delamination and matrix cracking occurs
			(90/0/90)x	**All***	90° Ply tension failure is followed by delamination (more controlled failure**)**
Charpy Impact Test	ASTM D6110	Energy absorbed upon impact	**(90)xs**	**All***	Transverse matrix cracking is dominant
Double Cantilever Beam	D5528	G_{1C} vs. Crack Length	**(0)x**	**Only Midplane**	Opening mode delamination and interlayer bridging effect occurs
End Notched Flexure	ASTM WK22949	G_{IIC}	**(0)x**	**Only Midplane**	Ensures crack initiation and growth from

					interlayered region.
Longitudinal Tensile Test	ASTM D3039	Tensile Strength Elastic Modulus Poisson's Ratio	**(0)x**	**All***	For UD carbon/epoxy composites, early matrix cracking and pre-mature failutre observed
			(0/90)xs	**All***	Premature failure and and edge delaminations are observed.
Transverse Tensile Test	ASTM D3039	Transverse Tensile Strength	**(90)x**	**All***	Direct observation of matrix toughening effect.
Open Hole Tension Test	ASTM D5766	Open Hole Tensile Strength	**(0/90)xs**	**All*, Around hole region**	Matrix cracking from the hole region and delaminations are observed.

| Custom Matrix Cracking Test | ASTM D3039 | Resistance to transverse matrix cracking | $(0_2/90_4)s$ | Between 90° blocks | Specific test measuring directly the transverse matrix cracking between 90° plies. (Specifics are explained below) |

(*): All interlaminar planes

Under various loading conditions the toughening of interlaminar regions mainly works against extensive matrix cracking and delaminations which can cause pre-mature failure of the composite laminates. Transverse matrix cracking in the unidirectional composite materials, for instance may arise within the individual plies or ply blocks (Johnson and Chang, 2011a, 2011b) where the stresses transverse to their fiber orientation are critical for the given loading conditions. Also interlaminar stresses at the interface of the adjacent plies due to the Poisson mismatch and mechanical anisotropy, and presence of the edge stresses or stress raisers such as joints (Shivakumar and Panduranga, 2013) are potential reasons for failure mechanisms.

Depending on the lamination sequence and loading conditions, the matrix cracks inside the laminate can cause a ply-by-ply failure, can induce both internal and edge delaminations and eventually facilitate fiber breakage by diminishing the effective load transfer between plies (Johnson and Chang, 2011a, 2011b). In that regard, the matrix cracking is an intermediate failure mode and mostly is not the direct cause of the ultimate

failure. On the contrary, delamination can lead the ultimate failure by totally separating subsequent composite plies.

A custom design test by the choice of $(0_m/90_n)_s$ with the blocks of 90° plies was studied to enforce the transverse cracking in composite laminates (Praveen and Readdy, 1998). Likewise, suppression of the matrix cracking and IFF can be assessed for by the interleaved/interlayered variations of $(0_m/90_n)_s$ as proposed here. Detailed investigation through this experiment design and the effect of nanofibrous interlayers on transverse matrix cracking is used as an example case to show crack suppression achieved through electrospun nanofibrous interlayers.

2.6. How Mechanism Works?

Under various loading conditions the toughening of interlaminar regions mainly works against extensive matrix cracking and delaminations which can cause pre-mature failure of the composite laminates. Transverse matrix cracking in the unidirectional composite materials, for instance may arise within the individual plies or ply blocks (Johnson and Chang, 2011a, 2011b) where the stresses transverse to their fiber orientation are critical for the given loading conditions. Also interlaminar stresses at the interface of the adjacent plies due to the Poisson mismatch and mechanical anisotropy, and presence of the edge stresses or stress raisers such as joints (Shivakumar and Panduranga, 2013) are potential reasons for failure mechanisms.

Depending on the lamination sequence and loading conditions, the matrix cracks inside the laminate can cause a ply-by-ply failure, can induce both internal and edge delaminations and eventually facilitate fiber breakage by diminishing the effective load transfer between plies (Johnson and Chang, 2011a, 2011b). In that regard, the matrix cracking is an intermediate failure mode and mostly is not the direct cause of the ultimate

failure. On the contrary, delamination can lead the ultimate failure by totally separating subsequent composite plies.

A custom design test by the choice of $(0_m/90_n)_s$ with the blocks of 90° plies was studied to enforce the transverse cracking in composite laminates (Praveen and Readdy, 1998). Likewise, suppression of the matrix cracking and IFF can be assessed for by the interleaved/interlayered variations of $(0_m/90_n)_s$ as proposed here. Detailed investigation through this experiment design and the effect of nanofibrous interlayers on transverse matrix cracking is used as an example case to show crack suppression achieved through electrospun nanofibrous interlayers.

Custom Matrix Cracking Test and Sound Assisted Failure Analysis for Nanofibrous Toughening Mechanism

A simple and yet effective way to detect the matrix cracking is also exemplified as uniaxial tension tests of custom select laminate. The interlayer(s) are incorporated at various positions through the thickness to correlate the toughening strategy. The base or reference laminate is $(0_2/90_4)_s$. Interleaving levels or cases are selected as $(0_2/90_4/I)_s$ where only midplane is toughened, $(0_2/90_2/I/90_2/I)_s$ with three interlayers between the blocks of two 90° plies and $(0_2/90/I/90/I/90/I/90/I)_s$ with seven interlayers between each 90° plies.

An efficient way of characterizing crack initiation and progression is to capture their acoustic signatures during the mechanical testing. The specimens are accompanied by a noise reducing microphone in order to capture the occurrence of minor and major cracks inside the laminates during the loading as each discrete, mostly invisible series of cracking events generate sounds. All of the recordings are started

in sync with the loading of the mechanical test (For details of sound assited failure analysis please find paper 1.1 [2] attached as appendix to this chapter.
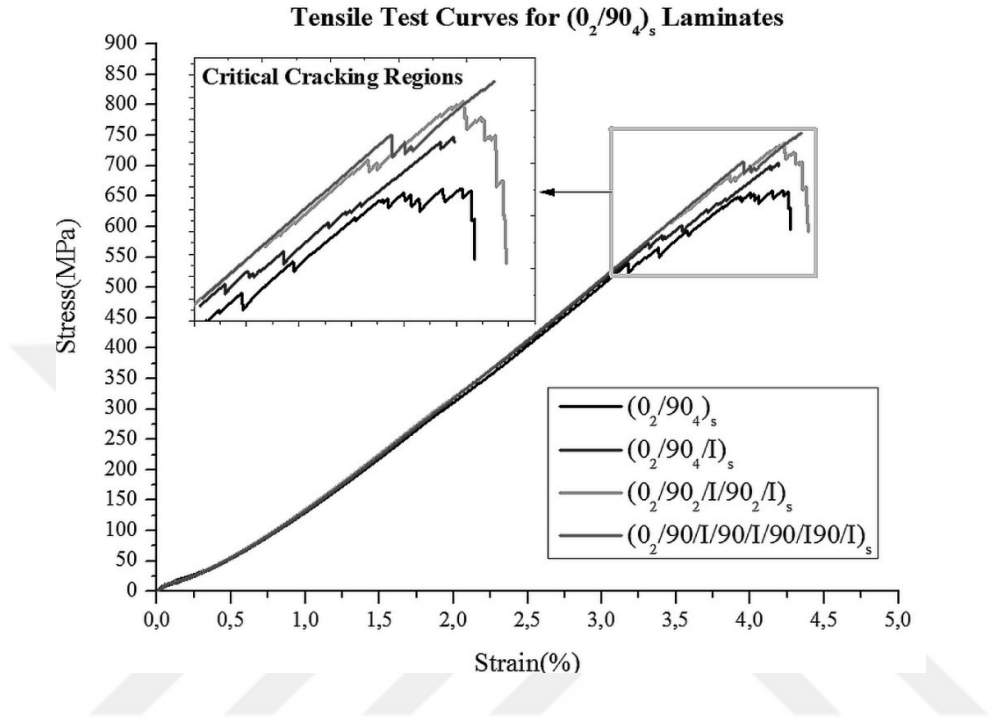
Figure 7: Tensile test results for custom matrix cracking test with $(0_2/90_4)_s$ laminates

Figure 7 corresponds to the representative stress-strain curves of the neat and interalyered/interleaved $(0_2/90_4)_s$ laminates where critical matrix cracking segments are also zoomed in. Test curves and observations suggested that the visible and degrading cracks of the custom select family of laminates occur progressively in the matrix until an ultimate catastrophic failure. Zoomed-in view to the critical matrix cracking segments shows that the critical transverse major matrix cracking in the neat laminates begins earlier than the interlayered counterparts. The resistance against transverse matrix cracking clearly increases with the addition and distribution of the electrospun interlayers. The laminate with the most dispersed interlayers nearly eliminated the damage progression and resulted in the highest

ultimate strength.
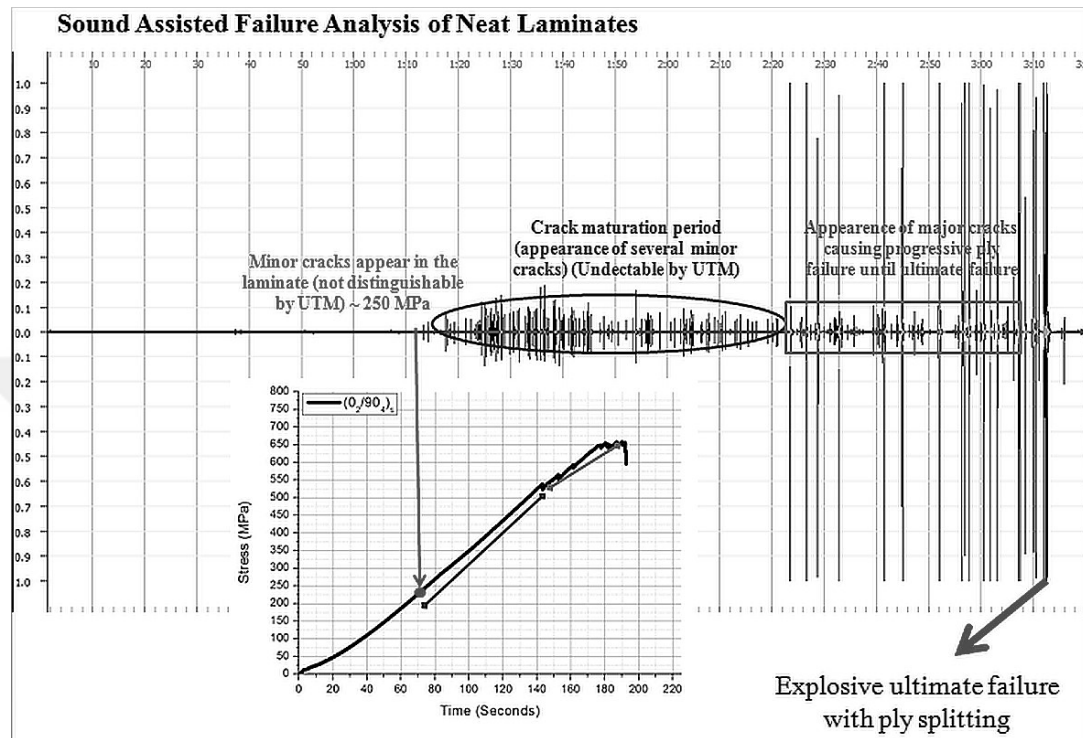
Figure 8: Sound spectrum corresponding to the tension test of neat $(0_2/90_4)_s$ laminates

Supportive evidence of improved cracking and failure behavior can be sought by the assistance of captured acoustic signatures. Figure 8 corresponds to the sound spectra of the neat laminate recorded during the mechanical tests. In correspondence with the previous discussions, discrete sound peaks are associated with the minor cracking inside the 90^0 ply blocks and are observed around 250 MPa (at an early stage of the test). As the load is increased such micro-cracks propagate through the 90^0 block thickness. Further load ramp-up induces multiple of such through-the-thickness cracks (IFF) and causes crack density to increase until the ultimate fracture is observed. Sound spectrum suggested that maturity and multiplication of internal

cracks seem to continue until around 550 MPa. After this maturity period critical or major cracks causing the failure of overall 90° blocks are correlated with higher amplitude peaks in the sound spectrum. This region exactly coincides with the observed load drops in figure 8. The load drops signify that a major crack was able to move between 90° plies and caused the localized whole block failure. After this block failure, stress is redistributed over the laminate and it can continue to carry loads until another major crack travels the whole ply blocks at another location. This process continues till the catastrophic ultimate failure which is differentiated by bold and high amplitude peak at the end of the test.

In $(0_2/90_4/I)_s$ case the first sound pick-up occurred at around 250 MPa as in the neat specimen test (Figure 9). This is again attributed to the initiation of minor cracks in 90° plies. However for this case the crack maturity and multiplication phase continued till around 560 MPa thanks to the interlayer addition in the midplane which suppressed the critical crack formation. Also both stress-strain curves and higher amplitude sound peaks suggest an increase of 6% in the ultimate tensile strength of laminates at a lower crack density (Table 3).
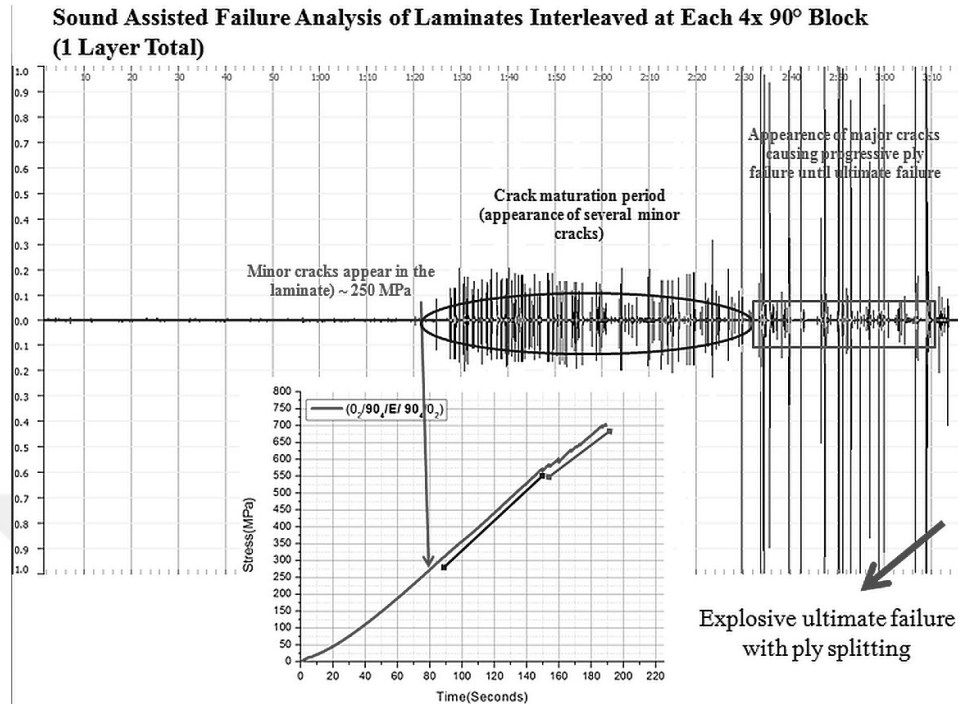
Figure 9: Sound spectrum corresponding to the tension test of interlayered $(0_2/90_4/I)_s$ laminates

For $(0_2/90_2/I/90_2/I)_s$ case minor crack initiation stress did not change. However, the interlayer addition for this case significantly delayed the occurrence of the major cracks and extended the crack maturity process upto around 680 MPa. Sound spectrum (Figure 10) and significant load drops in the stress-strain curve suggest that the number of critical major cracks were reduced. Hence, the ultimate failure stress was about 10% higher than the neat laminate result.
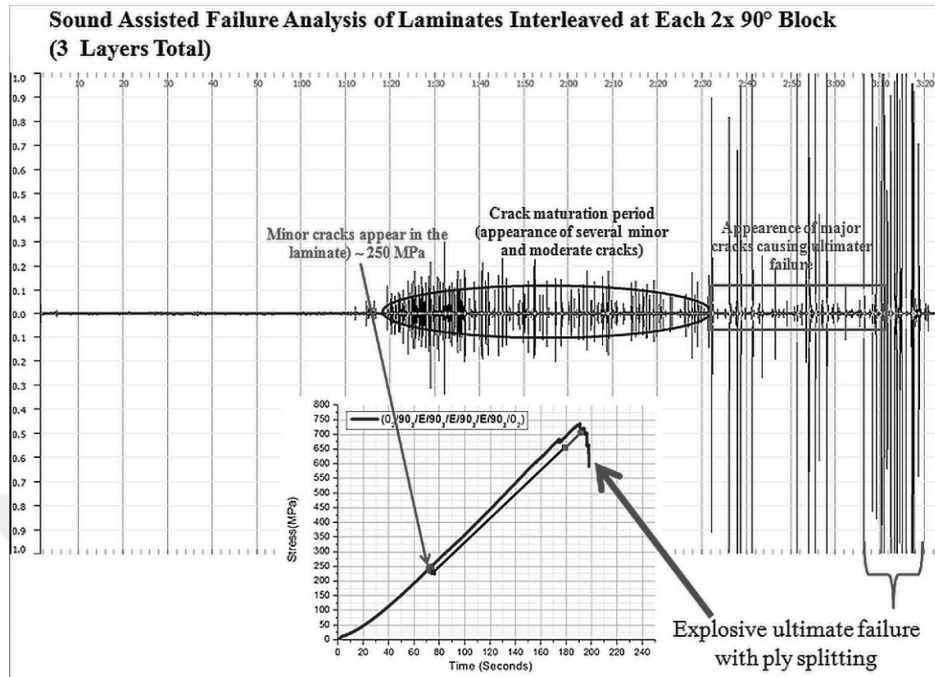
Figure 10: Sound spectrum corresponding to the tension test of interlayered $(0_2/90_2/I/90_2/I)_s$ laminates

In the final case with $(0_2/90/I/90/I/90/I)_s$ of 7 interlayers (between each 90° ply), the minor crack initiation again began at around 250 MPa whereas the crack maturity period was the longest. Hence critical matrix cracking was mostly avoided up until 700 MPa (Figure 11). In addition, the occurrence of load drops associated with the ply degradation was minimized and ultimate failure stress is up to 15% higher than the neat laminates.
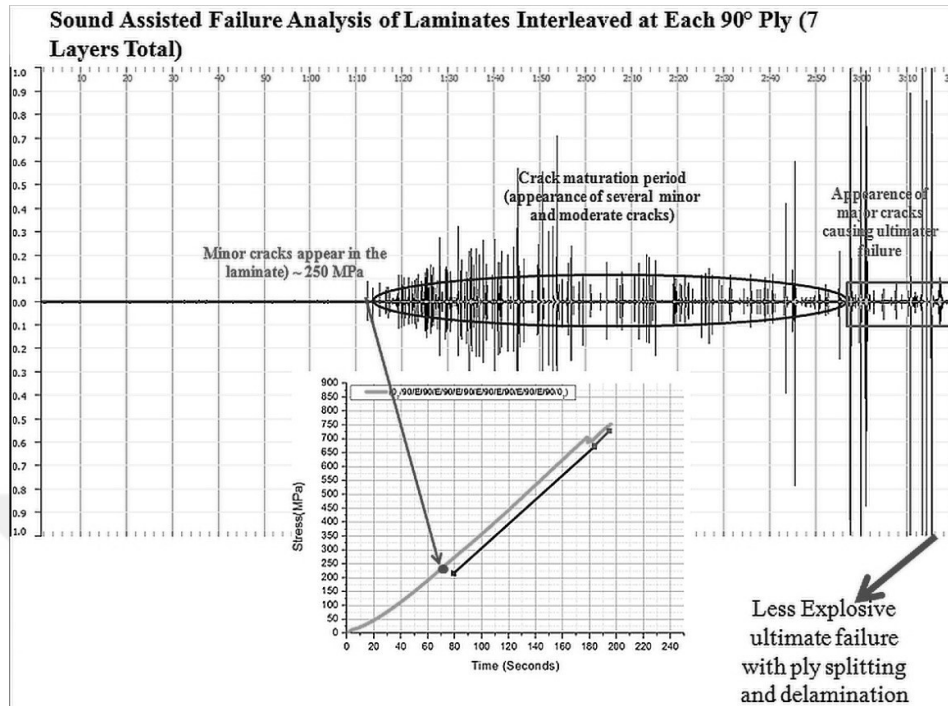
Figure 11: Sound spectrum corresponding to the tension test of interlayered $(0_2/90/I/90/I/90/I/90/I)_s$ laminates

This set of experiments on the interlayer toughening by the electrospun nanofibrous interleafs and the sound pick-up assisted failure analysis suggest the following:

- Presence of the nanofibrous interlayers does not seem to affect the initiation of minor-crack formations inside the 90° plies.

- Their main role is to suppress micro cracks, i.e. delay/avoid the growth and crossing through the interlaminar planes that can cause the ply block transverse failure (degradation). Hence their presence constrains the occurrence or growth of the major/critical cracks inside the laminates.

- The evaluation of crack progress inside a laminate can easily be spotted and recognized through a simple synchronous sound recording and its post-processing.

2.7 Changes in Mechanical Behavior

47

This section is to provide the supporting evidence for the toughening and mechanical behavior enhancement in the presence of nanofibrous interlayers/interleaves. For consistency with the earlier examples of materials&synthesis, processing and manufacturing sections, the mechanical property improvements achieved through the application of P(St-co-GMA) nanofibers are discussed. The resistance against transverse matrix cracking and delamination are explored as the primary interlayer toughening issues subject to in-plane and out of plane loading conditions. For the tests of out of plane loading conditions, addition of 1wt% of MWCNTs and case study of P(St-co-GMA)/MWCNT composite nanofibers are also provided.

Table 3: Mechanical property improvements for nanofiber interlayered composites

Test Type	Lay-up Sequence	Interlayer Type	Interlayered Sequence	Target Property	Neat	Interlayered
Custom Matrix Cracking	$(0_2/90_4)_s$	P(St-co-GMA)	$(0_2/90_4/I)_s$ $(0_2/90_2/I/90_2/I)_s$ $(0_2/90/I/90/I/90/I)_s$	Tensile Strength (MPa)	645±14	696±28 737±5 757±4
Transverse Tension	$(90)_6$	P(St-co-GMA)	$(90/I)_6$	Transverse Tensile Strength (MPa)	26,5±0,7	31,2±0,6
		P(St-co-GMA)/ MWCNT				33,6±0,7
3-point Bending	(0/0/0)	P(St-co-GMA)	(0/I/0/I/0)	Flexural Strength (MPa)	875±16	965±17
		P(St-co-GMA)/ MWCNT				1002±14
	(90/0/90)	P(St-co-GMA)	(90/I/90/I/90)		243±6	282±9
		P(St-co-GMA)/ MWCNT				296±6
End Notched Flexure	$(0)_4$	P(St-co-GMA)	(0/0/I/0/0) (only ahead of crack tip on midplane)	G_{IIc} (kJ/m^2)	0,95 ±0.03	1,47±0,04
		P(St-co-GMA)/ MWCNT				1,6±0,1

2.7.1 Improvements Under Out-of-Plane Loading

2.7.1.1 Three Point Bending Tests

Comparison of three point bending tests on laminates with and without fibrous interlayers showed that their addition led to increase in both flexural strength and modulus of the samples. The nanofibrous interlayers (denoted by I) within the laminates (0/I/0/I/0) resulted in 10% increase in the flexural strength (Table 3). Introduction of the nanotubes by 1% weight to the copolymer fibers led to a further improvement adding up to 15% increase in flexural strength compared to results without nanocomposite interlayers incorporated. Comparing (90/ 0/90) vs. (90/I/0/I/90) laminates, P(St-co-GMA) nanofibrous interlayers increased both the flexural strength of the samples by 16%. The increase in these values were 22% with P(St-co-GMA)/MWCNT interlayers. Post-failure SEM analyses on cross section of the specimens revealed that the lamination sequence was a factor in the fracture mode. Two distinct active failure mechanisms, transverse matrix cracking and/or delamination, were observed in (0/0/0) laminates (Figure 12). Co-existence of the two failure mechanisms on the samples is attributed to the inability of the three point bending test to create pure shear conditions.

An example is shown in the SEM image of a (0/0) interface represented in Fig. 15a where the two corresponding mechanisms were indicated with arrows (1: transverse matrix cracking and 2: delamination). Oblique intra-ply damage (Knops, 2008) initiated at the end of delamination growth occurred due to the presence of high stress regions at the contact of the loading tip. The flexural strength and modulus increase reported by the three-point bending tests characterized both delamination resistance and matrix

toughening introduced by the addition of the interlayer. This double effect of the interlayer was also studied and introduced by Sihn et al., 2008.
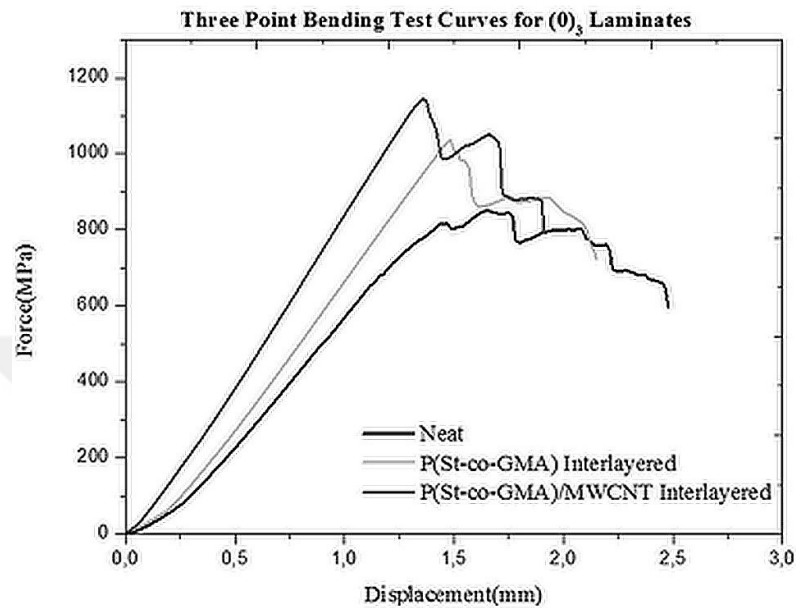
Figure 12: Representative 3-point bending curves for (0/0/0) laminates

With (90/0/90) lamination sequence, fracture mechanism was driven by 90° plies. The presence of 90 plies at the outer surface ensured the interlaminar stresses at 90/0 interface due to the stiffness mismatch. In addition the inherent weak links of 90° plies to tensile loads triggered a matrix crack induced failure on the bottom ply during bending loading (figure14). Figure 13 hows the representative flexural force–displacement curves of the specimens with and without nanofibrous interlayers/interleafs. The initial load drop corresponds to the first ply failure due to the critical matrix cracking on the bottom 90° ply subjected to tension. Note that the local matrix failure did not cause the ultimate failure. Instead a stable crack growth characterized by the load drops was observed and the final fracture occurred when 90 (degraded)/0 interface progressed to delamination. Hence the overall flexural performance was governed by two major failure mechanisms.
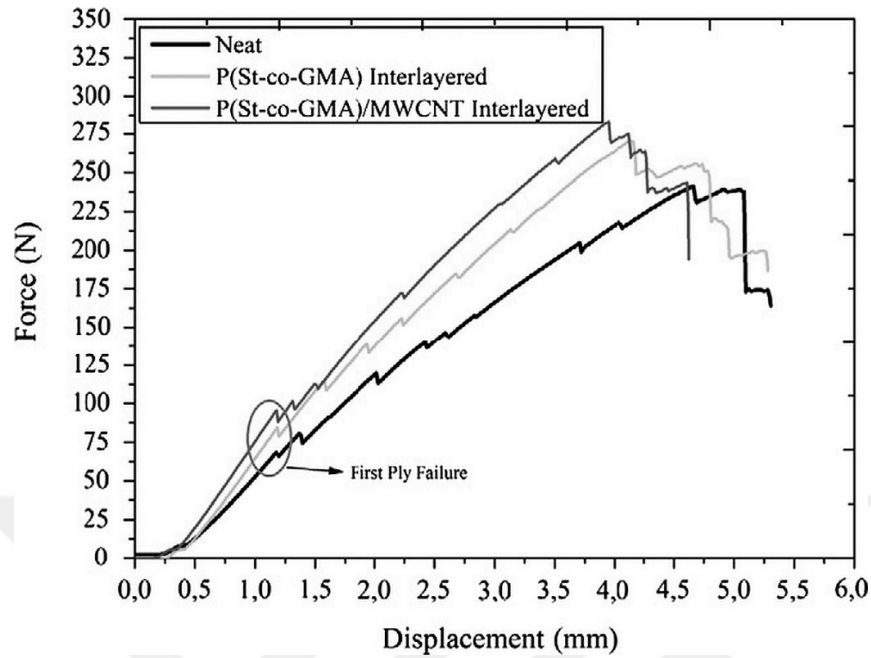
Figure 13: Representative 3-point bending curves for (90/0/90) laminates

The increased resistance against initial matrix cracking may be noted by comparing the first ply failure loads whereas the delamination resistance of laminates may be compared byhe ultimate load values. It is clearly visible from Fig. 14 that the interlayer addition worked well for both mechanisms as it was suggested for (0/0/0) laminates.
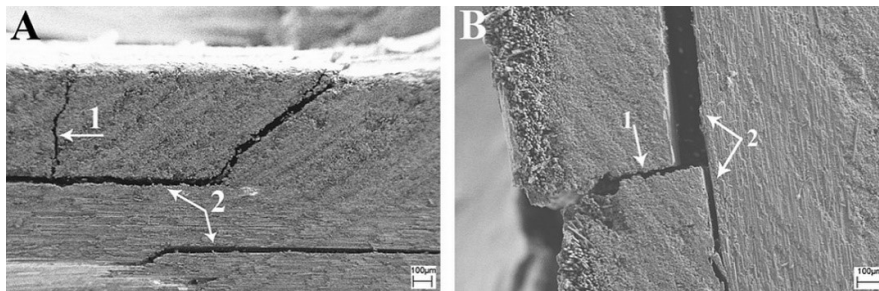
Figure 14: Cross-sectional view of fractured three point specimens. (a) (0/0/0) and (b) (90/0/90).

2.7.1.2 End Notched Flexure Tests

P(St-co-GMA) interlayer presence at the pre-crack tip increased G_{IIC} by 55% (Table 3). Further increase up to 70% in G_{IIC} by P(St-co-GMA)/MWCNTs interlayers suggests that the toughening is also correlated with the incorporation of the MWCNTs on electrospun fiber surfaces.
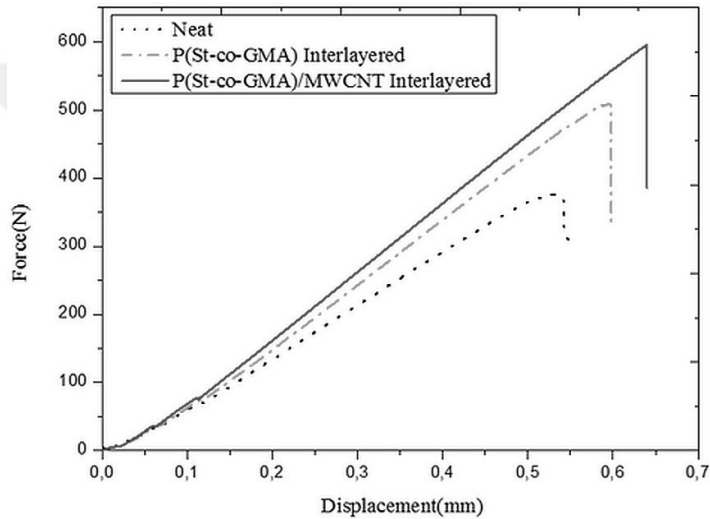
Figure 15: Representative end-notched flexure test for (0/0/0/0) laminates with interlayers located midplane ahead of the crack tip on the midplane

Failure of ENF specimens was observed as dominated by unstable crack growth parallel to the interlaminar plane with a sudden load drop (Figure 15). Formation of an unstable crack growth can be considered as an inherent characteristic in the testing of UD laminates under ENF test configurations with constant displacement rate (Stevanovic et. al, 2003). Further analysis of the fracture surfaces also suggested that the increase observed in G_{IIC} was directly associated with the active role of interlayers on the fracture resistance.

Common hackle patterns typically due to the micro-crack coalescence (Seyhan et. al, 2008) all along the crack pathway are clearly visible on specimens without the nanocomposite interlayers (Figure 16a). Whereas the hackle patterns for the interlayered specimens are either locally altered and replaced by a more complex structure or enlarged in size (Figure 16b). A different fracture mode was noted as the capillary-like damage marks indicated in figure 16c. These damage marks were observed both in the areas consisting of epoxy-interlayer complex (left and right arrows) and around carbon fibers (center arrow) that is surrounded by epoxy-interlayer complex (Figure 16d). Close examination of the fracture pattern seen in Figure 16d revealed the presence of micro-crack formation through the interlayer–epoxy complex. This observation can be further supported by the cut-like damage marks inside of the interlayer–epoxy complex for which a zoomed-in image is shown in figure 16e. Furthermore, the epoxy matrix and interlayers were not separated with a distinct interface, which was consistent with the structure shown in figure 6c (image taken on the ply).
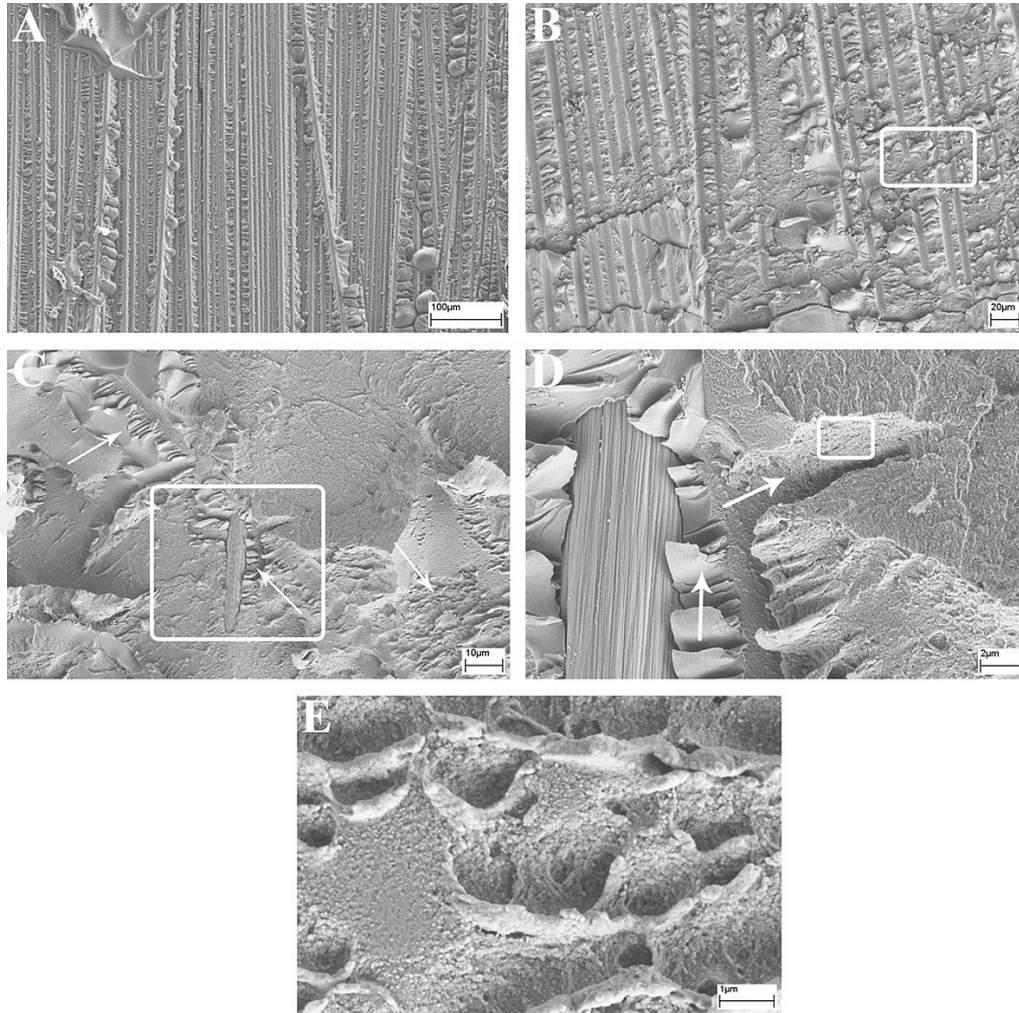
Figure 16: Fracture surfaces of (a) neat epoxy ply-to-ply interface (b) P(St-co-GMA)/MWCNT interlayered interface. Zoomed in views for (c) encircled area in (b). Arrows: the distinguishable damage marks (d) encircled area in (c), arrows: two distinct failure regions (carbon fiber interface and through interlayer/epoxy complex). (e) Encircled area in (d). Damage marks on interlayer/epoxy complex.

2.8 Applications and Future Trends

Nanofibrous interlayers may find extensive use in nearly all light-weight structural applications, where advanced composites are necessary, such as in aerospace, automotive and energy. They can be easily incorporated into existing manufacturing processes and provide substantially enhanced properties, while the weight and thickness increase associated with interleaving is nearly negligible. Additionally, as also exemplified here with the possibilities for combining the right selection of particles/fillers, the toughening performance can be further enhanced for both in- and out-of-plane loading conditions. Moreover, their full potential is even higher with multi-functional possibilities, such as tuning of mechanical, thermal and electrical properties by the right choices of nanofiber and filler combinations and proportions. With a complete understanding of impact on properties by using the nanofibrous interlayers, the opportunities are plentiful for developing characterization and scaled-up production capabilities and integration of the nanofibrous materials into conventional composite engineering design frameworks.

In regard to high potential of nanofibrous interlayer strategy, some of the key issues to address and intriguing research fronts to pursue may be noted as follows:

- Effective and safe-to-use, but scaled-up production capabilities incorporating emerging nanotechnology.

- Establishing the value-chain and materials supply for the industrial scale use

- Ability to tailor nanostructures and nanofiber morphology along with the nanofiller interactions for optimal benefits and multifunctionality

- New and direct characterization strategies for the nanofiber/filler properties, and their interface with the hosting matrix material

- Fractographic analysis and better understanding of the governing failure mechanisms of the nano-macro-scale interaction in composite applications.

- Multi-scale modeling strategies correlating well with the experimental development.

2.9 References in Alphabetic Order

Bilge, K., Ozden-Yenigun, E., Menceloglu, Y.Z., Papila, M. (2012) "Structural composites hybridized with epoxy compatible polymer/MWCNT nanofibrous interlayers", Composites Science and Technology, 72, 1639-1645.

Bilge, K., Venkataraman, S., Menceloglu, Y.Z., Papila, M. (2014) " Global and local nanofibrous interlayer toughened composites for higher in-plane strength", Composites Part A, 58,73-76.

Braun, D., Cherdon, H., Rehahn, M., Ritter, H., Voit, B. (2013), " Polymer Synthesis, Theory and Practice", 5th edition, Springer

Carlsson, A., Aksoy, A. (1991), "Analysis of interleaved end-notched flexure specimen for measuring mode II fracture toughness", International Journal of Fracture, 52(1),67-77

Carlsson, A., Aksoy, A. (1992), " Interlaminar shear fracture of interleaved graphite/epoxy composites", Composites Science and Technology, 43(1),55-69

Chen, Q., Zhang, L., Rahman, A., Zhou, Z., Wu, X.F., Fong, H. (2011), "Hybrid multi-scale epoxy composite made of conventional carbon fiber fabrics with interlaminar regions containing electrospun carbon nanofiber mats", Composites Part A, 42(12),2036-2042.

Coleman, J.N.N (2006), "Small but strong, a review of the mechanical properties of carbon nanotube-polymer composites" Carbon, 44,1624–1652.

Duarte, A., Hersxbewrg, I., Paton, R. (1999),"Impact resistance and tolerance of interleaved tape laminates", Composite Structures, 47(1-4),753-758

Dzenis, Y., Reneker, D. H.(2001), "Delamination resistant composites prepared by small diameter fiber reinforcement at ply interfaces." USPATENT 626533

Dzenis, Y. (2008), "Structural Nanocomposites", Science, 319(5862),419-420.
Feng, X.J., Jiang, L. (2006), "Design and creation of super wetting/anti wetting surfaces.", Advanced Mater,18(23), 3063–78.

Garcia. E.J., Wardle, B.L., Hart, A.J. (2008), "Joining prepreg composite interfaces with aligned carbon nanotubes", Composites, Part A, 39,1065–1070.

Gu, S.Y., Ren, J., Vansco, G.J. (2005a), "Process optimization and empirical modeling for electrospun polyacrylonitrile (PAN) nanofiber precursor of carbon nanofibers", European Polymer Journal, 41(11), 2559-2568.

Gu, S.Y., Ren, J., Wu, Q.L. (2005a), "Preparation and structures of electrospun PAN nanofibers as a precursor of carbon nanofibers", Synthetic Metals,155(1),157-161.

Hatada, K., Kitayama, T. (2004), "NMR Spectroscopy of Polymers", 7th edition, Springer Laboratory.

Heijden, S.V.D, Daelemans, L., Schoenmaker, B.D., Baere, I.D., Rahier, H., Paepegem, W.V., Clerck, K.D . (2014), "Interlaminar toughening of resin transfer moulded glass fibre epoxy laminates by polycaprolactone electrospun nanofibres", Composites Science and Technology, 10,66-73.

Hojo, M., Matsuda, S., Tanaka, M., Ochiai, S., Murakami, A. (2006), "Mode I delamination fatigue properties of interlayer toughened CF/epoxy laminates" , Composites Science and Technology, 66(5) , 665-675.

Hossain, M.K., Hossain, M.E., Dewan, M.W., Hosur, M., Jeelani. S. (2013), "Effects of carbon nanofibers (CNFs) on thermal and interlaminar shear responses of E-glass/polyester composites", Composites Part B, 44(1), 313-320.

Huang ,Y., Horn, J. (1998) , " Effects of thermoplastic additives on mechanical properties and glass transition temperatures for styrene-crosslinked low-shrink polyestermatrices", Polymer, 39(16),3683-3695.

Huang, Z.M., Zhang, Y.Z., Kotaki, M., Ramakrishna,S. (2003), " A review on polymer nanofibers by electrospinning and their applications in nanocomposites", Composites Science and Technology, 63,2223-2253

Ishai, O., Rosenthal, H., Sela, N., Drukker, E. (1988), " Effec of selective adhesive interleaving on interlaminar fracture of graphite/epoxy laminates", Composites, 19(1),49-54

Jiang,W., Tjon ,S.C., Chu, P.K., Li, R.K.Y. (2001), " Interlaminar fracture properties of Carbon Fibre/Epoxy Matrix Composites Interleaved with Polyethylene Terephtalate (PET) Films", Polymers & Polymer Composites, 9(2) ,141-145

Johnson, P., Chang F-K. (2001a), "Characterization of Matrix Crack-Induced Laminate Failure—Part I: Experiments", Journal of Composite Materials, 35, 2009-2035.

Johnson, P., Chang F-K. (2001b), "Characterization of Matrix Crack-Induced Laminate Failure—Part II: Analysis and Verifications", Journal of Composite Materials, 35, 2037-2074.

Khan, S.U., Kim, J.K. (2011), "Impact and Delamination Failure of Multiscale Carbon Nanotube-Fiber Reinforced Polymer Composites, A Review", International Journal of Aeronautical & Space Science, 12(2), 115-133

Khan, S.U., Kim, J.K. (2012), "Improved interlaminar shear properties of multiscale carbon fiber composites with bucky paper interleaves made from carbon nanofibers", Carbon , 50(14),5265-5277

Kim, J.S.,Reneker, D.H. (1999), "Mechanical properties of composites using ultra fine electrospun fibers", Polym Compos, 20(1), 124–131

Knops, M. (2008), "Analysis of Failure in Fiber Polymer Laminates", Springer.

Koenig, J.L. (2005), "Spectroscopy, NMR, Fluorescence, FT-IR", Advances in Polymer Science, 54(1984),87-154.

Lee, S.H., Lee, J.H., Cheong, S.K., Noguchi, H. (2008), "A toughening and strengthening technique of hybrid composites with non-woven tissue", Journal of Materials Processing Technology,207(1-3),21–9

Lee, S.H., Noguchi, H., Kim, Y.B., Cheong, S.K. (2002), "Effect of interleaved non woven carbon tissue on interlaminar fracture toughness of laminated composites, Part 1,mode II", Journal of Composite Materials, 36(18),2153-68.

 Li, L., Lee-Sullivan, P., Liew, K.M. (1996), "The Influence of Thermoplastic Film Interleaving on the Interlaminar Shear Strength and Mode I Fracture of Laminated Composites", J.Eng.Mater.Technol, 118(3), 302-309.

Li, P., Liu, D., Zhu, B., Li, B., Xiaolong, J., Wang, L., Li, G., Yang, X. (2015), "Synchronous effects of multiscale reinforced and toughened CFRP composites by MWNTs-EP/PSF hybrid nanofibers with preferred orientation", Composites Part A, 68,72-80.

Liu,. L., Huang, Z.M., He, C., Han, X.(2006), " Mechanical performance of laminated composites incorporated with nanofibrous membranes", Materials Science and Engineering, 435-436 (0), 309-17

Liu, L., Zhang, H., Zhou, Y. (2014), "Quasi-static mechanical response and corresponding analytical model of laminates incorporating with nanoweb interlayers", Composite Structures, 11,436-445.

Liu, J., Gao, Y., Cao, D., Zhang, L., Guo, Z. (2011) , "Nanoparticle Dispersion and Aggregation in Polymer Nanocomposites, Insights from Molecular Dynamics Simulation", *Langmuir*, *27*(12), 7926–7933

Liu, L., Huang, Z.M., Xu, G.Y., Liang, Y.M., Dong, G.H. (2008), "Mode II interlaminar delamination of composite laminates incorporating with polymer ultra thin fibers", ,29(3),285-92

Magniez, K., Chaffraix, T., Fox, B. (2011), "Toughening of a Carbon-Fibre Composite Using Electrospun Poly(Hydroxyether of Bisphenol A) Nanofibrous Membranes Through Inverse Phasen Separation and Inter-Domain Etherification", Materials, 4,1967-1984.

Masters, J.E. (1989), "Improved Impact and Delamination Resistance Through Interleafing", Key Engineering Materials, 37,317-0

Matsuda, S., Hojo, M., Ochiai, S., Murakami, A., Akimoto, H., Ando, M. (1999), "Effect of ionomer thickness on mode I interlaminar fracture toughness for ionomer toughened CFRP", Compos Part A ,30,1311–1319.

Moore, J.C. (1964), " Gel permeation chromatography. I. A new method for molecular weight distrubution of high polymers", Journal of Polymer Science Part A, General Paper, 2(2),835-843
.
Nuhiji, B., Attard, D., Thorogood, G., Hanley, T., Magniez, K., Fox, B. (2011), " The effect of alternate heating rates during cure on the structure–property relationships of epoxy/MMT clay nanocomposites", Composites Science and Technology, 71(15), 1761-1768.

Ozden, E., Menceloglu, Y.Z., Papila, M. (2010), "Engineering chemistry of electrospun nanofibers and interfaces in nanocomposites for superior mechanical properties", ACS Appl Mater Interfaces,1788-93.

Ozden, E., Menceloglu, Y.Z., Papila, M. (2011), "MWCNTs/P(St-co-GMA) composite nanofibers of engineered interface chemistry for epoxy matrix nanocomposites", ACS Appl Mater Interfaces 4(2),777-84.

Ozdil, F., Carlsson, A. (1992), "Mode I Interlaminar Fracture of Interleaved Graphite/Epoxy", Journal of Composite Materials, 26(3),432-459.

Palmeri,. M.J., Putz, K.W., Ramanathan, T., Brinson, L.C. (2011), "Multi-scale reinforcement of CFRPs using carbon nanofibers", Composites Science and Technology, 71(2),79-86.

Pham, S., Burchill, P. (1995), "Toughening of vinyl ester resins with modified polybutadienes" , Polymer, 36(17) , 3279–3285

Praveen,G.N, Reddy,J.N. (1998), "Transverse matrix cracks in cross-ply laminates: stress transfer, stiffness reduction, crack opening profiles", Acta Mechanica, 130, 227-248.

Qian, H., Greenhalgh, E.S., Shaffer, M.S.P., Bismarck (2010), "A. Carbon nanotube-based hierarchical composites, a review." J Mater Chem, 20(23), 4751–62.

Rodriguez, A.J., Guzman, M.E., Lim, C.S., Minaie, B. (2011), "Mechanical properties of carbon nanofiber/fiber-reinforced hierarchical polymer composites manufactured with multiscale-reinforcement fabrics", Carbon, 49(3),937-948.

Sadeghian, R., Gangireddy, S., Minaie, B., Hsiaio, K. (2006), "Manufacturing carbon nanofibers toughened polyester/glass fiber composites using vacuum assisted resin transfer molding for enhancing the mode-I delamination resistance", Composites Part A, 37(10),1787-1795.

Schartl, W. (2007), " Light Scattering Polymer Solutions and Nanoparticle Dispersions", Springer Laboratory.

Sela, N., Ishai, O. (1989), "Interlaminar fracture toughness and toughening of laminated composite materials, a review", Composites, 20(5), 423–435.

Seyhan, A.T., Tanoglu, M., Schulte, K. (2008), "Mode I and Mode II fracture toughness of eglass non-crimp fabric/carbon nanotube (CNT) modified polymer based composites", Eng Fract Mech,75(18),5151–62.

Shivakumar, K., Panduranga, R. (2013), "Interleaved polymer matrix composites, A review", 54th AIAA/ASME/ASCE/AHS/ASC Structures, Structural Dynamics, and Materials Conference, April 8-11, Boston, Massachusetts

Sihn, S., Kim, R.Y., Huh, W., Lee, K.H., Roy A,K. (2008) "Improvement of damage resistance in laminated composites with electrospun nano-interlayers." Compos Sci Technol ,68(3–4),673–83.

Sohn, M.S., Hu, X.Z., Kim, J.K., Walker, L. (2000), " Impoact damage chracterisation of carbon/fibre epoxy composites with multi-layer reinforcement", Composites Part B, Engineering, 31(8),681-691

Stevanovic, D., Kalyanasundaram, S., Lowe, A., Jar, P.Y. (2003), "Mode I and Mode II delamination properties of glass/vinyl-ester composite toughened by particulate modified interlayers", Compos Sci Technol,63(13),1949–64.

Subagia, I.D.G., Jiang, Z., Tijing, L.D., Kim, Y., Kim, C.S., Lim, J.K. (2014), "Hybrid multi-scale basalt fiber-epoxy composite laminate reinforced with Electrospun polyurethane nanofibers containing carbon nanotubes", Fibers and Polymers, 15(6),1295-1302.

Sun, L., Warren, G.L., Sue, H.J. (2010), " Partially cured epoxy/SWCNT thin films for the reinforcement of vacuum-assisted resin-transfer-molded composites", Carbon, 48(8),2364-2367

Tsotsis,T.K. (2009) , "Interlayer toughening of composite materials", Polym Compos ,30(1), 70-86

Veedu, V.P., Cao ,A., Li, X., Ma, K., Soldano, C., Kar, S., Ajayan, P.M., Ghasemi-Nejhad, M.N. (2006), "Multifunctional composites using reinforced laminae with carbon-nanotube forests", Nature Materials, 5,457-462.

Warrior, N.A., Turner, T.A., Robitaille, F., Rudd, C.D. (2004), "The effect of interlaminar toughening strategies on the energy absorption of composite tubes", Composites, Part A , 35,431–437.

Wang, Y., Serrano, S., Santiago-Avilles, J.J. (2003), "Raman characterization of carbon nanofibers prepared using electrospinning", Synthetic Metals, 138(3),423-427.

Wendorff, J.H., Agarwal, S., Greiner, A. (2012) "Electrospinning, Materials, Processing, and Applications", Wiley.

White, K.L., Sue, H.J. (2012), "Delamination toughness of fiber-reinforced composites containing a carbon nanotube/polymamide-12 epoxy thin film interlayer", Polymer, 53(1),37-42.

Wilkinson, S.P., Ward, T.C., McGrath, J.E. (1993),"Effect of thermoplastic modifier variables on toughening a bismaleimide matrix resin for high-performance composite materials", Polymer, 34(4), 870–884

Xuefeng, A.N., Shuangying, J.I., Bangming, T., Zilong, Z., Xiao-Su, Y. (2002), "Toughness improvement of carbon laminates by periodic interleaving thin thermoplastic films", Journal of Materials Science Letters, 21(22),1763-1765.

Yasaee, M., Bond, I.P., Trask, R.S., Greenhalgh, E.S.(2012a), " Mode I interfacial toughening through discontinous interleaves for damage suspension and control", Composites Part A, 43(1) , 198-207

Yasaee, M., Bond, I.P., Trask, R.S., Greenhalgh, E.S.(2012b) " Mode II interfacial toughening through discontinous interleaves for damage suspension and control", Composites Part A, 43(1) , 121-128

Ye,Y., Chen,H., Wu, J., Chan, C. M. (2011), "Interlaminar properties of carbon fiber composites with halloysite nanotube-toughened epoxy matrix," Composites Science and Technology, 71,717–723.

Yordem, O.S., Papila, M., Menceloglu, Y.Z. (2008), "Effects of electrospinning parameters on polyacrylonitrile nanofiber diameter, An investigation by response surface methodology", Materials & Design, 29(1),34-44.

Yudin, V.E., Svetlichnyi, V.M., Shumakov, A.N., Schechter, R., Harel, H., Marom, G. (2008), "Morphology and mechanical properties of carbon fiber reinforced composites based on semicrystalline polyimides modified by carbon nanofibers", Composites Part A, 39(1), 85-90.

Zhang,J., Lin, T., Wang, X. (2010), "Electrospun nanofibre toughened carbon/epoxy composites, Effects of polyetherketone cardo (PEK-C) nanofibre diameter and interlayer thickness", Composites Science and Technology, 70,1660-1666.

Zhang, J., Yang, T., Lin, C., Wang, C.H. (2012) "Phase morphology of nanofibre interlayers, Critical factor for toughening carbon/epoxy composites" , Composites Science and Technology, 72,256-262.

Zhou, Z., Lai, C., Zhang, L., Qian, Y., Hou, H., Reneker, D.H., Fong, H. (2009) "Development of carbon nanofibers from aligned electrospun polyacrylonitrile nanofiber bundles and characterization of their microstructural, electrical, and mechanical properties", Polymer, 50(13),2999-3006.

Zucchelli, A., Focarete, M.L., Gualandi, C., Ramakrishna, S. (2011)"Electrospun nanofibers for enhancing structural performance of composite materials. Polym Adv Technol, 22(3),339–49.

Zuchelli,A., Gualandi, C., Focarete, M.L., Donati, L., Minak, G., Ramakrishna, S. (2012), "Influence of electrospun Nylon 6,6 nanofibrous mats on the interlaminar properties of Gr-epoxy composite laminates", Composite Structures, 94(2),571-79

Zussman, E., Chen, X., Ding, W., Calabri, L., Dikin, D.A., Quintana, J.P., Ruoff, R.S. (2005), "Mechanical and structural characterization of electrospun PAN-derived carbon nanofibers", Carbon, 43(10),2175,2185

2.10 Additional Information on Sound Based Fracture Analysis

Reference (Paper B): **Bilge K.,** Yilmaz B., Papila, M. "Sound-tracking of failure events for cross-ply composite laminates under tension", Composite Structures, Volume 153, Pages 421-427, October 2016.

2.10.1 Abstract

The methodology being presented is an attempt to exemplify how a typical mechanical testing can be accompanied by easy to access, affordable pieces of equipment, but to reach a level of information substantially beyond somewhat standard practices. Fingerprints of discrete crack and damage formations during tensile testing are collected by a general purpose noise-reducing microphone in conjunction with a digital video microscope. Six cross-ply-like, specially ortohotropic laminates, $(0/90_5)_s$, $(0_3/90_3)_s$, $(0_5/90)_s$, $(0/90)_{3s}$, $(90/0)_{3s}$ and $(90_3/0_3)_s$ are studied. Mechanical test results suggest that the current methodology is able to identify progressive failure events/regimes characterized by unique audio signal profiles. Access to supplementary video and audio recordings are also provided to discuss and validate the efficiency and benefits of the proposed approach.

2.10.2 Introduction

Transverse matrix cracking can be considered as an initially minor-to-intermediate level failure mode where crack formations occur in relatively weak matrix phase [1-4]. Depending on the lamination sequence and loading conditions, formation of the transverse cracks may lead to ply-by-ply failure, induce delaminations [5-7] and eventually facilitate the progression to ultimate failure by loss of the effective load transfer between and within the plies [8-10]. Hence, real-time detection and posterior study of the formation and growth of these cracks during mechanical testing are of crucial importance to understand and better identify the progressive nature of the fiber reinforced composite materials failure [11-14]. Acoustic emission methodology should be noted as one of the established methods for real-time damage monitoring in loaded composite materials [15-19]. This method typically requires expensive instrumentation, detailed and profound data analysis along with expertise/specialization which may not be common and readily available for all composite practitioners with testing interests and needs.

An approach that is simple, affordable, easy to incorporate, yet capable of collecting useful information was exercised for this brief technical report. The set-up makes use of a general purpose noise reducing microphone. It can be attached to the specimens in order to capture the sound/acoustic signatures associated with the failure events and transmit the signal into a recording mobile device and/or computer.

Specific attention was given to family of cross-ply $(0_m/90_n)_s$ laminates where 90° ply blocks that are susceptible to transverse cracking under tension [8,9,20]. Laminates of $(0/90_5)_s$, $(0_3/90_3)_s$, $(0_5/90)_s$ stacking sequence were tested to capture the effect of different ply-to-ply load distributions changing with the repeats/blocks of 0°and 90° plies. A lay-up of dispersed ply orientations forming homogenized $(0/90)_{3s}$ laminate was also tested to demonstrate a straightforward example of the matrix crack suppression under tension. Lastly, rather unconventional/non-practical laminates of $(90/0)_3$ and $(90_3/0_3)_s$ layup

sequences were studied in order to enhance the discussion on the differences between the progressive failure on specimens of similar in-plane stiffness. Specific failure events in the damaging regimes were also observed and recorded synchronously by video capturing capable optical microscope.

2.10.3. Experimental

2.10.3.1 Specimen Manufacturing

Experimentation strategy herein implemented a test matrix using several $(0_m/90_n)_s$ laminates with m+n=6 and a relatively homogenized laminate of $(0/90)_{3s}$. Overall, four different lay-ups were studied to expedite the transverse cracking in composite laminates [8] each assuming different levels of matrix crack suppression as the 90°-ply-block thickness (n) varies. All of the composite laminates were manufactured out of unidirectional carbon fiber/epoxy prepreg provided by CMP Composites (CM-Preg–T-C- 150/ CP002 3). Two more choices of lay-ups were also included, $(90/0)_3$ and $(90_3/0_3)_s$, in order to create free surfaced matrix-cracking prone plies in the specimens.

Stacked plies of composites were vacuum bagged and hot pressed under 135^0C for 2 hours. Reported fiber volume fraction for prepreg plies were around 62%. Composite plates were cut into tensile test specimens per ASTM D3039 by a Diatrim diamond coated disc saw.

The tensile tests were carried out using Zwick Roell Z100 Universal Testing Machine with a constant cross-head displacement rate of 1 mm/min.

2.10.3.2 Sound Amplitude Based Analyses

The audio data were recorded by a noise-reducing RODE microphone which was attached to the middle of test specimen as barely touching without intruding/restraining the test procedure/specimen (figure 1).
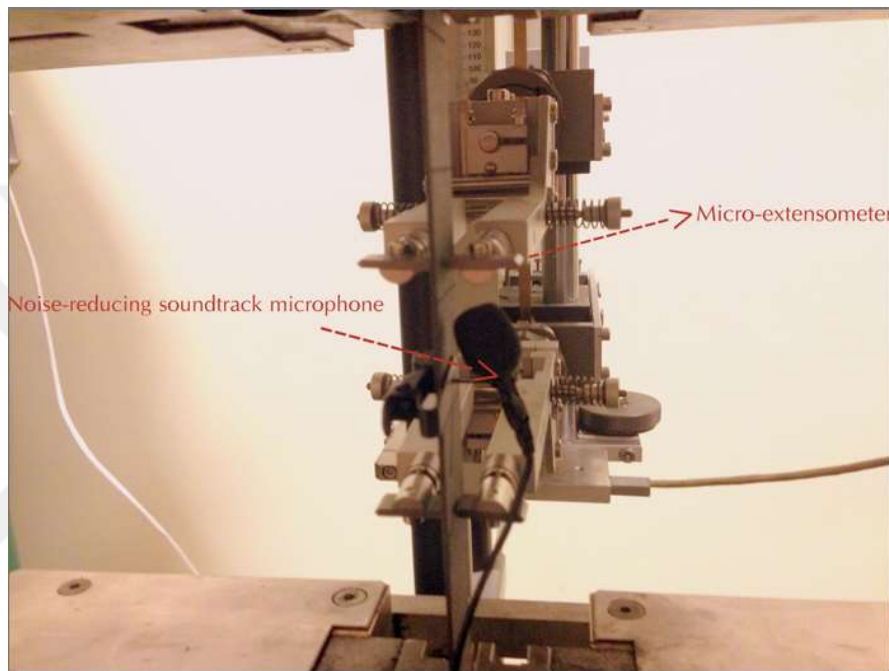
Figure 1: A view from experimental setup

The analog audio data have been digitalized with constant sample rate/frequency of f_s= 44100 Hz, which is almost standard for most general-purpose microphones. This sample frequency allows us to collect the digital sound data with the upper bound of 22050 Hz ($f_s \geq 2f_{\max}$) according to sampling theory. Since the limit of human hearing is between 20 Hz to 20 kHz, maximum frequency of the collected sound data is in limit of the human hearing.

Acquired sound or audio data were then post processed by using an open source software, Sonic Visualizer developed by Queen Mary University [21].

The normalized discrete sound peaks of the failure events reported in this work were reclaimed with Sonic Visualizer built-in acoustic analysis as the following:

For video capturing in the tensile tests, one edge of the specimens were carefully polished and the optical video microscope was located in-focus to the middle of the specimen. Sound and video recording were started in sync with the tensile loading to retrieve the exact times of cracking events and associate the stress-strain to the acoustic and visual data. The experimental procedure and audio signal discretization technique of Sonic Visualizer software is summarized in figure 2.
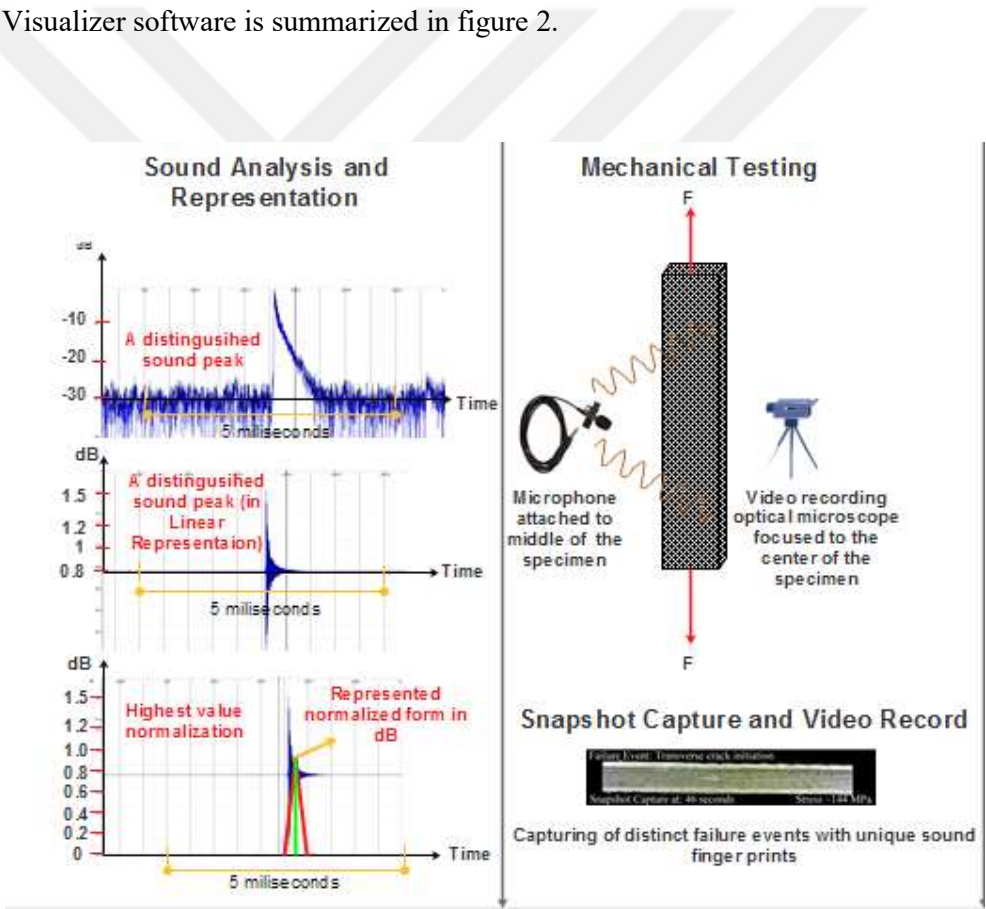
Figure 2 : Experimental procedure and sound analysis

The progressive failure observed in cross-ply laminates can be grouped into four categories by their specific acoustic signatures and crack characteristics as follows:

1- *Minor Failure Events* (⬤): The failure of cross-ply laminates is typically initiated by the transverse cracks in 90^0 plies due to lower strength and brittle nature of thermoset resins under tension [22].   These matrix dominated events are typically mode I cracks [22] and herein called the minor failure events considering their initial and not-dominating influences (presented as in Figures 2-6). They do not cause noticeable drops in typical load-deflection curves (or stress-strain data). From acoustics point of view, however these cracks generate frequent and low amplitude sound waves that can also be perceived by human ear. Depending on the laminate stacking sequence, the initiation stress of these cracks and the generated sound amplitude differs.

2- *Intermediate Failure Events* (⬛) : With increasing load, the density of the transverse matrix cracks increases along the loading axis as such potential sites for other failure modes are developed. For instance, second failure regime that can be considered as intermediate failure event typically includes the initiation of local interfacial debondings in 0/90 ply interfaces and narrow 0^0 ply strip splits due to ply interface discontinuities caused by the intensified transverse cracks. As for minor failure events, the intermediate or transitional events were not necessarily revealed by distint load drops in the typical stress/strain profile, but they typically generate a sharp and high pitched sound wave from the surface hence with higher wave amplitude as they emerged from the surface (presented as yellow squares in Figures 2-6).

3- *Major Failure Events* (▲) : Presence of the minor and intermediate failure spots in a laminate translates further into major failure events (presented as orange triangles in Figures 2). They are mostly identifiable also as load drops on the stress/strain profile. The major failure events are typically associated with the 0^0 plies They comprise severe ply splitting along the length of the specimen and extensive delaminations at the $0^0/90^0$ ply interfaces which are characteristically mode II cracks [23].   They also generate high

69

amplitude sound waves which are easily collectable/recordable using the general purpose microphone.

4- Ultimate Fracture (◆): Finally, abrupt and catastrophic failure occurs in conjunction with all the above mentioned failure modes and is marked by a broader and low pitched sound wave corresponding to simultaneously occurring of several failure events [17]

Note that the sound peaks corresponding to the failure events are already identifiable as un-processed sound wave output. However, the sound discretization by highest value transformation reported in figure 1 was performed for a better and simple representation in accordance with the stress-strain data.

2.10.4 Results and Discussion

2.10.4.1 Detection of Failure Events for $(0_m/90_n)_s$ laminates with m=1 n=5 under tension

Figure 3 reports the applied stress, audio data and several snapshots of the video captured failure events, all acquired in sync during uniaxial tensile testing of $(0/90_5)_s$ laminates. Note that the corresponding visual recording is provided as supplementary video 1. The first set of peaks on the sound data at early stages of the mechanical test suggest that initiation of minor events corresponds to stress around 75 MPa (40 seconds). The data showed the fact that laminate goes through a period of transverse matrix cracking. This period was dominated by smaller amplitude, but frequent audio peaks which are attributed to several random transverse cracks occurring in the 90°ply blocks. Also note that the initiation of these minor-cracks was not marked off as load drops in the stress-time curve, hence they are arguably undetectable by the basic and typical mechanical stress-strain test data. However, synchronous recording of acoustic signatures by the microphone effectively captured history/progress of the transverse cracking which continued till the

70

ultimate fracture. In the course of mechanical loading higher amplitude sound peaks emerged beyond 250 MPa (110 seconds). Early such highpitched sound peaks are attributed to localized/narrow 0^0 ply-strip splitting initiated from the discontinuities due to transverse matrix cracks [22]. The ply-strip splitting events occurred rather randomly in the laminate, and did not associate to any load drop mark in the stress strain curves. Exact timing of these splitting failures were also identified by following the acoustic signatures (e.g. at 122nd and 127th seconds). As the test progresses, a notable load drop occurred in the stress/strain curve which signifies a major failure event in the laminate. This failure event is captured both within the sound data profile (as a high pitch-high amplitude sound peak) and the captured video (please see supplementary information). At around 295 MPa (129 seconds); 0^0 ply split completely along the specimen length and the load was redistributed within the plies. The specimen was able to sustain increased stress till the next major failure event. The failure progression appeared to continue until the load transfer between the plies was lost and intact $0°$ plies were loaded for fiber failures resulting in an overall explosive ultimate fracture.
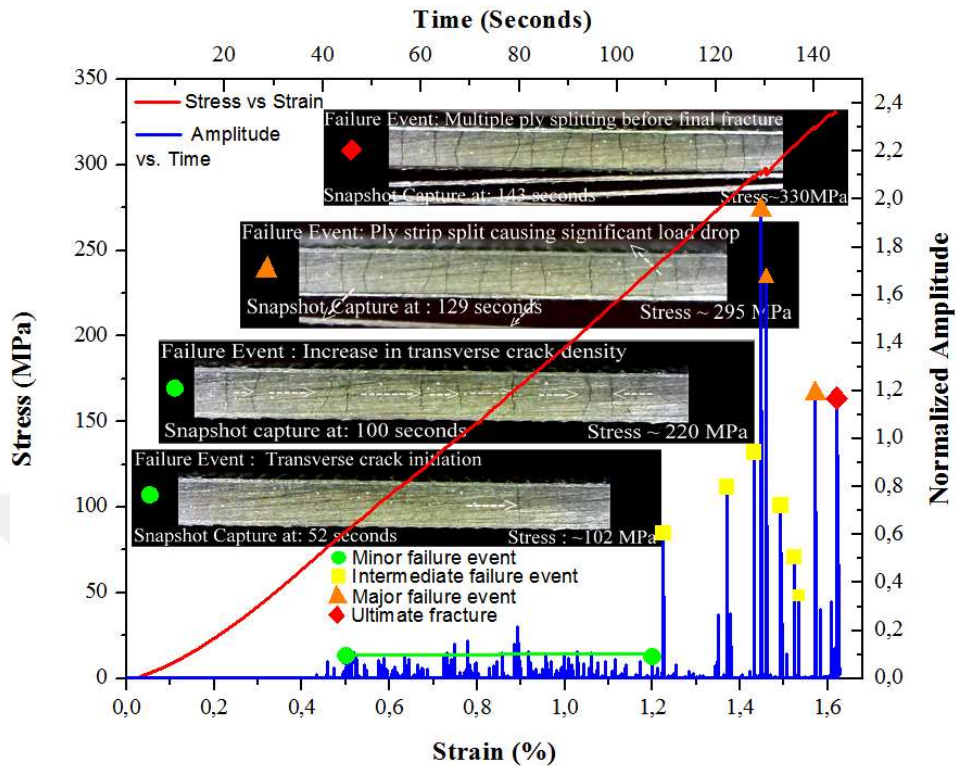
Figure 3: Stress vs. Strain , Amplitude vs. Time plots for $(0/90_5)_s$ laminates and snapshot captures from video 1.

2.10.4.2 Detection of failure events for $(0_m/90_n)_s$ laminates with m=3 n=3 under tension

Figure 4 reports the applied stress, audio data and representative snapshots of the captured failure events acquired synchronously during uniaxial tensile testing of $(0_3/90_3)_s$ laminates. Captured video of the tension test is provided in supplementary information labeled as video 2. As the proportion of 0° plies in this laminate was higher than the previous case, load share of matrix cracking prone 90° plies required higher overall applied stress.
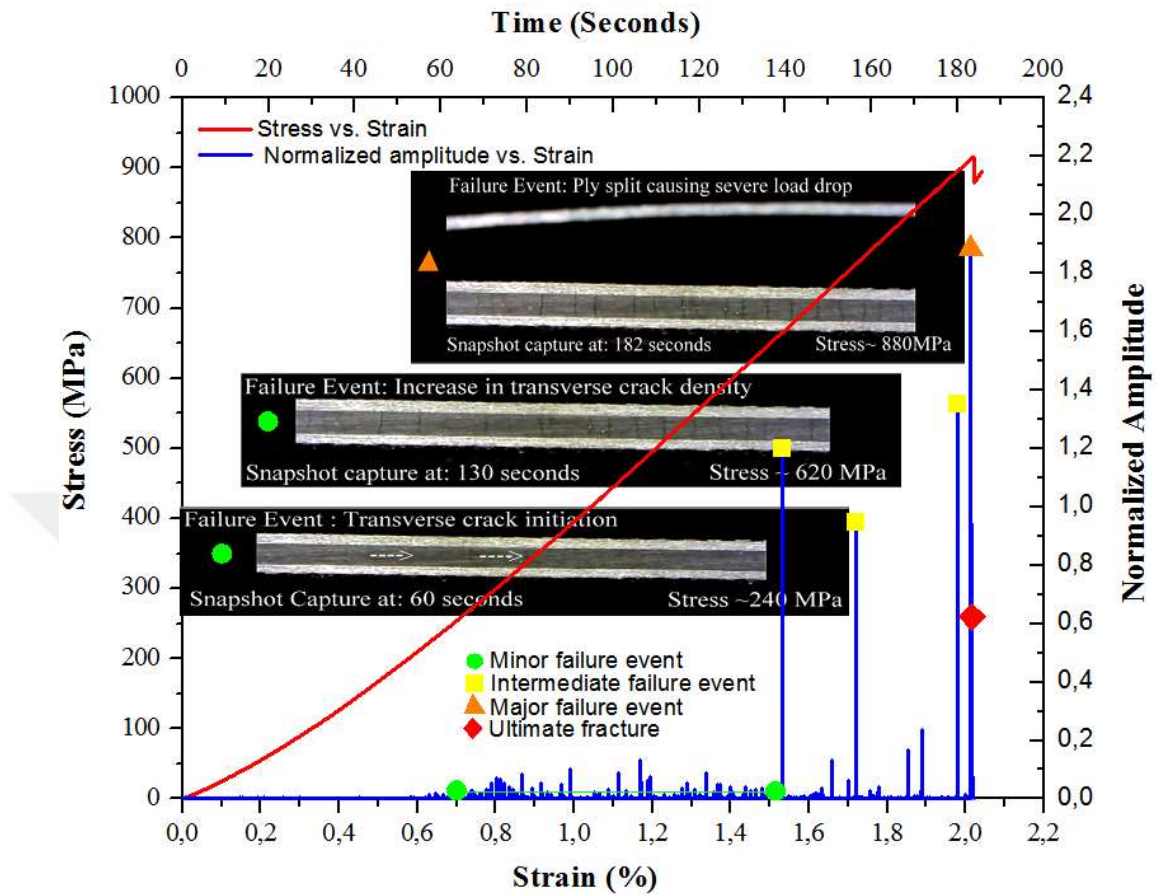
Figure 4: Stress vs. Strain , Amplitude vs. Time plots for $(0_3/90_3)_s$ laminates and snapshot captures from video 2.

Hence the transverse cracking was initiated at around 220MPa (~60th seconds from the start) and continued to densify along the specimen until the ultimate fracture. The first intermediate failure event was observed at overall stress of about 500 MPa (~140th seconds). This event can be attributed to a local delamination or ply-split event, but the visual identification was not possible since the failure event occurred outside of the recording window of the focused microscope. Compared to the $(0/90_5)_s$ case, the accumulation of the intermediate failure events for this case were less. The intermediate regime continued with no standing-out load drops in the stress-strain profile up until a

major event was observed at 880MPa (~182 seconds). This major failure event associated with the splitting of a large 0°ply strip was effectively captured within the sound signal profile. Tested laminate was not able to redistribute the loading since the damage was severe and total fracture instantaneously occurred just after the major failure event.

2.10.4.3 Failure of $(0_m/90_n)_s$ laminates with m=5 n=1 under tension

Figure 5 reports the audio data and several snapshots of the video captured failure events, all acquired in sync during uniaxial tensile testing of $(0_5/90)_s$ laminates. Visual recording of the tension test is provided in video 3. For this case, 90^0 ply block was 2 plies thick and centered at the lamininate mid-plane. The failure sequence was initiated by transverse cracking at about 800MPa (~140 seconds). Since the matrix-crack prone ply block thickness was smaller, sound peaks associated with the transverse cracks had relatively small amplitudes, but still distinguishable within the sound data profile. The data also suggested that intermediate failure events corresponding to local delaminations and ply splits were more frequent than the previous cases. A good example of a local delamination initiation from transverse cracks was captured at around 1320 MPa (~214 seconds) although it did not cause any load drops in the stress-strain profile. The observations suggest that the delamination occurs on the 0/90 ply interface which then propagates and translates into a major failure event. At around 1475 MPa (~227 seconds) 0° and 90° ply blocks were completely separated from each other. Second major event around 1480 MPa (~234 seconds) was also noted when a severe delamination occurred in the 0° plies. These two failure events were clearly distinguishable both in the captured video (video 3) and sound data profile. Upon redistribution of the stresses in the laminate, specimen was still able to sustain loads. Following these events, several ply strip splits have occurred in 0° ply blocks and the final fracture was explosive.
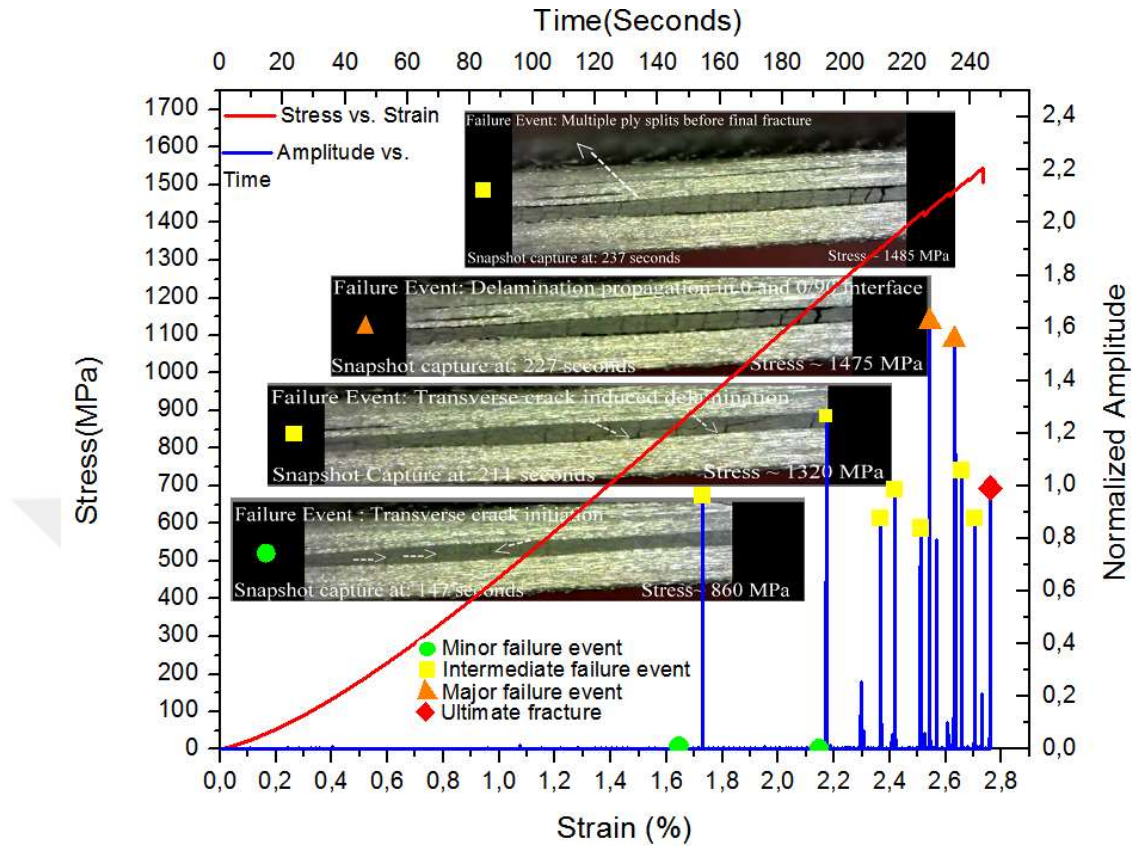
Figure 5: Stress vs. Strain , Amplitude vs. Time plots for $(0_5/90)_s$ laminates and snapshot captures from video 3.

2.10.4.4 Failure of $(0/90)_{ms}$ laminates with m=3(=n) under tension

Figure 6 reports the applied stress along with synchronous audio data and selected snapshots of the captured failure events during uniaxial tensile testing of $(0/90)_{3s}$ laminates. Visual record of the test is presented in video 4 of supplementary section. Note that 0°-90° plies were stacked subsequently, so that the thick block of multiple 90° plies were avoided except at the mid-plane, block of 2 plies due to symmetry. The lay-up of dispersed plies creates more homogenized load distribution in the laminate. The audio and video assisted mechanical test results suggested occurrence of the intermediate and major failure events due to transverse cracking were suppressed. Absence of the high

amplitude peaks is clearly notable in the audio data profile. Instead, the transverse cracking that was initiated around 300 MPa (~85 seconds) continued and densified within the dispersed 90 plies until the final fracture. Note that two laminates of the same in-plane stiffness [(0/90)$_{3s}$ vs (0$_3$/90$_3$)$_s$] were remarkably different in regard to the damage progression. From this perspective, homogenized laminate of (0/90)$_{ms}$ can be considered as a demonstration case where damage suppression was uniquely identified by the simple audio signature capturing method exercised hereby.
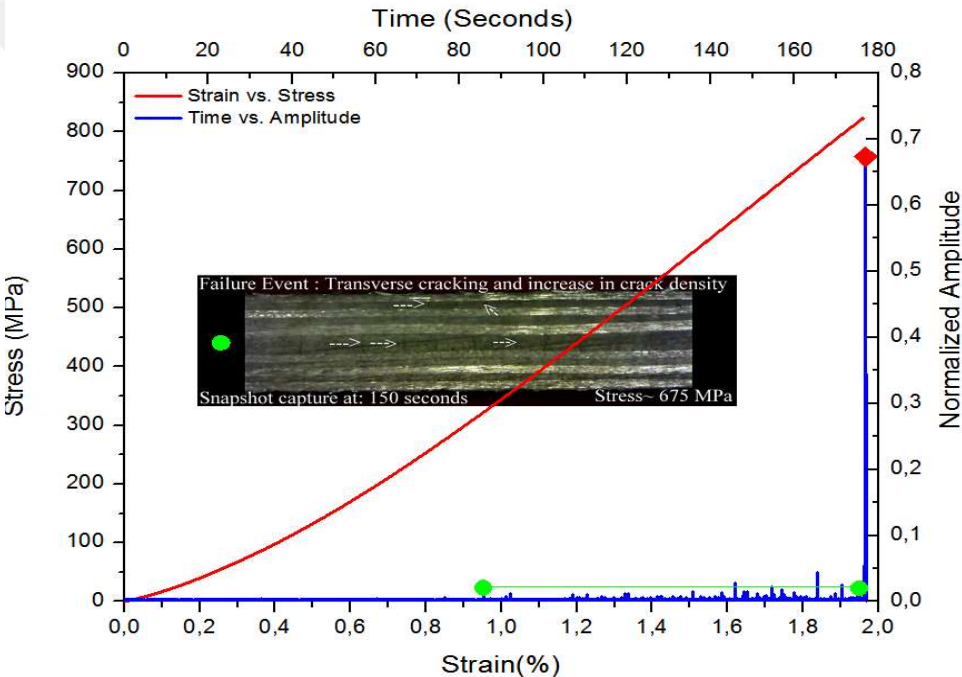
Figure 6: Stress vs. Strain , Amplitude vs. Time plots for (0/90)$_{3s}$ laminates and snapshot captures from video 4.

2.10.4.5 Failure of (90$_m$/0$_n$)$_s$ and (90/0)$_{ms}$ laminates with m=3 n=3 under tension

Two more, rather unconventional test cases with (90$_3$/0$_3$)$_s$ and (90/0)$_{3s}$ lay-up sequences which also result in the same in-plane stiffness with the cases of section 3.4. They were particularly included to investigated what happens if the matrix-cracked, failing plies were rather at the surfaces than being sandwiched between the 0^0 plies. As depicted in

figure 7 and video 5 of the supplementary section, the sound amplitudes acquired from $(90_3/0_3)_s$ specimens were rather high with respect to previous cases since the failure events associated with the 90^0 plies were also open to the free top and bottom surfaces of the specimens. First transverse cracking began at around 200 MPa (~60 seconds). Failure in
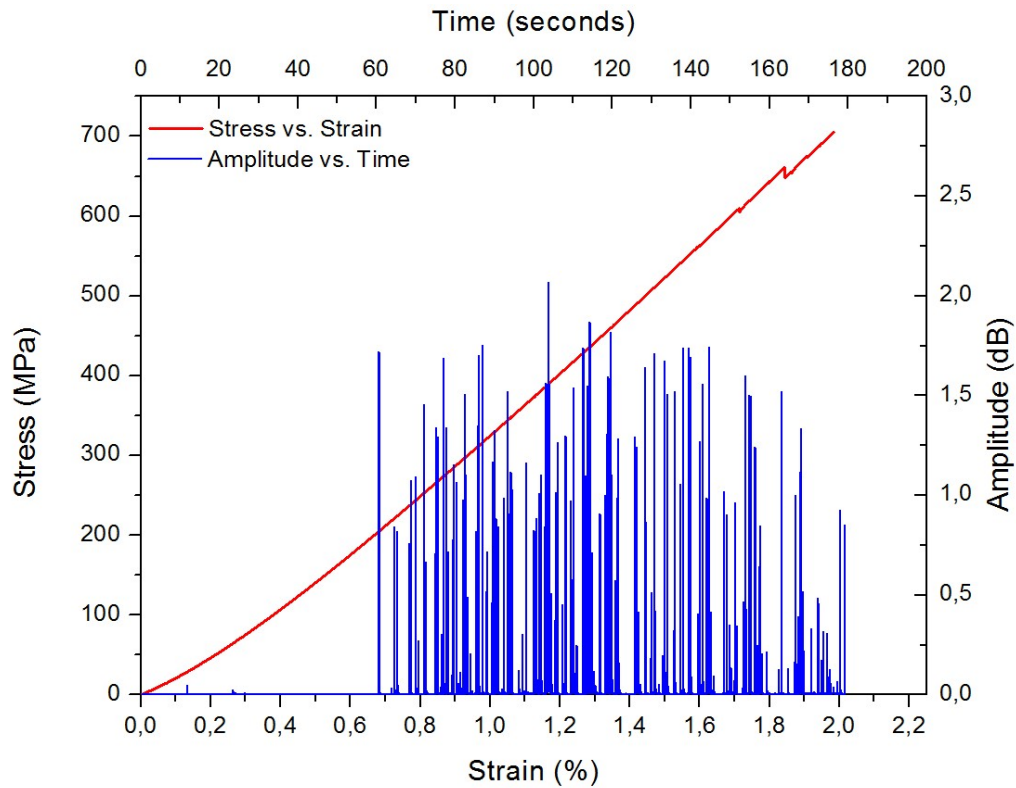
Figure 7: Stress vs. Strain , Amplitude vs. Time plots for $(90_3/0_3)_s$ laminates

the 90^0 plies continued and multiplied randomly throughout the specimens until around 160 seconds where blocks of the 90^0 plies were gotten separated from each other. Delamination at the 0/90 interfaces was then observed. This failure event caused a significant load drop in the stress-strain profile. However this specific event could not be identified with microphone based approach as it was successfully captured on previous cases where 90^0 plies were embedded between 0^0 plies. This is attributed to the fact that the sound output already spreading from the surface was intense and dominating. No fracture at the 0^0 plies occurred for this case.

On the other hand, the failure profile of the (90/0)₃ₛ specimens were quite similar to (0/90)₃ₛ where the failure was initiated by transverse cracking in 90^0 plies and finished with a sudden fracture at similar loads (Figure 8, video 6). The comparison of these two cases suggests the following about the proposed methodology: i) the amplitude based sound analysis is distance and lay-up sequence (hence the load distribution) sensitive. Large 90^0 ply blocks open to the specimen top and bottom free surfaces and the ones embedded inside generate different sound profiles. When the load distribution is more homogenized as in the case of (0/90)₃ₛ and (90/0)₃ₛ the discrete fracture events were prevented and the sound output generated from the specimens are nearly identical. This alone points out the advantage of the homogenized laminates of dispersed ply anlges.
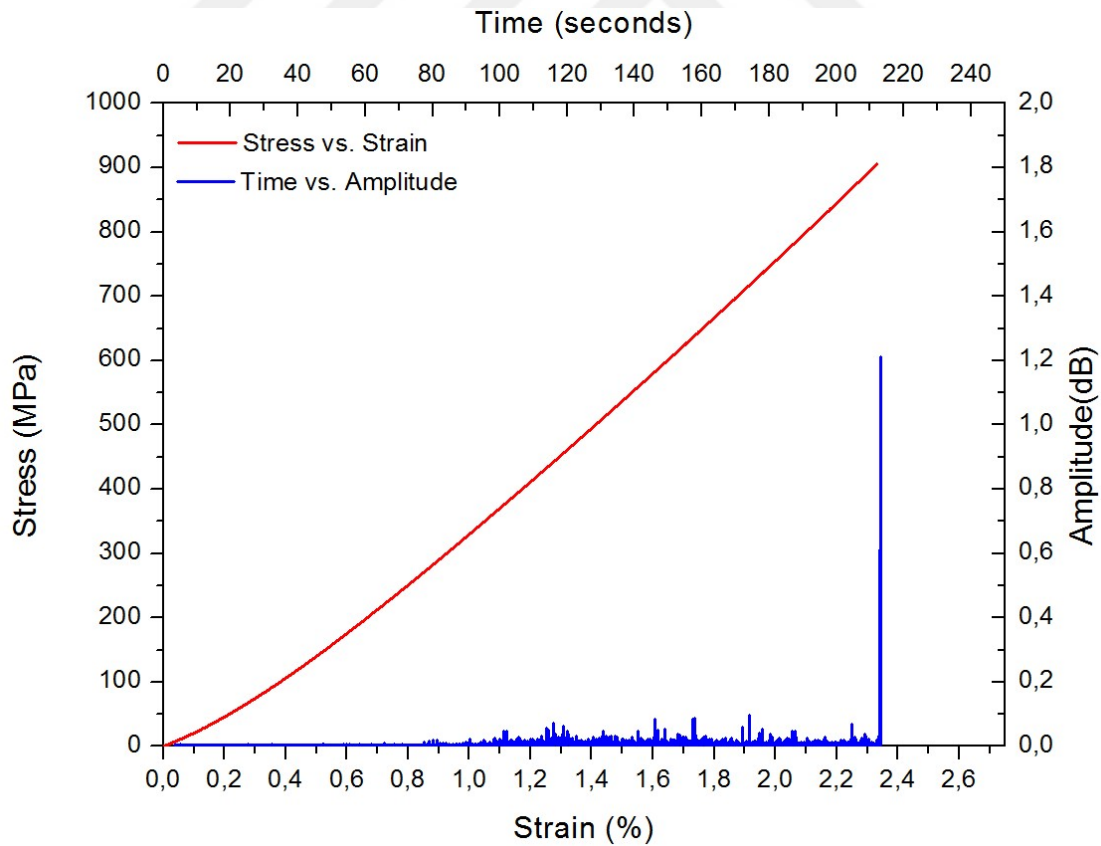
Figure 8: Stress vs. Strain , Amplitude vs. Time plots for (90/0)₃ₛ laminates

2.10.5 Conclusions

The progressive failure of $(0_m/90_n)_s$ laminates were effectively captured by a microphone assisted sound-tracking approach. Simultaneous video capturing of the polished specimen edges confirmed that the present simplified method is capable of capturing minor, intermediate, major and ultimate failure events as they produce sound fingerprints of their own. Audio and video assisted mechanical testing of $(0/90_5)_s$, $(0_3/90_3)_s$, $(0_5/90)_s$, $(0/90)_{3s}$, $(90/0)_{3s}$ and $(90_3/0_3)_s$ also demonstrated that the occurrence of the potent failure events and the corresponding sound outputs were significantly dependent on the lay-up sequence. This affordable, easy to set-up and quick method was found to be quite feasible and practical. The results presented herein suggest the proposed methodology provides valuable information by using the inherent acoustic signatures in testing/assessments rather than loosing completely when an acoustic emission toolset/software and associated expertise are not readily available..

2.10.6 References

[1] Camanho PP, Davila CG, Pinho ST, Iannuccic L, Robinson P. Prediction of in situ strengths and matrix cracking in composites under transverse tension and in-plane shear. Composites Part A 2006; 37(2): 165-176.

[2] Xia ZC, Carr RR, Hutchinson JW. Transverse cracking in fiber-reinforced brittle matrix, cross-ply laminates. Acta Metall.Mater 1993; 41(8): 2365-76.

 3] Tong J, Guild FJ, Ogin SL, Smith PA. On matrix crack growth in quasi-isotropic laminates I. Experimental investigation. Composites Science and Technology 1997; 57(11):1527-35

[4] Takeda N, Ogihara S. In situ observation and probabilistic prediction of microscopic failure processes in CFRP cross-ply laminates . Composites Science and Technology 1994;52(2):183-95.

[5] Takeda N, Ogihara S. Initiation and growth of delamination from the tips of transverse cracks in CFRP cross-ply laminates. Composites Science and Technology 1994;52(3):309-18.

[6] JM Berthelot. Transverse cracking and delamination in cross-ply glass-fiber and carbon-fiber reinforced plastic laminates: Static and fatigue loading . Applied Mechanics Reviews 2003; 56(1):111-47

[7] Ogihara S, Takeda N. Interaction between transverse cracks and delamination during damage progress in CFRP cross-ply laminates. Composites Science and Technology 1995; 54(4): 394-404.

[8] Johnson P, Chang FK. Characterization of Matrix Crack-Induced Laminate Failure Part I: Experiments. Journal of Composite Materials 2001; 35: 2009-35.

[9] Johnson P, Chang FK. Characterization of Matrix Crack-Induced Laminate Failure Part II: Analysis and Verifications. Journal of Composite Materials 2001;35: 2037-74,

[10] Greenhalgh ES. Failure analysis and fractography of polymer composites.Woodhead Publishing, 2009.

[11] Aymerich F, Meili S. Ultrasonic evaluation of matrix damage in impacted composite laminates. Composites Part B 2000; 31(1):1-6.

[12] Dvorak GJ, Laws N. Analysis of Progressive Matrix Cracking In Composite Laminates II. First Ply Failure. Journal of Composite Materials 1987; 21(4): 309-329.

[13] Tay TR, Liu G, Tan VBC, Sun XS, Pham DC. Progressive Failure Analysis of Composites. Journal of Composite Materials 2008; 42: 1921-1966

[14] Jen KC, Sun CT. Matrix Cracking and Delamination Prediction in Graphite/Epoxy Laminates. Journal of Reinforced Plastics and Composites 1992; 11(10): 1163-75.

[15] Surgeon M, Wevers M. Modal analysis of acoustic emission signals from CFRP laminates. NDT & E International 1999; 32(6): 311-22.

[16] Aggelis DG, Barkoula NM, Matikas TE, Paipetis AS. Acoustic structural health monitoring of composite materials : Damage identification and evaluation in cross ply laminates using acoustic emission and ultrasonics. Composites Science and Technology 2012; 72(10) : 1127-33.

[17] De Groot PJ, Wijnen PAM, Janssen RBF. Real-time frequency determination of acoustic emission for different fracture mechanisms in carbon/epoxy composites. Composites Science and Technology 1995; 55(4):405-412.

[18] Mizutani Y, Nagashima K, Takemotoa M, Onob K. Fracture mechanism characterization of cross-ply carbon-fiber composites using acoustic emission analysis. NDT & E International 2000; 33(2): 101-110.

[19] Baker C, Morscher GN, Pujar VV, Lemanski JR. Transverse cracking in carbon fiber reinforced polymer composites: Modal acoustic emission and peak frequency analysis. Composites Science and Technology 2015; 116: 26-32.

[20] Cannam C, Landone C, Sandler M. Sonic Visualiser : An Open Source Application for Viewing, Analysing, and Annotating Music Audio Files, in Proceedings of the ACM Multimedia International Conference 2010.

[21] Cannam C, Landone C, Sandler M. Sonic Visualiser: An Open Source Application for Viewing, Analysing, and Annotating Music Audio Files, in Proceedings of the ACM Multimedia 2010 International Conference.

[22] Zubilaga L, Turon A, Renart J, Costa J, Linde P. An experimental study on matrix crack induced delamination in composite laminates. Composites Strcutures 2015; 127:10-17.

[23] Aggelis DG, Barkoula NM, Matikas TE, Paipetis AS. Acoustic emission monitoring of degradation of cross ply laminates. JASA Express Letters 2010; 127(6).

:

CHAPTER 3

OUT-OF-THE BOX APPLICATIONS FOR NANOFIBROUS INTERLAYERS

Author's Note : This part of the thesis is based on the demonstration of the proof-of - concepts that have been offered by the author to the literature on nanofibrous toughening. Two papers are presented as three sections.

3.1 Global and Local Nanofibrous Interlayer Toughened Composites for Higher In-Plane Strength

3.1.1 Abstract

Epoxy compatible P(St-co-GMA) copolymer based nanofibrous mats are introduced by electrospinning onto uni-directional (UD) and 0/90 twill weave carbon fiber/epoxy prepreg systems as interlayers. Expecting in-plane strength improvement via higher matrix cracking resistance, nanofibrous interlayered composites are subject to uni-axial tension tests as $(0)_6$ and $(0/90)_{6woven}$ laminates. The ultimate tensile strength of the $(0)_6$ laminates is increased by 12% whereas the tensile strength of the woven fabric composites is increased by 18%. A localized interlayer approach where the interlayers are incorporated at the vicinity of the hole is evaluated via open hole tension (OHT) tests of $(0/90)_{6woven}$ laminates. An increase up to 9% on OHT strength is achieved.

3.1.2 Introduction

Science and engineering of fiber reinforced advanced composite materials (FRC) is an actively broadening research field with more and more emphasis on their multi-phase and multi-scale characteristics. Emerging manufacturing and characterization techniques provide ability to manipulate materials at all scales from traditional macro scale to relatively recent nano-scale. The property tailoring by incorporating nano-scale aiming to change the macro-level behavior of composite materials is at the focus of many research activities thanks to the promising and surprising nature of the nano-world. For instance, the addition of nano or sub-micron fibrous as interlayers for delamination of structural composites is a relatively recent approach introduced first by the works of Reneker [1] and Dzenis et al. [2],[3]. Several other studies have followed this novel idea and demonstrated the capabilities of the electrospun nanofibers [4] and the advanteges that can be achieved with their incorporation into different composite systems [5,6]. These studies have shown that the polymeric nanofibrous interlayers were quite effective in the improvement of out of plane material properties. However, less attention was given to the failure behavior of these hybrid structures under in plane loading conditions. Given the early matrix cracking is one of the troublesome characteristics of laminated composites, [7,8] under such loading conditions the ability of interlayers to act against transverse matrix cracking also becomes interesting and appealing.

Deriving from the idea that interlayer addition may also work against premature transverse matrix cracking (transverse to fiber direction) as well as delamination [9], our recent work first explored the effect of matrix compatibility by introducing electrospun P(St-co-GMA) based nanofibrous mats as interlayer materials into conventional UD carbon/epoxy composite laminates focusing primarily on the out of plane behavior and

toughness evaluated by three point bending, end notched flexure and Charpy impact tests. Whereas UD specimen tests under tension loads transverse to the fibers were also reported to indicate the transverse strength increase by the interlayers [10].

The present work compliments our previous works by exploring the longitudinal (parallel to fiber direction) uni-axial tension behavior of UD laminates reinforced with nanofibrous interlayers. In addition, it extends the application of P(St-co-GMA) based interlayer reinforcements to woven carbon fabric/epoxy laminates and demonstrates their ability to improve in-plane strength for these laminates. Finally, the concept of "localized interlayer toughening of composite laminates" at stress concentration locations such as holes is introduced. Open hole tension tests (OHT) were conducted on tensile specimens where nanofibrous interlayer reinforcement is localized to the near-hole regions as opposed to integrating them over the whole interlaminar planes. Overall, the results support that P(St-co-GMA) nanofibers are strong candidates for toughening and strengthening of structural composites subjected to in plane loads as well.

3.1.3. Experimental Procedure

3.1.3.1 Specimen Preparation and Mechanical Testing

Polymer synthesis, solution preparation and electrospinning parameters were set as reported in our earlier work [10], [11]. Polymer solution was electrospun directly onto prepreg layers. Two different carbon/epoxy prepreg systems from TCR Composites were used: twill weave carbon fabric/UF3369 epoxy and UD carbon fiber/UF3325 epoxy. For un-notched tensile test specimens, the nanofibrous interlayers were electrospun on the whole surface of each ply where weight addition due to electrospun interlayers was only

about 0.2%. The specimen dimensions and testing procedures were determined according to ASTM D3039. For open hole tension test specimens, the electrospinning was carried out onto the prepreg layers which were masked with a non-conducting and non-adherent plastic layer. As a result the electrospun nanofibers were only collected on the prepreg layers partially, at the intended area-the vicinity of to stress raisers (see Figure 1.a, 1.b, the holes to be drilled after the consolidation of the source laminate for the OHT specimens) and the weight addition was considered none. The specimen dimensions and testing procedures were determined according to ASTM D5766 . The hole diameter to width ratio is 1/6. Hence the open-hole tension test specimen had a 2.5 mm hole at the center and the interlayer toughened region was about 15x15 mm square centering the hole for each specimen.
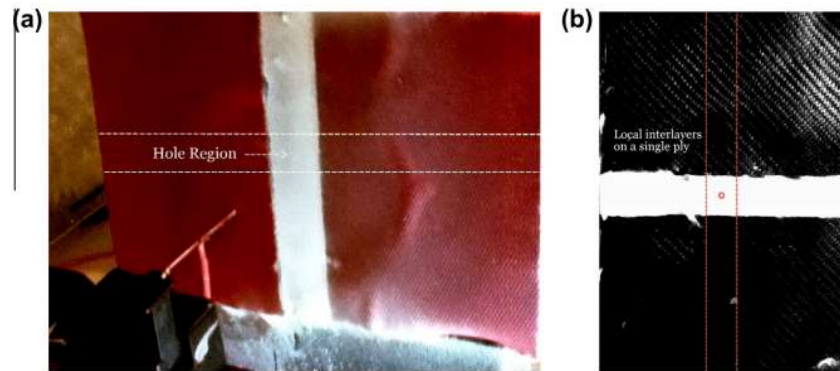
Fig. 1. (a) Electro-spinning with non-conductive mask for OHT specimen preparation. (b) Local interlayer addition over single prepreg ply. (For interpretation of the references to color in this figure legend, the reader is referred to the web version of this article.)

Figure 1: a) Electro-spinning with non conductive mask for OHT specimen preparation. b) Local interlayer addition over single prepreg ply.

For both tests, stack of 6 plies hosting 5 interlayers of electrospun nanofibers were prepared to form the final uncured composite laminates. The laminates were then vacuum bagged and cured at 100˚C for 24 hours. The laminates were cut with a diamond disc

cutter according to the specimen dimensions. Drilling of the center hole was later done by tungsten carbide drill. The mechanical tests were done using ZWICK Proline 100 with a 100kN load cell at a constant cross-head speed of 1mm/min.

3.1.4. Results and Discussion

3.1.4.1 Progressive Wetting of P(St-co-GMA) Interlayers at Laminate Curing Temperature

The structural compatibility of the P(St-co-GMA) interlayers within UF3325 epoxy matrix UD fiber composites was first reported in our earlier work [10]. Epoxy wettability/impregnation behavior of the interlayers on the present woven fabric carbon/epoxy prepreg surface at the curing temperature (100˚C) was checked as shown in Figure 2. The transition of the electrospun prepreg surface from white coated to visible carbon fiber architecture appearances (Figure 2.a to 2.b, respectively) shows the progress of the resin self-impregnation into the nanofibrous interlayers at 100° C (curing temperature) respectively in about an hour time. The electrospun fibrous mat was totally wetted by the epoxy resin on the prepreg despite no external stimulation was applied.
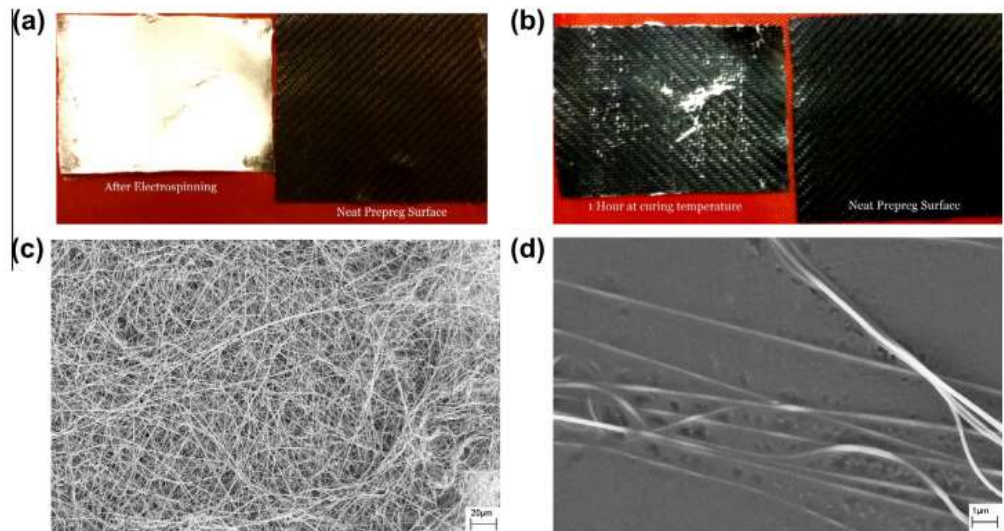
Fig. 2. Prepreg surfaces (a) just after electrospinning, at room temperature, (b) after 1 h hold at 100 °C, (c) nanofiber morphology on prepreg surfaces at room temperature and (d) nanofiber morphology on prepreg surfaces at 100 °C after 1 h hold. (For interpretation of the references to color in this figure legend, the reader is referred to the web version of this article.)

Figure 2: Prepreg surfaces a) just after electrospinning at room temperature b) After 1 hour hold at 100^0C. c) Nanofiber morphology on prepreg surfaces at room temperature and d) nanofiber morphology on prepreg surfaces at 100^0C after 1h hold.

This observation was further supported by SEM images taken from the prepreg surfaces. Figure 2.c corresponds to the prepreg surfaces at room temperature where the nanofibers are clearly visible. Figure 2d corresponds to higher magnification SEM image of the epoxy surface of Figure 2.b where the nanofibers embedded in epoxy can easily be noted. A detailed in-situ morphological study of nanofiber/ UF3325 epoxy complex including the fracture surfaces and cross-sectional SEM analysis was also provided in detail in our previous study [10].

3.1.4.2 Longitudinal Tensile Tests

The results of longitudinal tensile tests on $(0)_6$ UD specimens suggested that the presence of P(St-co-GMA) interlayers on the interlaminar planes increased the tensile strength of UD composite laminates by 12 %. The failure was thought to be initiated by matrix cracking from the free edges and the overall failure occured due to ply splitting as expected for the tensile tests of UD carbon/epoxy specimens (Figure 3). On the other hand the tensile strength of the $(0/90)_{6woven}$ laminates was increased by 18% (See Table 1). The fracture was observed as initiated by matrix cracks and finalized by fiber failure (Figure 3). For both tests the failure modes were similar for interlayered and neat laminates. In consistency with previously reported transverse tensile test results [10], these observations suggest that the presence of P(ST-co-GMA) fibrous interlayers increases the resistance of composite laminates against matrix cracking.
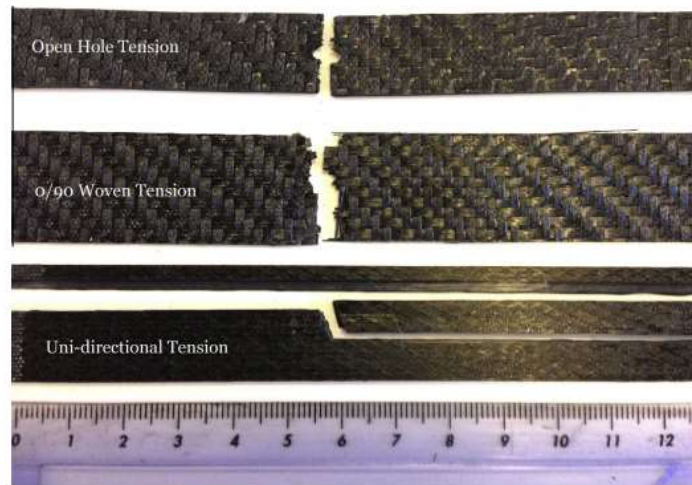
Fig. 3. Fractured $(0/90)_{6woven}$ OHT (top), un-notched $(0/90)_{6woven}$ tensile (middle), $(0)_6$ tensile (bottom) specimens. (For interpretation of the references to color in this figure legend, the reader is referred to the web version of this article.)

Figure 3: Fractured $(0/90)_{woven}$ OHT (top), un-notched $(0/90)_{woven}$ tensile (middle). $(0)_6$ tensile (bottom) specimens.

3.1.4.3 Open-Hole Tension Tests

Open-hole tensile strength of locally interlayered $(0/90)_{6woven}$ composite specimens was 9% higher than the specimens without the interlayers (see Table 1). For OHT specimens the failure was mostly dominated by a major crack formation from the periphery of the hole. This observation suggests the following: i) the inplane strength increase is attributed to the presence of interlayers since the crack moved through toughened region ii) the increase however was not as high as it was on the case of un-notched tensile test specimens. It is noteworthy that the amount of interlayer material to cover near hole region was smaller and the localization procedure provides efficiency in both use of time and material compared to the interlayer application on the whole ply surfaces.

Table 1
Summary of un-notched and open-hole tension test results.

Test result	Specimen/lay-up	No interlayers	With interlayers
Tensile strength (MPa)	$(0)_6$ UD laminate	1151 ± 70	1312 ± 65
	$(0/90)_6$ Woven laminate	493 ± 19	620 ± 11
Open hole tension (OHT) strength (MPa)	$(0/90)_6$ Woven laminate	393 ± 9	427 ± 8[a]

[a] Interlayers localized at the vicinity of the hole.

3.1.5 Conclusion

Electrospinning process was used to obtain nanofibrous P(St-co-GMA) interlayers on UD and woven fabric carbon/epoxy prepreg surfaces. Progressive wetting of P(St-co-GMA) nanofibers with the epoxy matrix were assessed. Uni-axial tensile tests of $(0)_6$ and

(0/90)$_{6woven}$ laminates showed increase in tensile strength by 12% and 18%, respectively, with almost no weight penalty associated with the nanofibrous interlayers. Moreover, the local toughening effect assessed by open hole tension (OHT) tests showed that interlayer addition just in the vicinity of the highly stressed regions was also effective increasing the maximum failure stress by 9%. Reported test results underlined that electrospun P(St-co-GMA) nanofibrous mat is a promising interlayer candidate thanks to their ability to work also under in-plane loads which makes them integrable to conventional composite design.

3.1.6 References

[1] Kim J.S., Reneker D.H. "Mechanical properties of composites using ultra fine electrospun fibers", *Polymer Composites,* 1999; 20(1):124–31.

[2] Dzenis Y, Reneker D H., "Delamination resistant composites prepared by small diameter fiber reinforcement at ply interfaces", USPATENT 626533,2001.

[3] Dzenis Y., "Structural nanocomposites", *Science,*2008; 319(5862):419- 20.

[4] Huang Z.M, Zhang Y.Z, Kotaki M., Ramakrishna S., "A review on polymer nanofibers by electrospinning and their applications in nanocomposites", *Compos Sci Technol*, 2003; 63: 2223–2253

[5] T.K. Tsotsis, "Interlayer toughening of composite materials**",** Polym Compos, 2009 ; 30 (1): 70–86

[6] Zucchelli A., Focarete M.L.,Gualandi C., Ramakrishna S. "Electrospun nanofibers for enhancing structural performance of composite materials." , *Polymers for Advanced Technologies,*2011;22(3):339–49.,

[7] Tsai. S. W. " Strength and Life of Composites" , JEC Composites, 2009

[8] M.S Kumar, K.Raghavendra, M.Anjanappa, M.A Venkatasvamy, H.V Ramachandra, "Fractographic Analysis of Tensile Failures of Aerospace Grade Composites", Materials Research. 2012; 15(6): 990-997

[9] Sihn S.,Kim R.Y.,Huh W.,Lee K.H.,Roy A.K. ,"Improvement of damage resistance in laminated composites with electrospun nano-interlayers. " *Compos Sci Technol,*2008; 68(3-4):673–83.

[10] Bilge K., Ozden-Yenigun E., Simsek E., Menceloglu Y.Z., Papila M., ,"Structural composites hybridized with epoxy compatible polymer/MWCNT nanofibrous interlayers." *Compos Sci Technol,*2012; 72(14):1639-45

[11] Ozden E., Menceloglu Y.Z., Papila M. "Engineering chemistry of electrospun nanofibers and interfaces in nanocomposites for superior mechanical properties" *ACS Applied Materials and Interfaces,* 2010;2(7):1788–93.

3.2 High Strain Rate Response of Nanofiber Interlayered Structural Composites

Reference (Paper D): E.O.Yenigün, **K.Bilge** , E.Sunbuloglu, E.Bozdag, M.Papila "High Strain Rate Response of Nanofiber Interlayered StructuralComposites", Composite Strcutures , under revision, November, 2016.

3.2.1 Abstract

Nanofibrous interlayer toughening strategy for laminated composite materials typically demonstrated at quasi-static loading is here evaluated under high strain rate deformation. Carbon fiber reinforced composite laminates of $(0/90)_{25s}$ stacking sequence are interlayered by P(St-*co*-GMA) nanofibers which are chemically tuned for interfacial compatibility when embedded in epoxy matrix. The cubical composite specimens are cut and subjected to high strain-rate deformation via Split Hopkinson pressure bar testing. Specimens are hit at their through-the-thickness (stacking) and side-to-side (in-plane) directions. The change in the dissipation of energy due to altered interlaminar microstructure is monitored and reported. Enhancement in the capacity of the energy dissipation due to the nanofibrous interlayers is as high as 80% in-plane and 40% through thickness directions, depending on the strain rate. The results overall suggest that interlayer toughening strategy used in this work prevents the formation of critical matrix cracks that can cause the formation of instantaneous mode II delamination. Incorporation of the nanofibers without causing notable weight penalty effectively toughen the matrix dominant interlaminar zones under high strain rate conditions as well.

3.2.2. Introduction

Several toughening strategies for structural laminated composites focus basically on reinforcing the interlaminar regions between two subsequent plies. These thin interfacial regions are relatively resin-rich, but exhibit different properties than the bulk resin depending on the matrix itself and the ply-interface interaction which is affected by the fiber-phase architecture, orientation and lamination sequence. Addition of sub-phases into the interlaminar planes have typically been proposed to avoid/delay extensive interply crack propagation and to prevent subsequent formation of interply delamination. They can be in the form of dispersed particles[2-4], films [5-7], fibrous/nanofibrous reinforcements [8-12] and their combinations [9, 13]. Moreover, recent studies by Daelemans *et. al* specifically defined the effect of reinforcement morphology (either as a film, nanofibrous mats or particulates) on the unique mechanical performance [14, 15]. This approach is referred as *interlayer toughening* in general [16]. The challenge has been to adapt the interlayer toughening strategies into the conventional materials and manufacturing techniques while aiming for both enhanced in-plane and out-of-plane mechanical behavior. In this regard, the nanofibrous interleaf/interlayer toughening is arguably more promising compared to the other sub-phase choices. Recent studies [8-10, 13-15, 17-20] demonstrated the potent of the nano and sub-micron sized fibrous interlayers to toughen the laminated composites. Our earlier and current work more focused on surface modified/reactive polystyrene-*co*-glycidyl methacrylate P(St-*co*-GMA).polymer on carbon/epoxy prepreg systems both under in-plane and out-of-plane loading conditions at the macro-scale [13].

Along with the out of plane and in-plane quasi-static performance, behavior of laminated composites under high strain rates is also intriguing, and especially crucial for their contribution against impact. There have been extensive efforts for the dynamic behavior of the conventional composite formations along with the other engineering materials [21]. Although such high strain rate phenomena have been extensively studied in conventional materials, such as metals, ceramics, polymers and conventional composite formations [21-43], to date the mechanical deformation of such interlayer toughened composites under large strains and at high strain rates has not been directly studied. Besides, there are even limited attempts to reveal the fracture behavior of layered structural composites [21, 29, 33-35, 42] and nanocomposites [44, 45] at high strain rates. On the other hand, published data and associated knowledge on high strain rate mechanical deformation of nanofiber-interlayer toughened composites appear to be lacking. As such, the contributions of nanoscale morphologies and toughened interfaces to the high strain rate characteristics are yet to be thoroughly explored. To the best of our knowledge, investigations specific to the high strain rate deformation of nanofiber interlayered structural composites for the development of new protective materials are still needed.

This study attempts to reveal the effects of nanofibrous interlayers at high strain rate. The research hypothesis states that exceptional mechanical performances of nanofibrous-interlayered structural composites are not limited at quasi-static rates, but also lead to the superior properties of these composites at high deformation rates. That is, performance of these nanofibrous interlayers in the structural composites under the extreme condition of high deformation rates and to large strains complements their proven advantages in increasing the resistance to delamination and transverse matrix cracking. As a continuation of our earlier work [8, 9, 13, 17], lab synthesized surface modified/reactive

polystyrene-*co*-glycidyl methacrylate P(St-*co*-GMA) nanofibers with epoxide functional groups were used. The carbon fiber reinforced composite laminates' of $(0/90)_{25s}$ stacking sequence were interlayered by these nanofibers. The experimental plan employed split Hopkinson pressure bar (SHPB) test both through fiber and transverse to fiber directions to examine the mechanical characteristics of composite structures evolving with the strain rates and the dynamic characteristics of the nanofibrous interlayers as their effects on the dissipated energy and ultimate compressive strength. The nanofibrous interlayers were examined by their effects on the dissipated energy and ultimate compressive strength of composite structures subject to the various strain rates.

3.2.3 Materials and Methods

3.2.3.1 Electrospinning of P(St-co-GMA) Nanofibers and laminate manufacturing:

The procedure for the synthesis of P(St-co-GMA) (Figure 1) with 10 wt.% GMA content was explained in detail in our previous works [8, 9, 13, 17]. Polymer solutions were prepared by dissolving P(St-*co*-GMA) 30 wt.% in DMF and stirring for 3 hr. Applied voltage, solution flow rate and tip to ground distance were set at 15 kV, 30 μL/h and 10 cm, respectively during the electrospinning. The polymer solution was electrospun directly onto the carbon/epoxy prepreg layers (Aldila Composites, 34-700 (24k)-AR2527). Consequently, a thin homogenous layer of nanofibers (mean fiber diameter of 400 nm), was deposited on the prepreg surface forming the interlayer with an additional weight as low as 0.1% of the prepreg ply weight. For Split-Hopkinson bar tests, the specimen thickness of 10 mm was to be aimed which ultimately required the lamination of 100 subsequent prepreg plies that each forming 99 interlaminar region to be toughened. In order to decrease the electrospinning process time, we have firstly stacked each (0/90)

plies and and carried out the electrospinning only over these 90^0 plies. Hence each specimen with $(0/90)_{25s}$ lay-up sequence contained 49 toughened interlaminar regions.
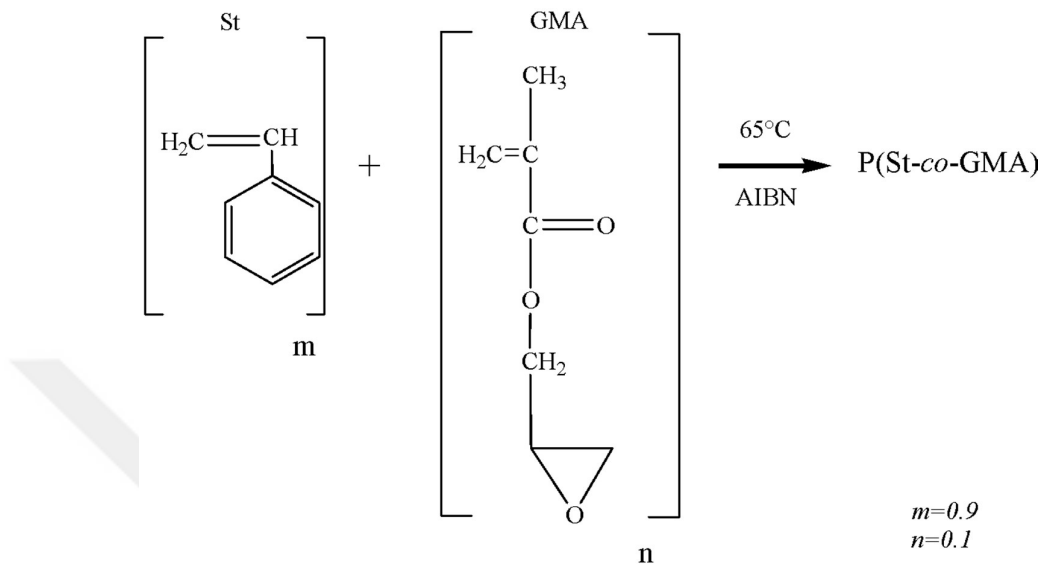
Figure 1: Chemical Structure of P(St-*co*-GMA)

After stacking the plies for intended laminates, each stack was put on a metallic tooling plate along with a release film and peel ply. Another sheet of peel ply was then laid on the pile of plies followed by a nonwoven breather layer. Next, the whole lay-up was vacuum bagged and kept under vacuum during the cure cycle. Prepreg stacks were cured at 100˚C and so the glass transition temperature of P(St-*co*-GMA) copolymer fibers which is also around 100 ˚C was not exceeded [8]. Cured 10 mm thick laminates were cut into 10 mm x 10 mm x 10 mm cubic SHPB specimens by waterjet.

3.2.3.2 Compressive Split-Hopkinson Pressure Bar (SHPB) apparatus

The standard compressive-type SHPB apparatus as shown in Figure 2a was used in this study. The main parts of the compressive SHPB apparatus are: propelling mechanism, striker, incident bar, transmitter bar and support stand. The diameter of the incident and transmitter bars is 22.2 mm and the length is 1510 mm. The bars are made of Maraging-

350 High Strength Steel which has Young's modulus of 210 GPa and density of 8100 kg/m^3. The specimen is positioned between the incident and transmitter bars (see the inset in Figure 2a). Prior to the testing, 3M^{TM} paper tape are attached to the impact face of incident bar as a practical pulse-shaper. When the striker hits the incident bar, an elastic stress pulse is generated and travels along the incident bar [46]. Once the compressive strain pulse (ε_i) reaches the specimen-incident bar interface, due to the mismatch between their impedance values, some portion of the strain pulse is reflected back (ε_r) into the
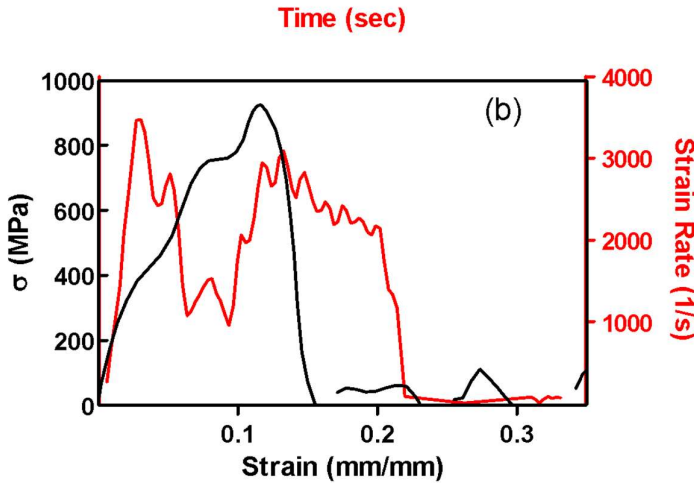
Figure 2: (a) The standard compressive-type SHPB apparatus used in this study **(b)** A sample of stress-strain data and strain-rate of the tests.

incident bar. The other part of the pulse is transmitted through the specimen into the transmitter bar (ε_t). Strain gages mounted on the incident and transmitter bars are used to collect and resolve the strain-wave signals. The 1st gage on the incident bar measures both the incident and reflected pulses whereas the 2nd strain gage on the transmitter bar merely measures the transmitted pulse. The output of the strain gages is fed through Wheatstone-Bridge circuit into a digital storage oscilloscope, where the signals are digitized and stored at a sampling rate of 400 kHz on a PC.
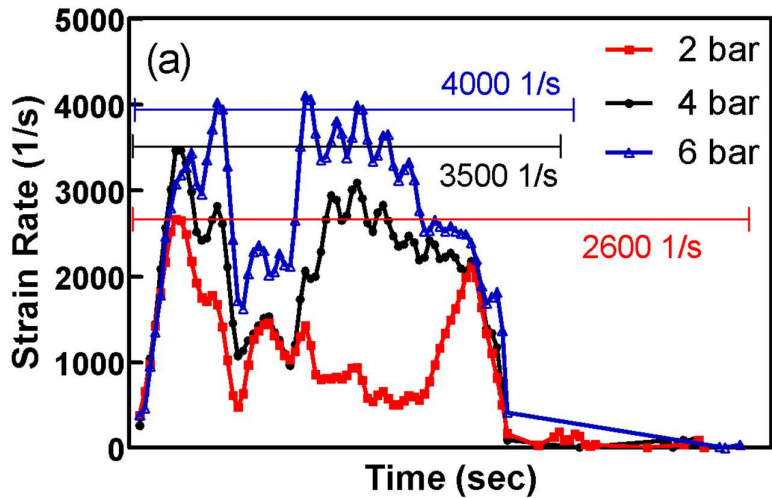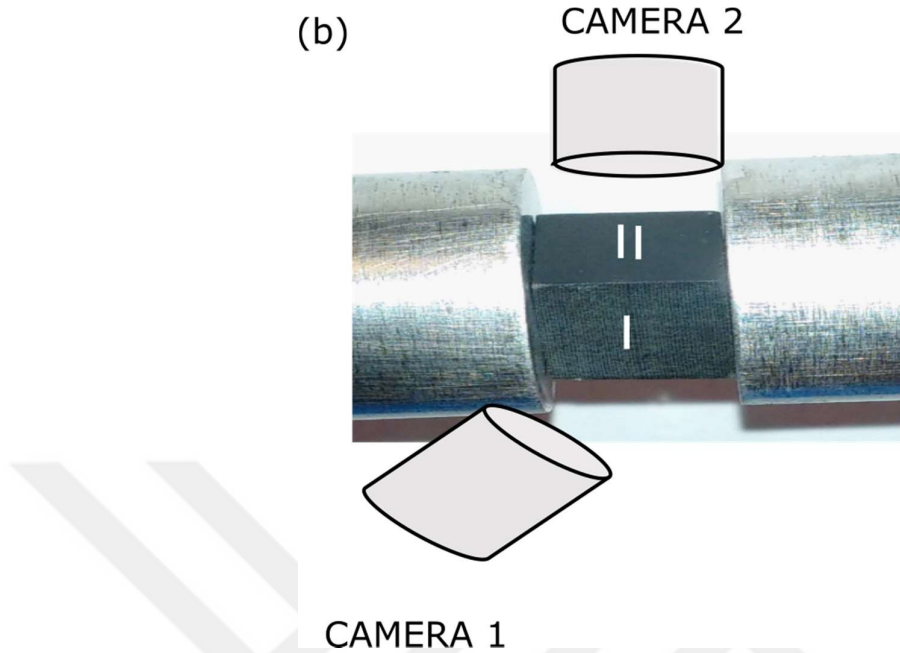
Figure 3: (a) Strain rate evolution depends on impact pressure (b) The illustration of mounted cameras for monitoring progressive damage.

Lindholm gives the expression for stress predictions in terms of the measured strain pulses. The stresses on the loaded front face (Eq 1) and rear face (Eq 2) of the specimen are calculated as:

$$\sigma_{sfi} = \left[E_0 \frac{A_0}{A_S} \right] (\varepsilon_i + \varepsilon_r) \tag{1}$$

$$\sigma_{sft} = \left[\frac{E_0 A_0}{2 A_S} \right] (\varepsilon_i + \varepsilon_r + \varepsilon_t) \tag{2}$$

where A_0 and E_0 refer to the area of the cross-section and modulus of elasticity of the incidence bar, respectively, ε is the axial strain corresponding to axis of the bar, and indices t and r indicate the recorded transmitted wave in the transmission bar and reflected wave in the incident bar, respectively. Considering the specimen to be in axial-force-

balance state, $\varepsilon_t(t) + \varepsilon_r(t) = \varepsilon_i(t)$ and then the equation system may be obtained in the form of

$$\sigma_s(t) = E_0 \frac{A_0}{A_s} \varepsilon_t(t) \tag{3a}$$

$$\dot{\varepsilon}_s(t) = -2\frac{c_0}{L_s} \varepsilon_r(t) \tag{3b}$$

$$\varepsilon_s(t) = \int_0^{T_{pulse}} \dot{\varepsilon}_s(\tau)d\tau \tag{3c}$$

with c_0 being the velocity of propagation of a longitudinal wave in the bar with a mass density of ρ_0 [48] defined as $c_0 = \sqrt{E_0 / \rho_0}$.

Also in [48], the influence of geometry is investigated for non-circular cross sections to check for radial inertia and axial equilibrium assumptions to hold. The ideal slenderness of a non-circular specimen (which is almost a must while testing composites with SHPB systems) is defined by $\lambda = \dfrac{L}{\sqrt{I/A}}$ and $1.4 \leq \lambda \leq 2.8$ in [48], and for a nominally 10mmx10mmx10mm specimen utilized in this study, the value exhibits a slight deviation, with $\lambda_s \approx 3.4$ considering measured sample dimension tolerances. However, smaller specimens are foreseen to introduce higher error leading to loss of continuum assumption as too few repeating (0/90) sub-laminate of carbon fibers exist in the specimen and shorter specimens lead to too high strain rates than observed here, thus, the current geometry has been adopted as an optimum for our purpose of high strain rates (on the order of 10^3s^{-1}). Also, it should be noted that the derivation in accounts of isotropic/homogeneous material, and indeed may not fully cover the current anisotropic case [48].

Dimensions of each specimen were measured before the test. The test conditions were also recorded. The specimen stress-strain curve, and the strain-rate of each test were adopted using the initial set of pulses. Dissipated energy values for each test were also

calculated. Specimens after the tests were kept for further scanning electron microscopy (SEM) analysis. The SHPB system was calibrated initially to account of the strain-gage positions away from the specimen interfaces. A sample of stress-strain data and strain-rate of the tests are given in Figure 2b. Each test associated with the types of specimen/loading (for instance, interlayered/impact through-the-thickness) was repeated at least 5 times for data analysis.

3.2.4 Results And Discussion

The effect of interlayers on ultimate compressive strength and dissipated energy was investigated. Reference carbon fiber reinforced composite laminates with $(0/90)_{25s}$ lay-up sequences and the laminates interlayered by P(St-*co*-GMA) nanofibers were subject to high strain-rate deformation in through-the-thickness and side-to-side (in-fiber-plane) directions. Furthermore, fiber-matrix interface strengthening mechanism and its influence on strength and dissipated energy were also explored by varying the strain rates. As the strain rate is sensitive to the entry gas barrel pressure (impact pressure of the striker on the input bar), it was alternated at 2, 4 and 6 bar which corresponds to the strain rates of 2600 s^{-1}, 3500 s^{-1}, 4000 s^{-1}, respectively (see Figure 3a). Two high-speed cameras were mounted to monitor the failure modes of the reference/neat and nano-interlayered composite laminates with $(0/90)_{50s}$ lay-up sequences, as seen in Figure 3b. Post-SEM analyses were used to trace the interface strengthening mechanism at the fracture surfaces.

3.2.4.1 Effects of Nanofiber Interlayers on High Strain Rate Stress–Strain Responses and Progressive Damage

The composite specimens tested through-the-thickness and longitudinally (in-fiber-direction) directions, as illustrated in Figure 4. First, engineering stress and strain were

measured until failure through-the-thickness direction (Figure 5a) where the high strain rate tests were conducted using a split Hopkinson bar at 4 bars which corresponds to strain rate of 3500 s^{-1} (Figure 5b).
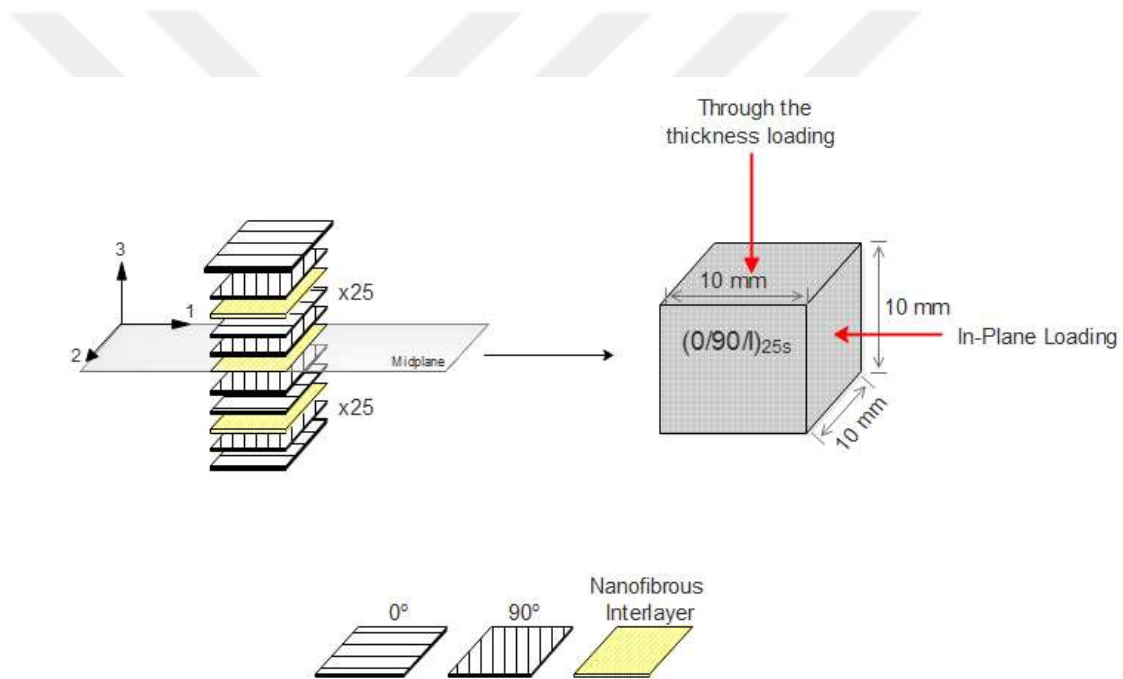
Figure 4: Illustration of interlayered ply sequences whereas the arrows indicated the incident impact direction through the thickness and side-to-side (in-fiber-plane) directions.

Figure 5a clearly demonstrated that incorporation of the nanofibers increases the ultimate compressive strength by about 13% without worthy to note weight penalty (which is as

low as 0.1%). Moreover, much higher energy (see Table 1) was dissipated through the thickness due to the presence of the surface reactive nanofibers between the plies.

Tarfaoui *et al*. [42] studied the effect of the reinforcing fiber orientation on mechanical properties of the laminated polymer composites subjected to out-of-plane high strain rate compressive loadings. They stated that damaging mode in composite laminates with $(0/90)_{40s}$ lay-up sequences was the result of the propagation of V shaped damage zone and subsequently forming macro-cracks led to failure. In nanofiber interlayered composites, improvement at the high strain rate can also be attributed to retardation of the formation and propagation of cracks by the presence the polymeric nanofibers between each plies in-line with the quasi-static behavior [13]. As seen in Figure 5a, stress versus strain curves were initially linear, and then to gradually became nonlinear up to the ultimate failure stress. Haque *et al*. [29] explained that the nonlinearity observed in the stress-strain plots results from the matrix-cracking and debonding. Same characteristics can also be noted in Figure 5a, as such the failure of the specimens is attributed to the macro-cracks and debonding due to out-of-plane loading. This behavior is also highlighted in post fracture analysis section. In order to examine the extent of damage during the dynamic compression, high-speed photography was used to follow the damage in the samples, as seen in Figure
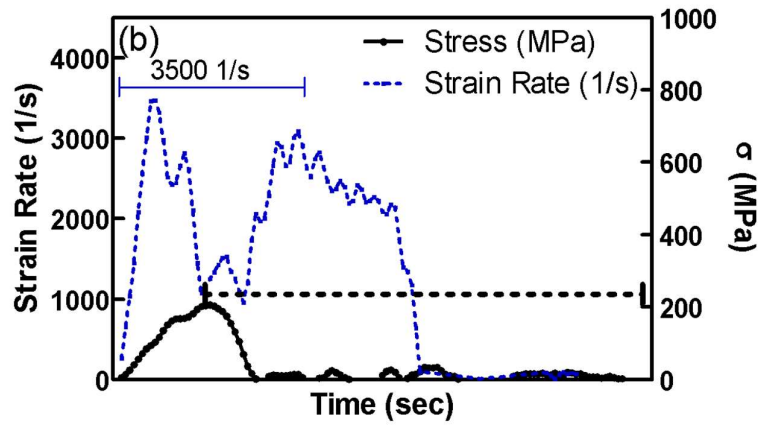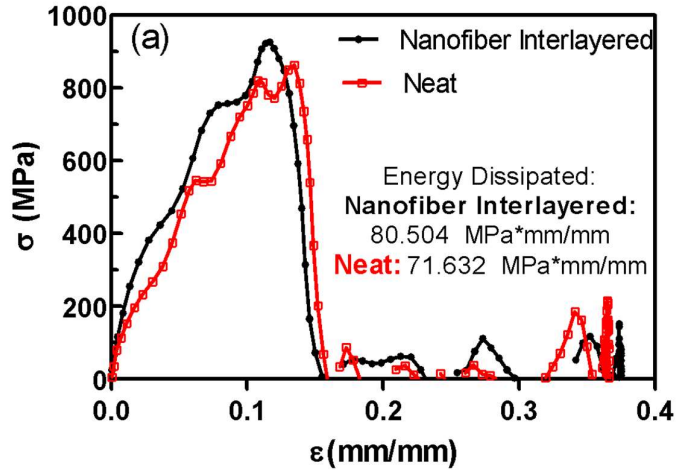
Figure 5: (a) Stress–strain (σ–ε) and (b) Strain rate and stress versus time plots of neat $(0/90)_{25s}$ and nanofiber interlayered $(0/\,90/I)_{25s}$ laminates through thickness loading at strain rate of 3500 s^{-1}

Figure 6 shows progressive damage of nanofiber interlayered $(0/90)_{25s}$ composites with applied load in the thickness direction at strain rate of 2600 s^{-1}, the images are taken from *Camera 1*.
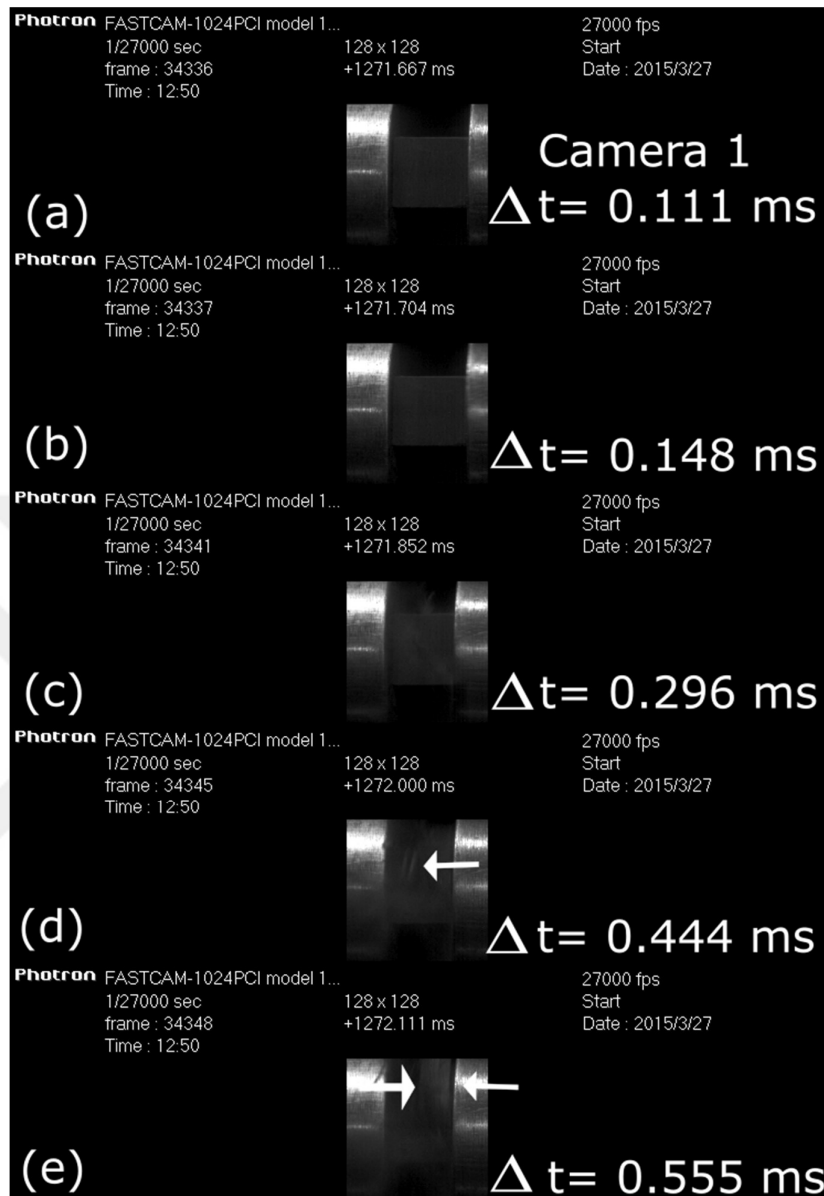
Figure 6: Progressive damage of nanofiber interlayered $(0/90)_{25s}$ laminates with applied load in thickness direction at strain rate of 2600 s^{-1}, high speed photography images are taken from mounted *Camera 1*. (t=0, time of impact)

In supporting information (supporting videos 1-4), real-time video of both neat/reference and nanofiber interlayered $(0/90)_{25s}$ composites are also provided in both directions. The reference $(0/90)_{25s}$ composite specimens break into individual ply

pieces, this leads to extensive matrix cracking and resulting extensive fiber splitting, and debonding [29].
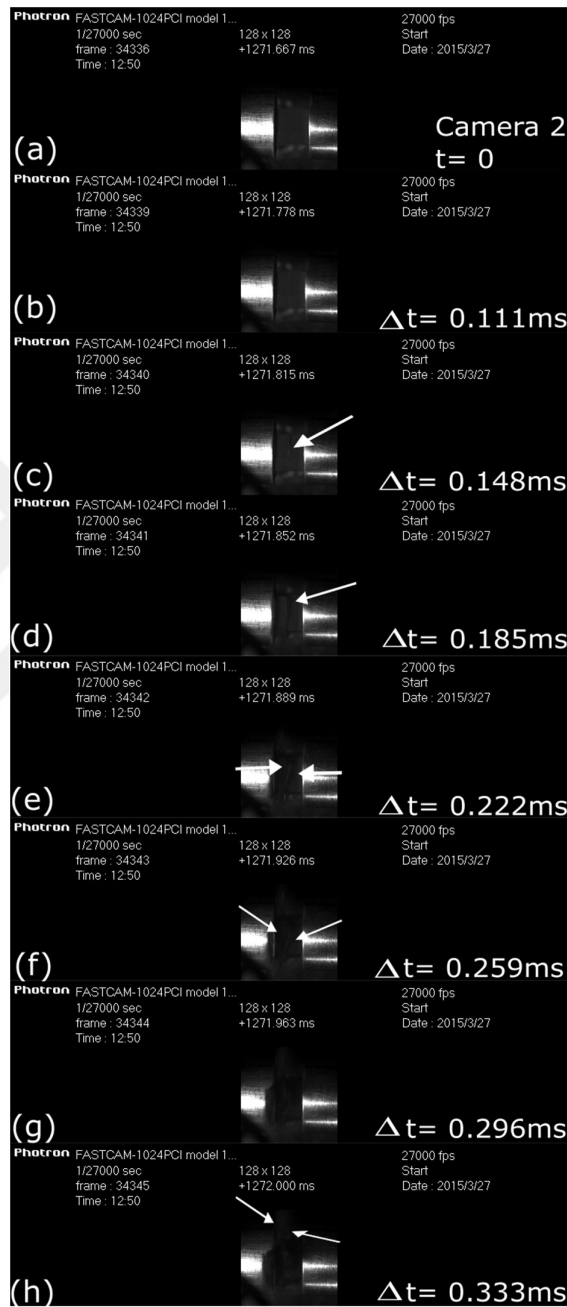
Figure 7. Progressive damage of nanofiber interlayered $(0/90)_{25s}$ composites with applied load in thickness direction at strain rate of 2600 s^{-1}, high speed photography images are taken from mounted *Camera 2*. (t=0, time of impact)

Thus, the composites without the interlayer toughening exhibit lower ultimate compressive strength and dissipation energy at all strain rates (Table 1). As seen in Figure 6 (*Camera 1*) and Figure 7 (*Camera 2*), plies are attached much

stronger in the case of nanofiber interlayered composites compared to reference specimens. Stronger interfacial bonding provides higher ultimate compressive strength (~up to 13%) in the layer-to-layer direction. Ply-block fragmentation was observed in nanointerlayered specimens, and led to delayed matrix cracking in the failure process. The observations suggest that the nanofibers incorporated at the ply-interfaces assist energy dissipation during high rate damage progression and cause higher ultimate compressive failure strength. Haque *et al.* [29] also noted that the failure mode in through the thickness direction was mostly matrix dominant.

Neat and nanofiber interlayered $(0/90)_{25s}$ composites were also tested subject to in-plane loading (loading is in-plane of the plies) to examine the matrix cracks and delamination which occur in the privileged interlaminar planes for this loading direction [42]. Figure 8 shows the stress–strain (σ–ε) plots of neat and nanofiber interlayered $(0/90)_{25s}$ composites in-plane loading at strain rate of $3500 \ s^{-1}$. Compared to Figure 5a, it is clear that for out-of-plane plane tests, both neat and nanofiber interlayered composites show greater ultimate strength and dissipation energy values. However, for the in-plane loading, the effect of nanofibers on ultimate compressive strength, failure strain and failure mechanism was much more remarkable. The compressive failure strength and the failure strains increased by almost 40% and 15%, respectively. Furthermore, the stress–strain (σ–ε) plots in Figure 8 were almost linear up to the maximum failure stress since the failure mode is primarily fiber dominant [29].
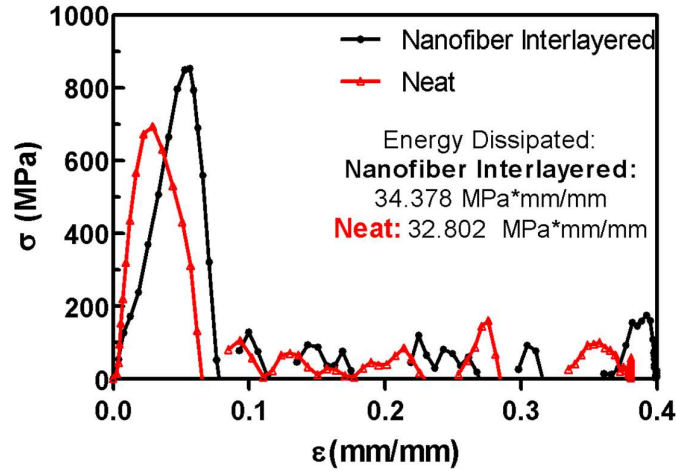
Figure 8. Stress–strain (σ–ε) plots of neat $(0/90)_{25s}$ and nanofiber interlayered $(0/90/I)_{25s}$ composites in-plane loading at strain rate of 3500 s^{-1}

Progressive damage of the neat and nanofiber interlayered $(0/90)_{50s}$ composites for in-plane loading at strain rate of 3500 s^{-1}, were monitored via *Camera 1 & 2*, as depicted in Figure 9 (a) and (b). When analyzed framewise through the recorded progression, as in Figure 9 (a) the initial form of damage occurring in neat laminates under in-plane compression was random matrix cracking either forming inside 90^0 plies or at 0/90 interlaminar regions. We should note that this damage formation was recorded as the progressive formation of random voids inside the specimens. The ultimate final failure of neat laminates was due to extensive delamination initiated from appearing matrix cracks. Nevertheless, the matrix crack formation and sudden catastrophic delamination behavior can be partly prevented by interlayer addition. Interlayered laminates have rather gone through layer kinking and layer compression resulting in delayed matrix cracking and micro-buckling in the failure process, as seen in Figure 9b. Thus, interlayered nanofibers resisted void-like formation between the plies, resulting in increased ultimate compressive strength and failure strain.

(a) Neat (0/90)$_{25s}$ composites
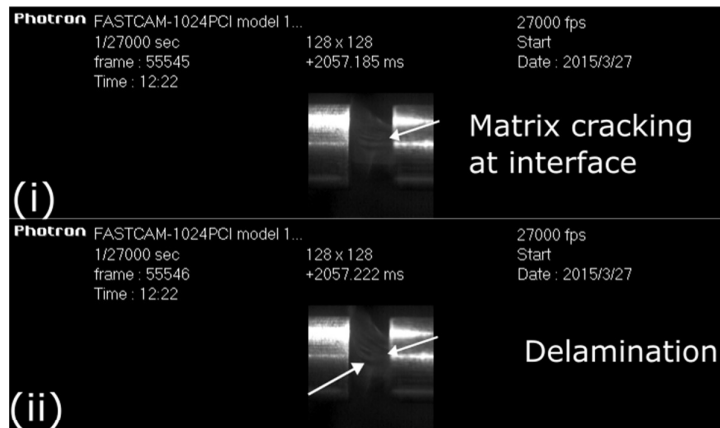
(b) Nanofiber interlayered (0/90/i)$_{25s}$ composites
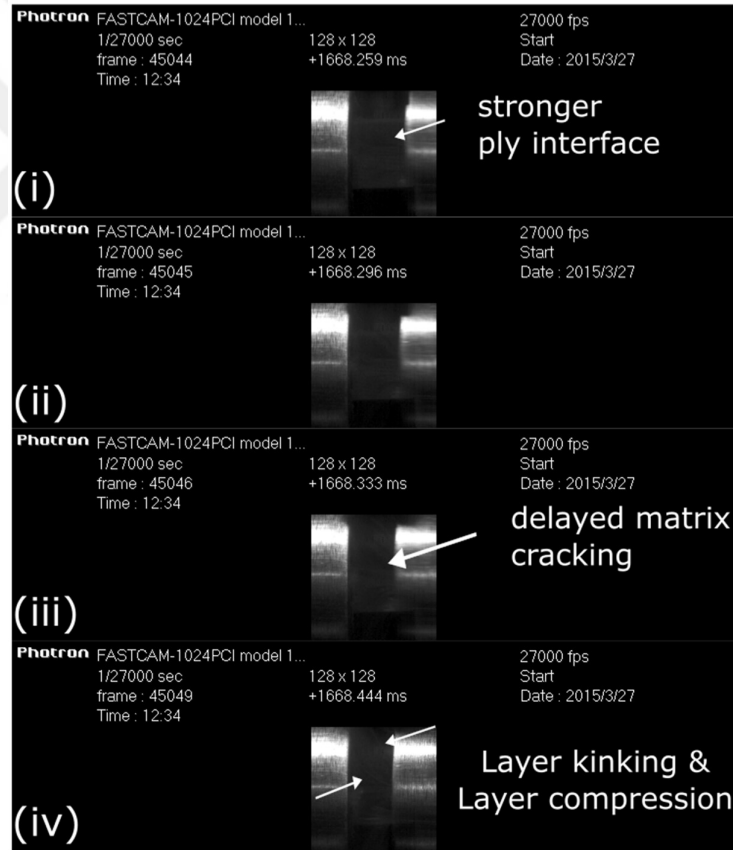
Figure 9. Progressive damage of (a) neat (0/90)$_{25s}$ and (b) nanofiber interlayered

(0/90/I)$_{25s}$ composites in in-plane loading at strain rate of 3500 s^{-1}, are monitored via

Camera 1.

3.2.4.2 Effects of Strain Rate on Stress–Strain Responses of Nanofiber Interlayered Composites

Strain rate dependency of ultimate strength and failure strain of laminated composites under compressive dynamic loading was shown, [42] but full understanding of the effect of strain rate not has not been established. This is arguably due to the different initiation and propagation of failure mechanisms in different the fiber types and architectures such as unidirectional and woven composites. Kara *et. al.* [33] expressed that the modulus and maximum stress of the (±45) symmetric E-glass/polyester composites increased with increasing strain rate. Yokoyama *et. al.* [21] pointed that the strain rate-ultimate compressive strength correlation was positive for the plain-weave glass/epoxy laminated composite, but negative for the cross-ply and plain-weave carbon/epoxy laminated composites whereas the ultimate compressive strain for all three laminated composites decreased marginally with the increasing strain rate.

The effect of strain rate on stress–strain responses of nano-interlayered composites was explored, to our knowledge for the first time. Through thickness and in-plane directions focused testing were carried out as seen in Figure 10a and Figure 10b, respectively. Results suggest that absorbed energy for both the reference/neat and nanointerlayered composites increased marginally with increasing strain rate (See Table 1). In addition, for the out-of-plane testing, neat and nanointerlayered composites demonstrated much greater ultimate strength and dissipation energy. In relevance, Tarfaoui *et al.* [42] expressed that the most pronounced effect of increasing the strain rate is the changes in the failure modes. All in all, composite specimens failed by fiber kinking at low rates while delamination and interfacial separation dominated at the higher strain rates [42].

Thus, the variations in ultimate strain pointed out different failure mechanisms depending on the strain rate, where laminated composites exhibited significant nonlinear and strain dependent behavior.
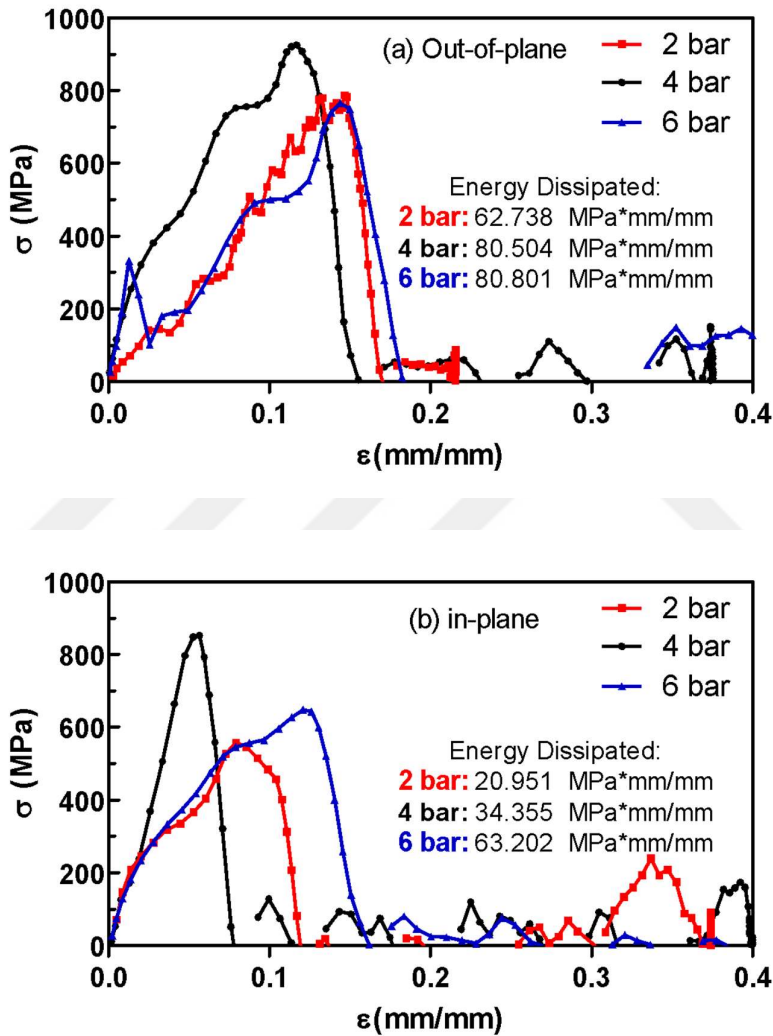
Figure 10. Stress–strain (σ–ε) plots of nanofiber interlayered $(0/90/I)_{50s}$ composites (a) through thickness (out-of-plane) (b) in-plane loading at strain rate of 2600 s^{-1}(2 bar), 3500 s^{-1}(4 bar), 4000 s^{-1}(6 bar).

Table 1: Strain rate dependencies of neat $(0/90)_{25s}$ and nanofiber interlayered $(0/90/I)_{25s}$ composites. Ultimate compressive strength (MPa) and dissipated energy values are reported at both directions.

Specimen	Gas Barrel Pressure	Ultimate Compressive Strength (MPa)	Dissipated Energy (MPa*mm/mm)
		Through Thickness Loading	
$(0/90)_{25s}$	2 bar	481±5	45.2±3
$(0/90)_{25s}$	4 bar	820±3	71.6±3
$(0/90/I)_{25s}$	2 bar	788 ±5	62.7±2
$(0/90/I)_{25s}$	4 bar	925±5	80.5±2
$(0/90/I)_{25s}$	6 bar	766±8	80.8±5
		In-plane Loading	
$(0/90)_{25s}$	2 bar	524±5	11.7±5
$(0/90)_{25s}$	4 bar	606±5	32.8±4
$(0/90/I)_{25s}$	2 bar	558±8	21.0±6
$(0/90/I)_{25s}$	4 bar	852±8	34.4±8
$(0/90/I)_{25s}$	6 bar	648±11	63.2±11

3.2.4.3 Post Fracture Analysis

Fracture of the neat laminates under high strain loading was explosive. All of the tested laminates were instantaneously burst apart into very small dust like particles. Hence no surfaces suitable for fractography were left to collect. On the other hand, interlayered

specimens responded to the high pressure loading such that chunks of the cubic specimens have remained intact for which fracture surfaces can be accessible. As the interlayer toughening strategy was to introduce nanofibrous interlayers between each (0/90) block, interlayered specimens contained untoughened regions. Figure 11a and b corresponds to an untoughened 0-90 interlaminar region where the two plies were separated with a clear delamination onset. The damage propagation in that plane caused the formation of hackle markings of the epoxy matrix, typical for Mode II fracture events. Experimental observations suggest that the sudden high strain loading of the neat laminates caused extensive delamination followed by instantaneous compressive fiber and resin fracture. On the other hand, Figure 11c and d show the interlayer toughened (90-0) ply interface where the resin morphology was highly altered due to the nanofibers/epoxy impregnation, forming nanocomposite interlayer. No hackle markings were found on the failure surfaces of the interlayer. This observation suggests the nanofibrous interlayers played a significant role in preventing severe delamination formation and helped the specimens to partially remain intact rather than bursting apart in contrast to the untoughened specimens. Furthermore, Figure 11e shows a fracture zone of a laminate where the fractured resin and reinforcing carbon fiber phases as well as the polymer nanofibers are clearly visible. Interconnected sight of the nanofibrous mat between fractured resin chunks also underlined their significant role in matrix/interlayer toughening even under high strain loading conditions.
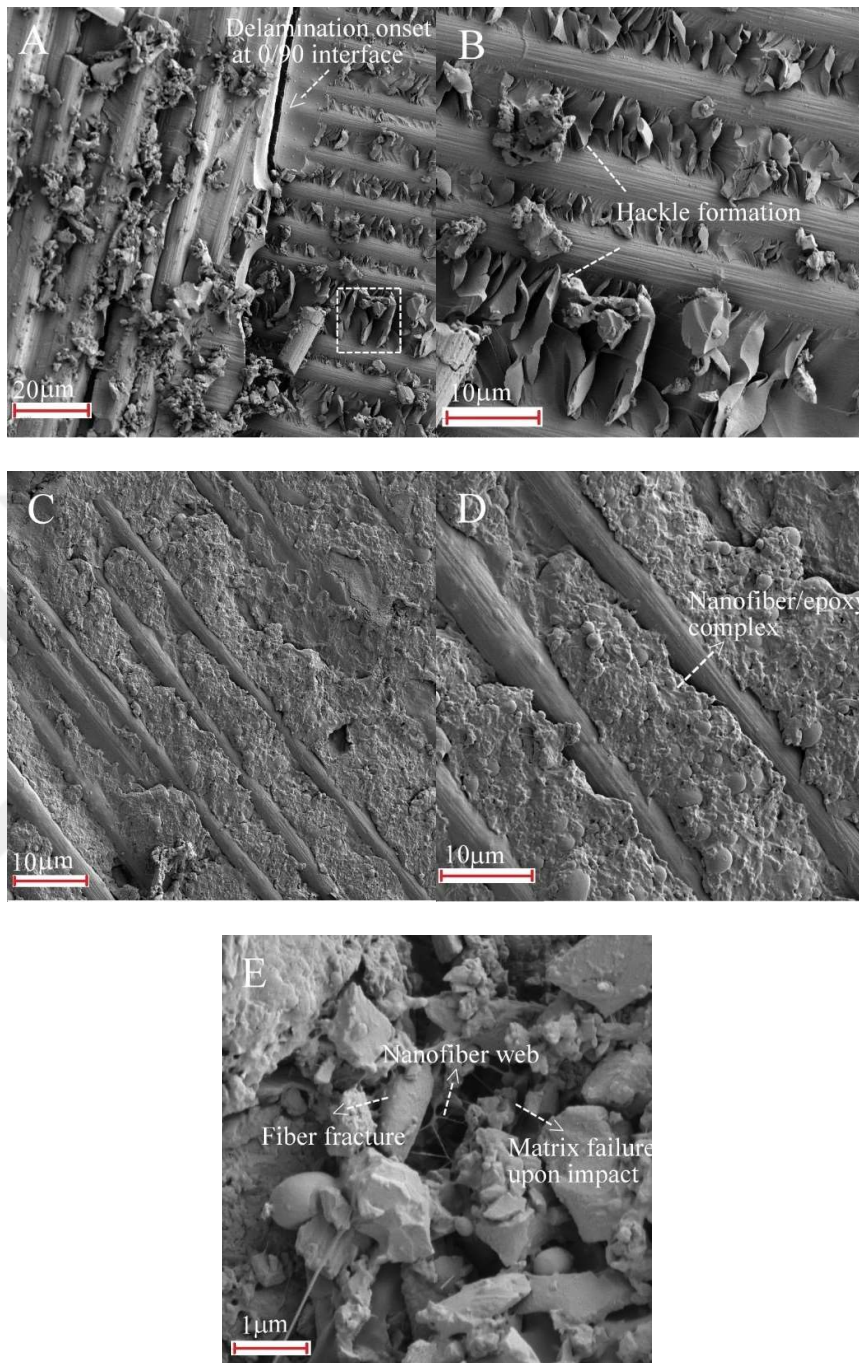
Figure 11: a,b) Unreinforced 0/90 interface and **c,d)** Nanofiber reinforced 90/0 interface

for interlayered laminates. e) A randomly fractured composite part showing all of the

constituents

3.2.5 Conclusion

High strain rate response of the carbon fiber reinforced composite laminate of $(0/90)_{25s}$ stacking sequence and its toughened counterpart by P(St-*co*-GMA) nanofibrous interlayers were investigated both for in-plane and through the thickness loadings via SHPB. The compressive stress–strain behavior of the laminates was shown to be strain rate sensitive. Nanofibrous interlayered laminate was superior in regard to the through-the-thickness compressive characteristics at all high rates of strain tested in this study. Through-the-thickness, reference $(0/90)_{25s}$ composite specimens broke into individual ply pieces caused by extensive matrix failure leading to delamination and fiber fracture. Whereas block-of-plies fragmentation was observed in nanointerlayered specimens due to stronger and tougher interlaminar bonding, resulting in suppression of matrix cracking and subsequent failure events. At the in-plane loading, the effect of nanofibers on ultimate compressive strength, failure strain and failure mechanism was much more remarkable, enhancement in the energy dissipation due to the nanofibrous interlayers is as high as 80% whereas 40% improvement was also recorded through thickness directions. Interlayer nanofibers are concluded to be resistive against crack formation between the plies, resulting in increased ultimate compressive strength and failure strain.

3.2.6 REFERENCES

[1] Tsotsis TK. Interlayer Toughening of Composite Materials. Polymer Composites. 2009;30:70-86.

[2] Pham S, Burchill PJ. Toughening of Vinyl Ester Resins with Modified Polybutadienes. Polymer. 1995;36:3279-85.

[3] Huang YJ, Horng JC. Effects of thermoplastic additives on mechanical properties and glass transition temperatures for styrene-crosslinked low-shrink polyester matrices. Polymer. 1998;39:3683-95.

[4] Warrior NA, Turner TA, Robitaille F, Rudd CD. The effect of interlaminar toughening strategies on the energy absorption of composite tubes. Composites Part a-Applied Science and Manufacturing. 2004;35:431-7.

[5] Ishai O, Rosenthal H, Sela N, Drukker E. Effect of Selective Adhesive Interleaving on Interlaminar Fracture-Toughness of Graphite Epoxy Composite Laminates. Composites. 1988;19:49-54.

[6] Carlsson LA, Aksoy A. Analysis of Interleaved End-Notched Flexure Specimen for Measuring Mode-Ii Fracture-Toughness. International Journal of Fracture. 1991;52:67-77.

[7] Khan SU, Kim JK. Improved interlaminar shear properties of multiscale carbon fiber composites with bucky paper interleaves made from carbon nanofibers. Carbon. 2012;50:5265-77.

[8] Ozden E, Menceloglu YZ, Papila M. Engineering Chemistry of Electrospun Nanofibers and Interfaces in Nanocomposites for Superior Mechanical Properties. Acs Applied Materials & Interfaces. 2010;2:1788-93.

[9] Ozden-Yenigun E, Menceloglu YZ, Papila M. MWCNTs/P(St-co-GMA) Composite Nanofibers of Engineered Interface Chemistry for Epoxy Matrix Nanocomposites. Acs Applied Materials & Interfaces. 2012;4:777-84.

[10] Kim JS, Reneker DH. Mechanical properties of composites using ultrafine electrospun fibers. Polymer Composites. 1999;20:124-31.

[11] Dzenis Y. Materials science - Structural nanocomposites. Science. 2008;319:419-20.

[12] Palmeri MJ, Putz KW, Ramanathan T, Brinson LC. Multi-scale reinforcement of CFRPs using carbon nanofibers. Composites Science and Technology. 2011;71:79-86.

[13] Bilge K, Ozden-Yenigun E, Simsek E, Menceloglu YZ, Papila M. Structural composites hybridized with epoxy compatible polymer/MWCNT nanofibrous interlayers. Composites Science and Technology. 2012;72:1639-45.

[14] Daelemans L, van der Heijden S, De Baere I, Rahier H, Van Paepegem W, De Clerck K. Damage-Resistant Composites Using Electrospun Nanofibers: A Multiscale Analysis of the Toughening Mechanisms. Acs Applied Materials & Interfaces. 2016;8:11806-18.

[15] van der Heijden S, Daelemans L, De Schoenmaker B, De Baere I, Rahier H, Van Paepegem W, et al. Interlaminar toughening of resin transfer moulded glass fibre epoxy laminates by polycaprolactone electrospun nanofibres. Composites Science and Technology. 2014;104:66-73.

[16] Bilge K, Papila M. 10 - Interlayer toughening mechanisms of composite materials A2 - Qin, Qinghua. In: Ye J, editor. Toughening Mechanisms in Composite Materials: Woodhead Publishing; 2015. p. 263-94.

[17] Bilge K, Venkataraman S, Menceloglu YZ, Papila M. Global and local nanofibrous interlayer toughened composites for higher in-plane strength. Composites Part a-Applied Science and Manufacturing. 2014;58:73-6.

[18] Magniez K, Chaffraix T, Fox B. Toughening of a Carbon-Fibre Composite Using Electrospun Poly(Hydroxyether of Bisphenol A) Nanofibrous Membranes Through Inverse Phase Separation and Inter-Domain Etherification. Materials. 2011;4:1967-84.

[19] Palazzetti R, Zucchelli A, Gualandi C, Focarete ML, Donati L, Minak G, et al. Influence of electrospun Nylon 6,6 nanofibrous mats on the interlaminar properties of Gr-epoxy composite laminates. Composite Structures. 2012;94:571-9.

[20] Zucchelli A, Focarete ML, Gualandi C, Ramakrishna S. Electrospun nanofibers for enhancing structural performance of composite materials. Polymers for Advanced Technologies. 2011;22:339-49.

[21] Yokoyama T, Nakai Y. High strain-rate compressive characteristics of carbon/epoxy laminated composites in through-thickness direction. Advances in Experimental Mechanics. 2004;1-2:11-6.

[22] Bi J, Xiao BL, Ma ZY. High strain rate superplastic deformation behavior of powder-metallurgy processed 17%SiCp/2024 Al composite. Acta Metallurgica Sinica. 2002;38:621-4.

[23] Chan KC, Wang CL, Zhang KF. Low temperature and high strain rate superplasticity of Ni-1 mass% SiC nanocomposite. Materials Transactions. 2004;45:2558-63.

[24] Chen DM, Wang G, Sun JF, Shen J. Deformation behavior of tungsten wires enhanced Zr-based bulk metallic glass composite at high strain rate. Acta Metallurgica Sinica. 2006;42:1003-8.

[25] Goldberg RK, Gilat A. Experimental and computational characterization of the high strain rate tensile response of polymer matrix composites. Composite Materials: Testing and Design, Fourteenth Volume. 2003;1436:207-23.

[26] Goldberg RK, Roberts GD, Gilat A. Incorporation of mean stress effects into the micromechanical analysis of the high strain rate response of polymer matrix composites. Composites Part B-Engineering. 2003;34:151-65.

[27] Greenfield MJ, Hunter TF, Kalika DS, Penn LS. Improvement of interfaces by tethered polymer chains. Part II: Evaluation of a particulate composite at very high strain rate. Journal of Composite Materials. 2001;35:175-86.

[28] Guden M, Hall IW. High strain rate deformation behavior of a continuous fiber reinforced aluminum metal matrix composite. Computers & Structures. 2000;76:139-44.

[29] Haque A, Ali M. High strain rate responses and failure analysis in polymer matrix composites - An experimental and finite element study. Journal of Composite Materials. 2005;39:423-50.

[30] Hu H, Zhen LA. High Strain Rate Superplastic Deformation Behavior of TiN(P)/2014Al Composite. Manufacturing Science and Engineering, Pts 1-5. 2010;97-101:1633-6.

[31] Iwasaki H, Mori T, Mabuchi M, Higashi K. Improvement of post-deformation properties by static annealing for a high strain rate superplastic composite. Advances in Engineering Plasticity, Pts 1-2. 2000;177-1:667-72.

[32] Iwasaki H, Yada Y, Mori T, Mabuchi M, Higashi K. Cavitation control by static annealing after deformation at a high strain rate of a Si3N4p/Al-Mg-Si composite. Scripta Materialia. 1996;34:1179-84.

[33] Kara A, Tasdemirci A, Guden M. Modeling quasi-static and high strain rate deformation and failure behavior of a (+/- 45) symmetric E-glass/polyester composite under compressive loading. Materials & Design. 2013;49:566-74.

[34] Kim W, Argento A, Lee E, Flanigan C, Houston D, Harris A, et al. High strain-rate behavior of natural fiber-reinforced polymer composites. Journal of Composite Materials. 2012;46:1051-65.

[35] Lee OS, Lee JY, Kim GH, Hwang JS. High strain-rate deformation of composite materials using a Split Hopkinson Bar technique. Fracture and Strength of Solids, Pts 1 and 2. 2000;183-1:307-12.

[36] liozberg YR, Hoy RS, Mrozek RA, Lenhart JL, Andzelm JW. Role of entanglements and bond scission in high strain-rate deformation of polymer gels. Polymer. 2014;55:2543-51.

[37] Luo XT, Yang GJ, Li CJ, Kondoh K. High strain rate induced localized amorphization in cubic BN/NiCrAl nanocomposite through high velocity impact. Scripta Materialia. 2011;65:581-4.

[38] Mabuchi M, Iwasaki H, Higashi K. An investigation of shear deformation in a semi-solid state of a high strain rate superplastic Si_3N_4p/Al-Mg-Si composite. Acta Materialia. 1998;46:5335-43.

[39] Mishra RS, Valiev RZ, McFadden SX, Islamgaliev RK, Mukherjee AK. Severe plastic deformation processing and high strain rate superplasticity in an aluminum matrix composite. Scripta Materialia. 1999;40:1151-5.

[40] Niu JT, Han LH, Hu H. High strain rate superplastic deformation of 30 vol.% ALN(P)/6061Al composite. Hot Deformation of Aluminum Alloys Iii. 2003:193-8.

[41] Salas PA, Benson DJ, Venkataraman S, Loikkanen MJ. Numerical Implementation of Polymer Viscoplastic Equations for High Strain-Rate Composite Models. Journal of Aerospace Engineering. 2009;22:304-9.

[42] Tarfaoui M, Choukri S, Neme A. Effect of fibre orientation on mechanical properties of the laminated polymer composites subjected to out-of-plane high strain rate compressive loadings. Composites Science and Technology. 2008;68:477-85.

[43] Wang LL, Sun ZJ. Studies on rate dependent damage evolution in polymer blends in high strain rates. Plastics Rubber and Composites. 2008;37:246-50.

[44] Demir MM, Horzum N, Tasdemirci A, Turan K, Guden M. Mechanical Interlocking between Porous Electrospun Polystyrene Fibers and an Epoxy Matrix. Acs Applied Materials & Interfaces. 2014;6:21901-5.

[45] Lee JH, Veysset D, Singer JP, Retsch M, Saini G, Pezeril T, et al. High strain rate deformation of layered nanocomposites. Nature Communications. 2012;3.

[46] Kolsky H. An investigation of the mechanical properties of materials at very high rates of loading. Proceedings of the Physical Society B. 1949;62:676-700.

[47] U.S. L. Some experiments with the split Hopkinson bar. J Mech Phys Solids. 1964;12:317-35.

[48] Sen O, Tekalur SA, Maity P. On the use of non-cylindrical specimens in a split-Hopkinson pressure bar. Journal of Strain Analysis for Engineering Design. 2011;46:866-78.

CHAPTER 4

DISCOVERY AND EXPANSION OF INTERLAYER MATERIAL LIMITS

4.1 Stabilized Electrospinning of Heat Stimuli/In-situ Cross-linkable Nanofibers and Their Self Same Nano-composites

4.1.1 Abstract

We present a strategy for stabilizing the morphological integrity of electrospun polymeric nanofibers by heat stimuli in-situ cross-linking . Amorphous polymer nanofibers, such as polystyrene (PS) and its co-polymers tend to lose their fiber morphology during processing at temperatures above their glass transition temperature (T_g) typically bound to happen in nanocomposite/structural composite applications. As an answer to this problem, incorporation of the cross-linking agents, phtalic anhydride (PA) and tributylamine (TBA), into the electrospinning polymer solution functionalized by glycidylmethacrylate (GMA) copolymerization, namely P(St-co-GMA), is demonstrated. Despite the presence of the cross-linker molecules, the electrospinning polymer solution is stable and its viscosity remains unaffected below 60°C. Cross-linking reaction stands-by and can be thermally stimulated during post-processing of the electrospun P(St-co-GMA)/PA-TBA fiber mat at intermediate temperatures (below the T_g). This strategy

enables the preservation of the nanofiber morphology during subsequent high temperature processing. The cross-linking event leads to an increase in T_g of the base polymer by $30\degree$C depending on degree of crosslinking. Cross-linked nanofibers are able to maintain their nanofibrous morphology above the T_g and upon exposure to organic solvents. In-situ crosslinking in epoxy matrix is also reported as an example of high temperature demanding application/processing. Finally a self-same fibrous nanocomposite is demonstrated by dual electrospinning of P(St-co-GMA) and stabilized P(St-co-GMA)/PA-TBA, forming an intermingled nanofibrous mat, followed by a heating cycle. The product is a composite of cross-linked P(St-co-GMA)/PA-TBA fibers fused by P(St-co-GMA) matrix.

KEYWORDS: Electrospinning, cross-linking, glass transition, nanofiber, self-same nanocomposite

4.1.2 Introduction

Thanks to versatility of electrospinning and tailorable properties of its products for a wide range of applications, the research efforts on nanofibrous structures have consistently increased over the years. One of the promising field of application is their usage as reinforcement materials in nanocomposites [1-7] and structural composites [8-29]. Morphology [30, 31], compatible chemistry [1,32,33] and high surface area of preferably polymeric nanofiber mats are crucial for the anticipated performance in such applications [34]. Comprehension of the proposed material choices, limits and their adaptation within conventional engineering processes should also be established for the coherent nanofiber based solutions. For instance, a relevant property especially in the case of highly amorphous polymers, is the glass transition temperature (T_g) as processing above which

(likely with the composite/nano-composite thermal processing cycles) can lead to distortion of the nanofibrous structure and morphology

Potential solution to this problem is to facilitate chemical cross-linking of the polymer. Cross-linking can be induced to readily available electrospun polymeric nanofibers by exposing them to the corresponding cross-linking medium [1, 35, 36]. Such an ex-situ implementation is arguably the conventional and direct way to achieve the cross-linked fibers. The major drawback of this method is that it causes permanent changes in chemistry and morphology of the nanofibrous structures prior to a subsequent application/integration step, e.g. their use as interlayers in the laminated composites (2, 8, 10). Alternatively, in situ cross-linking methodology is relatively new bulk cross-linking technique. The term "*in-situ*" comes from the fact that ingredients for the cross-linking are readily available "*in*" the base polymeric solution during electrospinning process [37-42]. The initiation of the cross-linking reaction is sought "*on-site*" by an external source of energy or stimuli (heat, UV light etc.). To the best of our knowledge, main problem for the proposed in-situ cross-linking methods in the literature is that they either require extra instrumentation or the continous/stable electrospinning time is limited [42,43] due to increasing solution viscosity in the presence of cross-linking agents.

Present work offers a unique in-situ cross-linking mechanism which stands by at the room/regular operating temperature or lower and allows the continuous electrospinning from the polymer solutions. The crosslinking mechanism is activated by a designed heat stimulus so that electrospun nanofibers can keep the pristine morphological characteristics at elevated temperature uses/applications. Hence it is both possible to incorporate amorphous nanofibrous reinforcement into conventional raw composite materials (such as resin film and prepregs) at room temperature and then follow required

processes (e.g. curing of epoxy) at elevated temperatures without the loss of nanofibrous morphology.

Efficiency of this method is exemplified in the use of highly amorphous PS which was firstly functionalized by GMA copolymerization The choice was made due to the fact that the fibrous network/mat is likely to lose the morphology when further processed above its T_g. The effect of the temperature increase on the nano-structure of P(St-co-GMA) nanofibers is shown by SEM analyses of samples treated beyond the polymer T_g (around 100°C). To circumvent the unwanted morphological changes, additions of an anhydride chemical cross-linking agent, PA (phatalic anhydride) and an appropriate tertiary amine catalyst, TBA (tributylamine) are herein considered. Continuously processable and yet heat stimuli- crosslinkable P(St-co-GMA) electrospun nanofibers were produced. Chemical cross-linking reaction onset temperature was found to be 60°C, that is sufficiently far below the polymer T_g, as suggested in different epoxy/anhydride/tertiary amine cross-linking studies [19-22]. Any cross-linking reaction at the room temperature that can easily hinder consistent electrospinning due to an increase in solution viscosity is avoided. The stoichiometric ratio (R), PA volume with respect to the available epoxide rings in GMA groups, is tuned for maximum cross-linking and minimum morphological change above the T_g. Cross-linking characteristics and efficiency is measured by FTIR and swelling tests. Also a systematic investigation of the temperature –morphology relation is presented by calorimetric and scanning electron microscopy (SEM) analyses. The implementation and potential of the in-situ crosslinking mechanism was demonstrated in two case studies. In the first demonstration, heat stimuli crosslinkable nanofibers were introduced onto high temperature curing epoxy surfaces. The last demonstration was done by the manufacturing of a self-same composites of uncross-linked and in-situ cross-linkable nanofibers by dual electrospining.

126

4.1.3. Experimental

4.1.3.1 Copolymer Synthesis and Crosslinking Agents.

The purified monomers of styrene (St) and glycidylmethacrylate (GMA), solvents dimethylformamide and methanol, initiator azobisisobutyronitrile (AIBN) were purchased from Aldrich Chemical Co. Free radical solution polymerization technique was used for copolymer P(St-co-GMA) synthesis. Styrene and GMA (by mole fractions m=0.9styrene and n=0.1GMA) were mixed at the round bottom reaction flask contained in an ice bath. Dimetylformamide (DMF) was then added into reaction flask with a 3:2 volume proportion solvent to monomer. The initiator AIBN was then added into monomer solvent mix and the reaction flask flushed with nitrogen.

The tube containing the dissolved monomers was then kept for 5 days in the constant temperature bath at 65˚C for the polymerization reaction. Finally, the polymer solution was poured out by drop wise into a beaker containing methanol and the methanol/polymer mixture was filtered and dried in a vacuum oven at 60˚C for 1 day. The synthesized P(St-co-GMA) copolymer structure was determined by proton magnetic resonance spectroscopy (^{1}H-NMR). Molecular weights and polydispersities (PDI) were measured by a gel permeation chromatography (GPC) system and the molecular weight recorded as 220,000 g/mole with 1.54 PDI. As for the in-situ crosslinking mechanism, the polymer solution recipe incorporates PA (phatalic anhydride) and an appropriate tertiary amine catalyst, TBA (tributylamine), puchased from   Sigma Aldrich.

4.1.3.2 Electrospinning

In the framework for developing heat-stimuli in-situ crosslinking mechanism, we also aimed to optimize the process and material parameters so that the electrospining is

continuous and forming bead-free nanofibers. Associated screening study was further discussed in the results section.

Execution of typical electrospining procedure used throughout this work can be summarized as follows i) electrical charge (via Gamma high voltage ES 30P-20W) was applied to polymer solutions contained in 2 mL syringe, which has an alligator clip attached to the blunt stainless steel syringe needle (diameter 300 μm). ii) The grounded collector covered with aluminum foil and a syringe pump (NewEra NE-1000 Syringe Pump) was used. iii) The applied voltage, solution flow rate and tip to collector distance were set at 15 kV, 0.4 ml/h, and 10 cm respectively during the electrospinning. In the absence of crosslinker agents, the electrospinning parameters were chosen as reported in our previous works [1,8,32,33] (See table 1) where the applied voltage was 10kV and polymer solution concentration was 30 wt%.

4.1.3.3 Thermal Characterization

The thermal properties of reference P(St-co-GMA) nanofibers along with stabilized P(St-co-GMA)/PA-TBA (prior to a heating scheme- SC, cross-linking stands by) and cross-linked P(St-co-GMA)/PA-TBA (posterior to the heating scheme- C) nanofibers were characterized with differential scanning calorimetric analyzer (Netzsch DSC 204). An initial study aiming to determine onset and peak temperatures of the cross-linking reaction was performed on the stabilized (SC)-P(St-co-GMA)/PA-TBA nanofibers with R=2. The sample as received was analyzed by DSC as such the heat stimuli cross-linking reaction was triggered during the thermal scan in N_2 environment. Figure 1 shows the reaction graphic for P(St-co-GMA)/PA-TBA nanofibers (R=2). The first heating cycle demonstrate that the exothermic reaction was acquired and the onset, peak and end

temperatures are 65 ºC, 125 ºC, 150 ºC respectively. The second thermal cycle resulted in neither an exothermic nor endothermic reaction, it only revealed glass transition temperature (T_g: 135 ºC). According to these characteristics the cross-linking reaction occurs exothermically, subsequent cycle shows after a heating cycle there is not an exothermic reaction pattern therefore it can be concluded that the cross-linking reaction was completed.
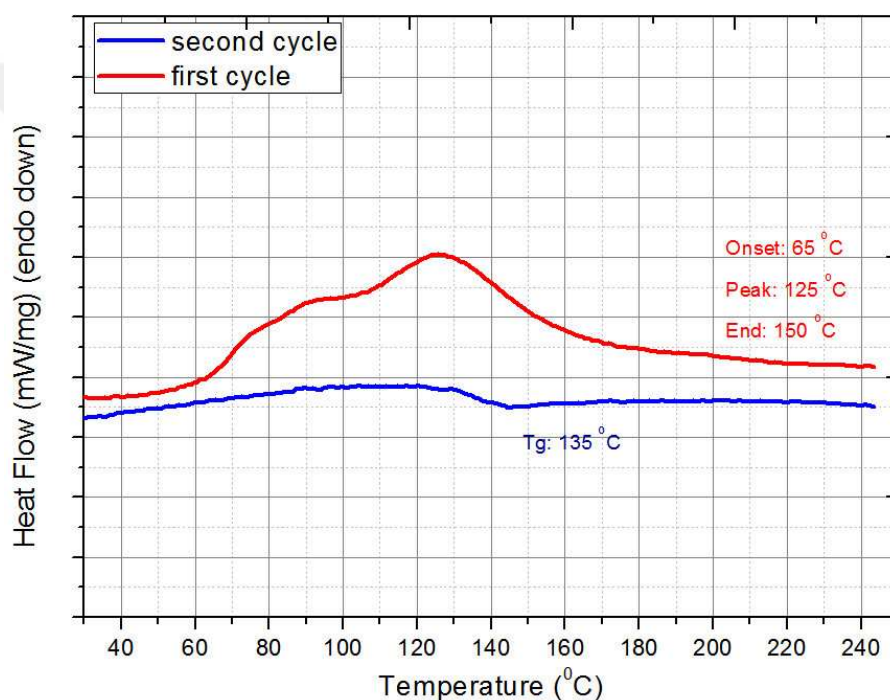
Figure 1 : two subsequent cycled DSC analysis for stabilized (SC)-P(St-co-GMA)/PA-TBA nanofibers with R=2

This preliminary study showed that by the proposed cross-linking strategy we are able to crosslink P(St-co-GMA) nanofibers far below their T_g around 100°C [1] (figure 5). Note that, this characterization may not precisely reflect the thermal nature of the reaction in a real life application such as curing of polymeric composites since the overall reaction is not carried out in an inert gas ambient in contrast to DSC.

By referring to the observed onset and peak temperatures, P(St-co-GMA)/PA-TBA nanofibers were also crosslinked during a post heat treatment in an oven after electrospinning. The heat cycle was 2 hours at 90 ºC (just below polymer T_g to prevent morphological changes), and ramping up to 150 ºC (above T_g) at 2 ºC/min heating rate to dwell for 1 hour at 150 ºC. Cross-linked (C)-P(St-co-GMA)/PA-TBA nanofibers were then studied by DSC within a single heat cycle. Glass transition temperatures for different samples with R= 1, 2, 5, 10 are reported.

4.1.3.4 Viscosity Measurements

Viscosity of the stabilized (SC)-P(St-co-GMA) nanofibers were determined via Anton Paar MCR302 rheometry with a shear rate control of 1-100 1/s through a gap size of 0.208 mm.

4.1.3.5 Spectroscopic Characterization

The structures of stabilized (SC)- and cross-linked (C)-P(St-co-GMA)/PA-TBA nanofibers were characterized by Attenuated Total Reflection Fourier transform infrared spectroscopy (ATR-FTIR). Analyses were performed with Thermo Scientific iS10 FT-IR Spectrometer in the mid-infrared 4000 cm^{-1} to 550 cm^{-1}.

4.1.3.6 Swelling Tests

The degree of cross-linking was determined by sol-gel analysis. Cross-linked (C)-P(St-co-GMA)/PA-TBA fibers were put into an aggressive solvent (DMF) effective on the base system P(St-co-GMA) and kept soaked for 72 hours at room temperature. The swollen fibers were then cleaned with DMF and de-ionized water which was followed by

drying step in a vacuum oven at 70°C. Cross-linking ratio is determined by measuring the gel fraction available in the specimens as follows :

% gel fraction = 100 - [((m_i – m_f) / m_i)* 100

where m_i and m_f corresponds to the initial mass and the dried mass of the sample respectively.

4.1.3.7 Microscopic Characterization

The morphologies of stabilized (SC) P(St-co-GMA)/PA-TBA and cross-linked (C) P(St-co-GMA)/PA-TBA electrospun mats were compared. Scanning electron microscope. SEM LEO 1530VP was utilized employing secondary electron detector and in-lens detector at 2-5 kV after coating the specimens with Au-Pd for better electrical conduction. The fiber diameter analyses were carried out using ImageJ software.

4.1.4. RESULTS AND DISCUSSION

4.1.4.1 Electrospinning Process Parameters for Continuous and Bead Free Crosslinkable Nanofibers

In presence of the reaction initiator and cross-linking agent it is essential to avoid any premature cross-linking reaction which can obstruct the electrospinning process. Therefore, we performed a preliminary screening study (see Table 1) to determine correct amounts of these agents so that the polymer solution is continuously electrospinnable without any viscosity problems at fixed process parameters.

Table 1: Electrospinnability of different polymer solutions with different initiator ratio, crosslinking

Initiator Ratio (TBA/Polymer by weight)	Solution Concentration (Polymer/DMF by weight)	Cross-linking agent Ratio (R) (PA/GMA functional group ratio)	Nanofiber Formation	Electrospinability Time (Reason if = 0)
0.1 %	10%	1	N	0
		2	N	
		5	N	
		10	N	(Bead formation due to low solution viscosity)
	15 %	1	Y	> 4 days
		2	Y	> 4 days
		5	Y	> 4 days
		10	Y	> 4 days
	20 %	1	Y	< 2 hours
		2	Y	< 1 hours
		5	N	0 (Pre-mature cross-linking)
		10	N	0 (Pre-mature cross-linking)
	30 % [1,8,32,33]	1	N	0
		2	N	
		5	N	(Pre-mature cross-linking)
		10	N	
0.2 %	All combinations	All combinations	N	0 (Pre-mature cross-linking)

Table 1 suggests that the excessive catalyst TBA/polymer ratio in electrospinning may not be tolerated by tuning the overall solution concentration. With the addition of 0.2 wt.% TBA, the polymer solution suffered from pre-mature cross-linking as such the electrospinning process was not applicable regardless of the solution concentration. Hence the first decision was to decrease its set value to nominal 0.1 wt.%. More

practically, the amount of TBA corresponds to a single drop of TBA from a Pasteur pipette. The effect of the cross-linking agent (PA) amount, was monitored in reference to the molar ratio of available active sites (epoxide ring) of P(St-co-GMA) in the solution. Four PA/Epoxide ring molar ratios, R, at 1, 2 ,5 and 10 were investigated. For instance R=5 means that the mole number of PA added to P(St-co-GMA)/DMF solution is 5 times more than the mole number of available epoxide rings. In accordance with the PA ratio the solution concentration was also tuned. In our previously reported studies on P(St-co-GMA) [1,8,32,33] the solution concentration was fixed at 30 % resulting in stable nanofiber formation. However, in the presence of PA and TBA we were not able perform electrospinning continuously due to increased polymer viscosity and pre-mature cross-linking at room temperature depending on the choice of R. Hence the solution viscosity was scanned in the solution concentration range of 10-30 wt. %. At the lower end, the continuous nanofiber formation was not accomplished despite no pre-mature cross-linking. Instead polymeric beads were formed. . However, when the solution concentration was increased to 15 % the stable nanofiber formation was atainable and no-premature cross-linking was observed due to presence of TBA and PA (amounts given in Table 1). The electrospinning process at room temperature was continuous without any unfavorable changes in the fibrous jet formation until we stopped monitoring after straight 10 hours. These observations were supported by rheology measurements carried out on the polymer solutions after 4 days of storage at room temperature without any stirring application (shaded rows in Table 1, i.e polymer solutions with 15 % solution concentration with R=1, 2, 5, 10). Figure 2 shows the corresponding shear rate vs. viscosity measurements. As a result of these measurements, it can be deducted that the crosslinking at room temperature was standing by and there was not any viscosity change in the polymer solutions with increasing shear rates.
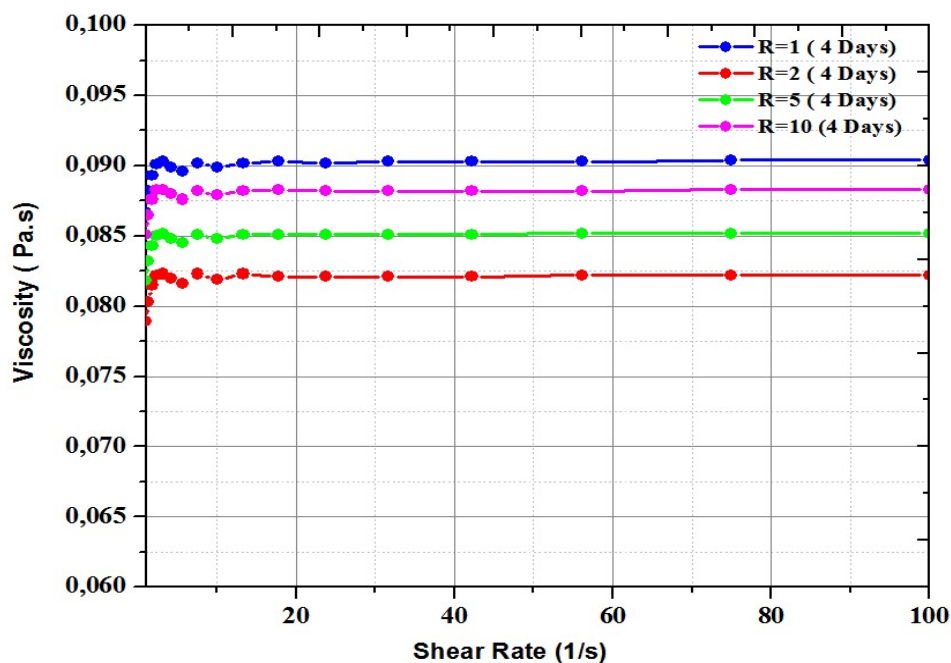
Figure 2: Preliminary viscosity vs. shear rate measurements for stabilized P(St-co-GMA)/PA-TBA nanofibers with R=1,2,5,10

4.1.4.2 Nature and Degree of Cross-linking

Proposed heat-stimulated reaction for the cross-linking of P(St-co-GMA)/PA-TBA is reported in [46].

FT-IR measurements were performed on samples of electrospun P(St-co-GMA)/PA-TBA nanofibers before and after the heat treatment. The samples were, so called here, stabilized (SC) and cross-linked (C), respectively, along with the reference P(St-co-GMA) nanofibers. The results confirmed the anticipated cross-linking and its dependence to the ratio R. Figure 3 shows the FT-IR spectra for nanofibers indicating the effect of various R ratios. The characteristic bands of the reaction are at 1851 cm^{-1} and 1787 cm^{-1}

[$\nu_{s,(C=O)}$ and $\nu_{as,(C=O)}$ of the anhydride ring], 902 cm^{-1} [$\nu_{s,(C-O)}$ overlapping epoxide (907 cm^{-1}) and anhydride (902 cm^{-1}) absorptions]. The intensities of these characteristic peaks decrease due to the reacting species during the cross-linking (SC vs. C). On the other hand, they increase with the increasing PA/Epoxide ring ratio R from 1 to 5 among the stabilized nanofibers (not heat treated).

Moreover, the characteristic epoxide ring stretching at 902 cm^{-1} remains distinguishable after the cross-linking reaction due to the remaining oxirane ring moiety. But, these moieties decay with the increasing PA/Epoxide ring ratio due to larger extent of the cross-linking. Additionally intensity of the peak at 1727 cm^{-1} [$\nu_{s,(C=O)}$ ester] increases with the formation of the ester groups, which is also a proof of the anticipated cross-linking [47-49].
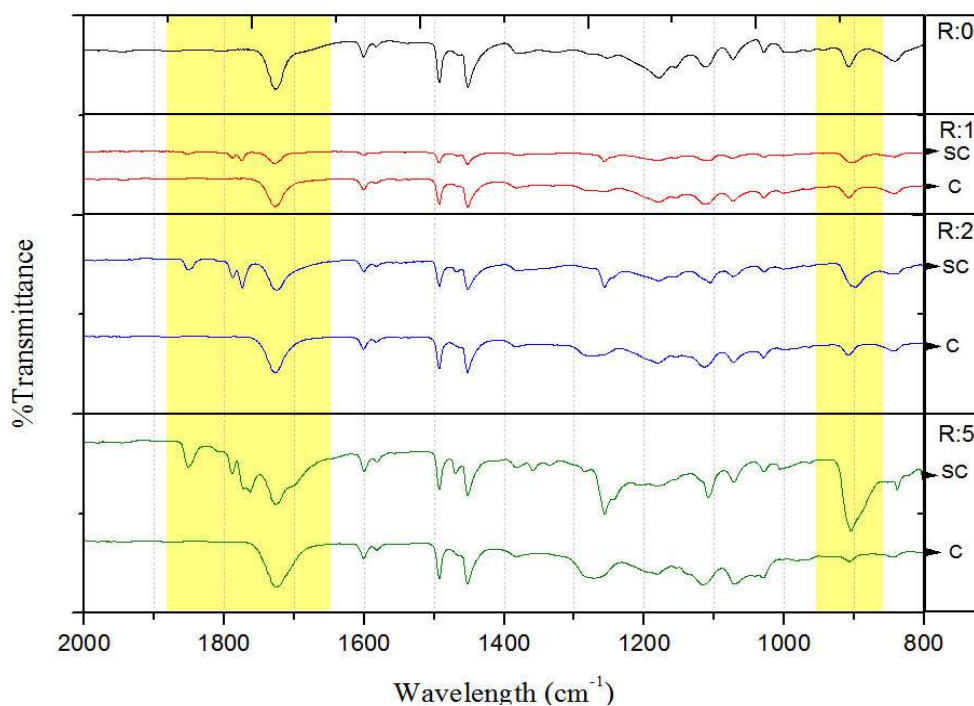
Figure 3: FT-IR spectrum of P(St-co-GMA) (R:0), stabilized (SC) and cross-linked (C) P(St-co-GMA)/PA-TBA nanofibers. Each boxed out row includes stabilized (above) and

cross-linked (below) nanofibers' spectrum pairs for an identical PA/Epoxide ring ratio marked at the right column of the graph. Shaded areas involve characteristic bands of the system.

Swelling test results also confirmed that the chemical cross-linking is achievable with applied heating scheme. They showed that the gel fraction for cross-linked nanofibers increased from 95% to 98.3% (Table 2) with increasing R ratio whereas the reference P(St-co-GMA) nanofibers were completely soluble in DMF solutions. Swelling associated morphological features/changes are shown by SEM images (Figure 3) after storing the nanofibers in DMF solvent.

Table 2: Gel fraction, glass transition temperature and average fiber diameter values for cases considered in the study.

PA/GMA Molar Ratio	Gel Fraction (%)	Glass Transition Temperature (T_g)	As spun average Fiber Diameter (nm)	Above T_g average fiber diameter(nm)
R=0 (un-crosslinked)	-	98±4	450±40	-
R=1	95	103±9	270 ±65	320±150
R=2	97.7	111±8	250±80	310±105
R=5	98.2	128± 4	320±100	310±90

They suggest that the nanofibrous microstructure becomes stable and is preserved as the degree of cross-linking increases. It can be noted that the cross-linked nanofibers, which are with a PA/GMA ratio R=5, are arguably unaffected by the solvent exposure. Transformation into the ribbon-like or notably swelled fibrous morphology was avoided unlike in cases of R=1 and R=2, respectively, for which the swelling with surface erosion [11] is considered to be the root-cause.
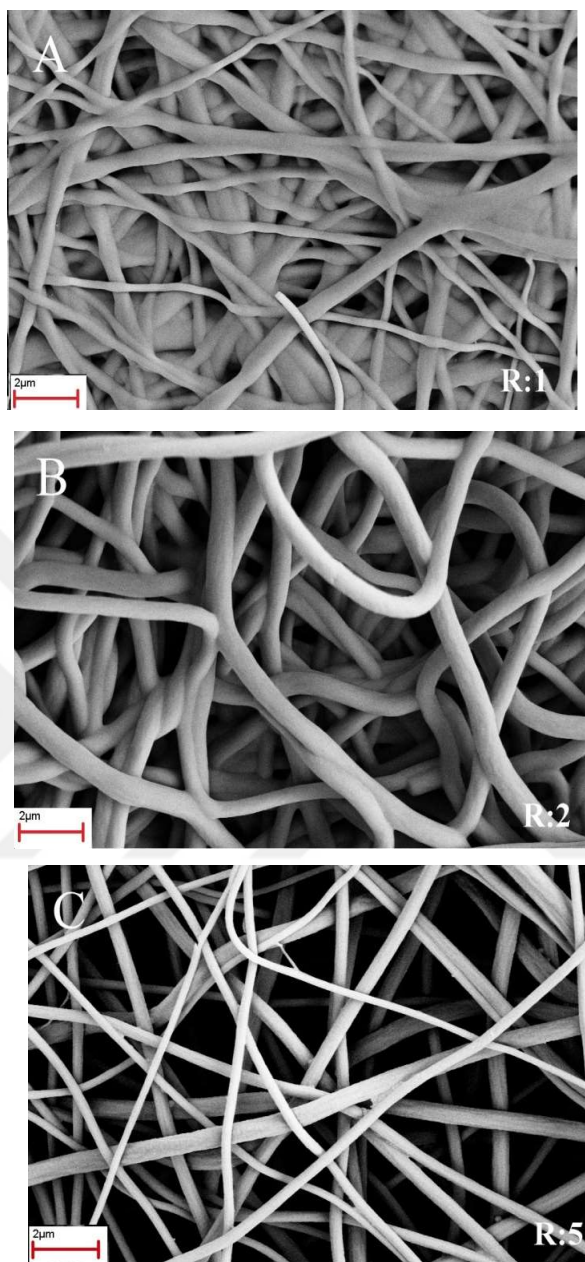
Figure 4: SEM micrographs of P(St-co-GMA)/PA-TBA nanofibers with PA/GMA ratios R:1(a) , R:2 (b) and R:5 (c) after immersion in DMF 72 h.

4.1.4.3 Glass Transition: Overcoming the Barrier

The DSC analyses of the cross-linked P(St-co-GMA)/PA-TBA (after the heating scheme applied) and reference P(St-co-GMA) nanofibers were carried out in order to identify the effects of the cross-linking on the thermal transitions (Figure 5). Glass transition temperature was raised from 98 ºC (reference by P(St-co-GMA) sample) up to 128 ºC with the increasing PA/Epoxide ring ratio R. This is attributed to the decreasing flexibility of polymer chains with the increasing extent of the cross-linking.
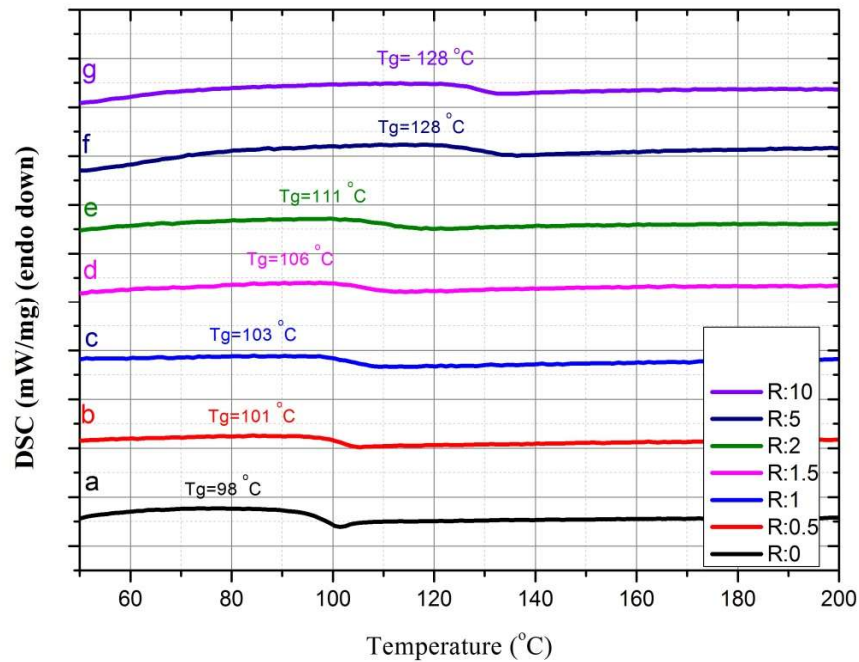
Figure 5: DSC curves of uncross-linked P(St-co-GMA) (a, R:0) and crosslinked (b-g) P(St-co-GMA)/PA-TBA nanofibers. PA to epoxide ring ratio (R) for b-g 0.5, 1, 1.5, 2, 5, 10 respectively.

Beyond R=5, the cross-linker amount can be considered saturated in regard to the resultant cross-linking density and associated thermal stability, that is the cross-linking ratio was found to converge and remained unchanged despite increase of PA. It is also important to point out that with the applied heating cycle on the nanofibers cross-linking reactions were complete as such no distinguishable exothermic reaction peak was observed in the individual DSC runs.

Fiber morphologies of the reference P(St-co-GMA), stabilized (SC) P(St-co-GMA)/PA-TBA and cross-linked (C) P(St-co-GMA)/PA-TBA nanofibers were examined for the selected PA/Epoxide ring ratios R. The SEM images of the nanofibers prior and posterior to the heat treatments are given in figure 6. Fiber diameter distribution charts are also attached onto the images. Recall that (section 2.2) applied voltage for no-crosslinker case (R=0) was 10kV in compliance with our earlier work (8, 32, 33), whereas 15kV was found to work better for homogenous fiber formations in the cases of the crosslinking agent (R=1, 2, 5: less spread in the fiber diameter can be noted in figure 6.d, g, 300-400nm). Despite the increased voltage no disruptive jet instability was observed. The morphological change along with the preserved continuity of the jet can be attributed to the increase in the electrostatic repulsive forces in the existence of cross-linker agents [50,51]

Substantiating our motivation for this work, un-crosslinked/reference P(St-co-GMA) nanofibers were found losing their form/morphology when processed above their glass transition temperature $T_g \approx 100^0C$ (figure 6c).

	Prior to heat treatment	After heat treatment at 90 ºC 2h	After additional post heat treatment at 150 ºC 1h
R:0	A	B	C
R:1	D	E	F
R:2	G	H	I
R:5	J	K	L
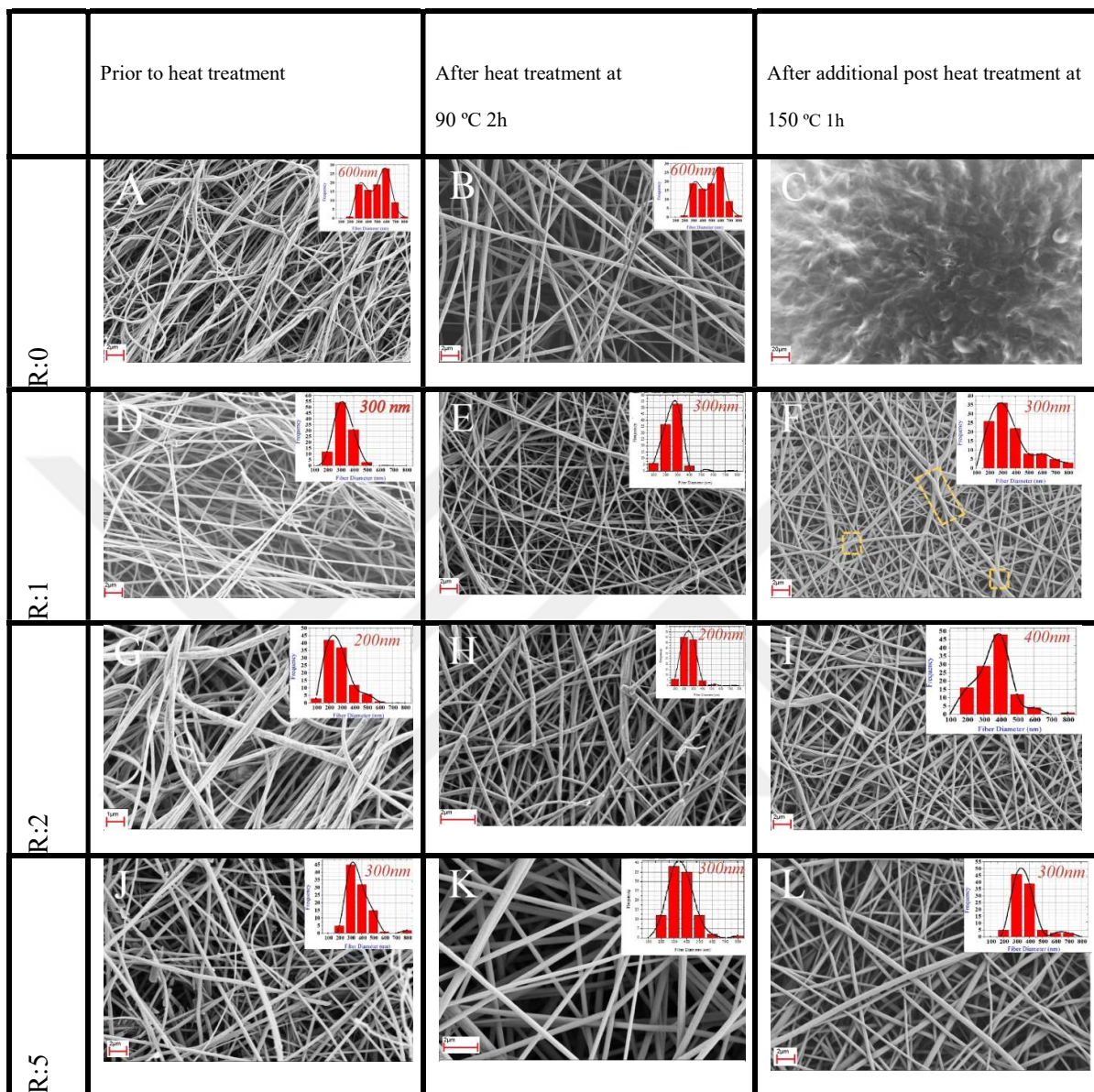
Figure 6: SEM micrographs of electrospun fibers. Each raw includes SEM images of the fibers prior to heat treatment (left image column), after the heat treatment at 90 ºC 2h (center image column), post heat treatment at 150 ºC (right image column). Scale bars: 2μm for a,b,d-l: and 20μm for c. Nanofiber diameter distribution charts reports fiber diameters ranging from 100 to 800nm where each bar is of a hundred nm bin width. Numbers over the distribution graphs notes the fiber diameter of the highest count in the respective image analysis. yellow dashed circle/ellipse: fusing/branching of the fibers onto the other

This is attributed to highly amorphous nature of P(St-co-GMA) nanofibers and associated softening effect above the T_g. We conclude that unconstrained mobility of the polymer chains promoted interactions between the individual fibers ultimately causing the loss of fibrous structure. On the contrary, in the cases of P(St-co-GMA)/PA-TBA nanofibers with R=1,2,5 (figures 6f, 6i and 6l, respectively) the fibrous morphologies were preserved beyond the T_g as a consequence of the heat stimuli/in-situ crosslinking as anticipated. Furthermore fiber diameter distribution along with the morphological changes suggest the transition into more discrete/uniform nanofibers is correlated with the level of intra-molecular crosslinking [43] (figures 6d&e for R=1, figures 6g&h for R=2 and figures 6j&k for R=5). It is worth noting the existence of somewhat flattened fibers and fusing/branching at the fiber interactions in R =1 and 2 cases (dashed line enclosures on figures 6h and 6k) as opposed to R=5 case (figure 6l) which was considered herein the maximum corsslinking configuration. It can also be claimed that the proposed heat stimulated/in-situ crosslink mechanism enforced nanofibers to shrink volumetrically, hence the diameter distributions were likely to converge into a narrower band as sampled and analyzed from the images.

4.1.4..4 An application example of High Temperature Processing: In-situ crosslinking of nanofibers during epoxy matrix cure cycle.

The heat-stimuli crosslinkable nanofibers can be used in composite materials as reinforcing and toughening agents. High performance epoxy resin systems demand processing at elevated temperature typically above the T_g of many amorphous polymers. In this specific demonstration, heat stimuli crosslinkable P(St-co-GMA)/PA-TBA (with R=5) and pristine/reference P(St-co-GMA) nanofibers were electrospun onto

carbon/epoxy prepreg surfaces (Aldila Composites, 34-700 (24k)-AR2527). The nanofiber coated epoxy matrix prepreg plies were cured at 150°C for 2 hours which is above the T_g of P(St-co-GMA) nanofibers (figure 5). Heat-stimuli crosslinking methodology was adopted as an intermediate hold-time of 120 minutes at 90°C, in order to treat the nanofibers on the prepreg ply before its ultimate cure at 150°C. As it can be seen in figure 7a and 7c the nanofibrous morphology of the reference P(St-co-GMA) nanofibers was totally lost, similar to figure 6b. However, P(St-co-GMA)/PA-TBA nanofibers were exposed to the proposed in-situ crosslinking process effectively and kept their nanofibrous formation while being embedded into epoxy matrix (figure 7c). Furthermore, they formed an effective interface with the epoxy matrix (figure 7d) which is in line with our previously reported composite application studies [1,8,32,33].
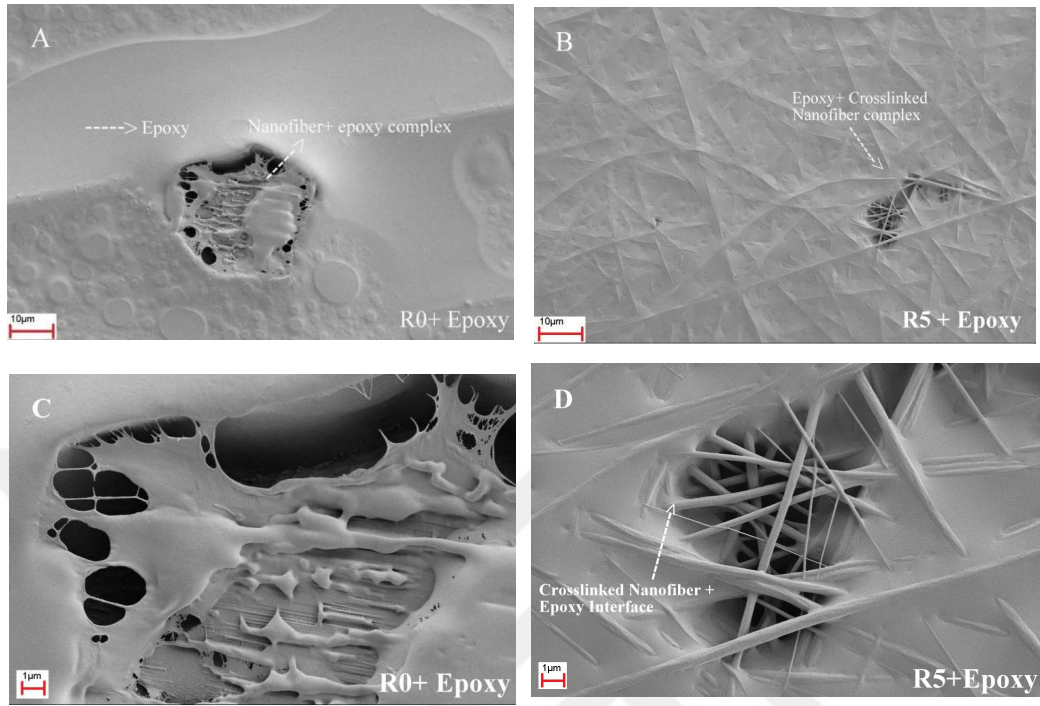
Figure 7: SEM micrographs of P(St-co-GMA) (a,c) and P(St-co-GMA)/PA-TBA (b,d) on cured epoxy surfaces.

4.1.4.5 Self Same Nanofibrous composites

The effect of cross-linker ratio R and associated morphological changes above the T_g can be taken advantage of to facilitate what we called a "self-same nanofibrous composites". In order to demonstrate this, we propose dual electrospinning of the reference (backbone) polymer P(St-co-GMA) (R=0) together with the stabilized cross-linkable P(St-co-GMA)/PA-TBA (R=5) nanofibers. The two polymer solutions were electrospun simultaneously from different syringes onto the same collector. Resultant intermingled fibrous web of the two polymeric nanofibers was obtained (Figure 8a).

143
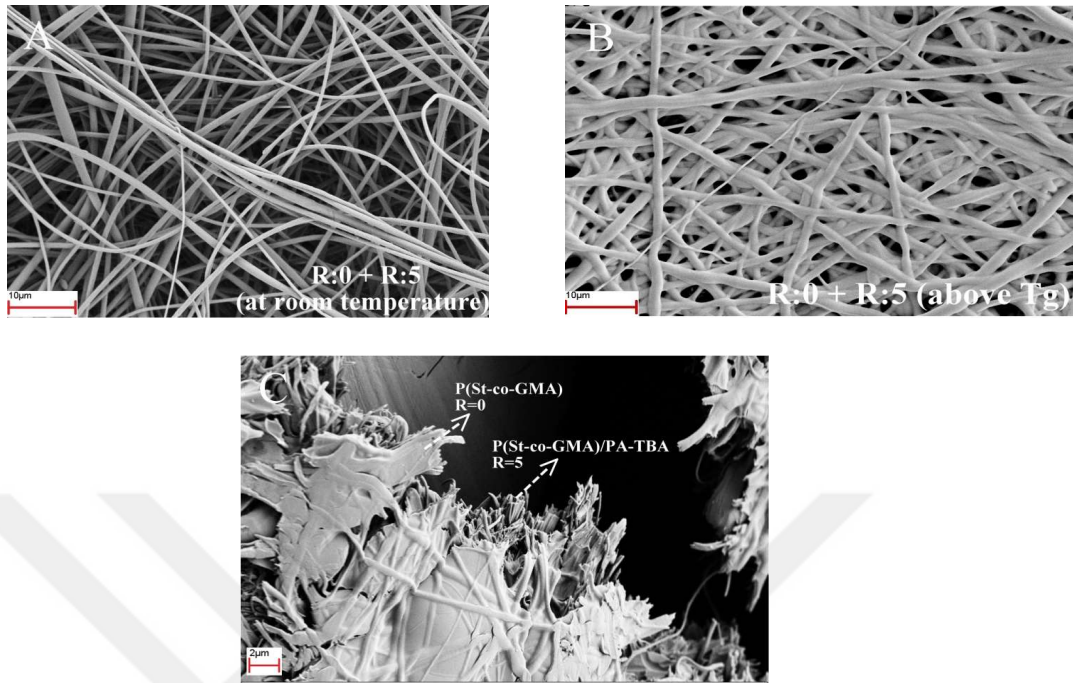
Figure 8: SEM micrographs of dual electrospun P(St-co-GMA) (R:0) and stabilized P(St-co-GMA)/PA-TBA (R:5) nanofibers at room temperature (a) at 150°C (b) cross-sectional view at 150^0C (c)

When this initially intermingled web was heat processed above the T_g condition, morphological changes of the two different fibers of their own occurred in concert as described in the previous section. That is, stabilized nanofibers were to crosslink and shrink, and backbone nanofibers were to lose their fibrous morphology by spreading. Clear change in the fibrous structure is shown in figure 8b where cross-linked nanofibers can be spotted. The morphology after the heat cycle is unique and different than the ones reported in figure 6. Observations in figure 6-8 suggest that the un-cross-linked backbone polymer P(St-co-GMA) wraps/fuses onto the cross-linked fibers creating a self-same nanofibrous composite film. In other words, un-cross-linked nanofibers processed above the T_g interacted with the cross-linkable fibers and hereby acted as a self-same matrix

144

material for the cross-linked nanofibers. Cross-sectional view presented as figure 8c also confirmed that with the application of the proposed processing, it is possible to create a polymeric film reinforced by nanofibers just by heating. We believe that this concept is worth of further considerations by a dedicated work.

4.1.5. Conclusions

Heat-stimulated cross-linking capability was introduced into amorphoıus P(St-co-GMA) nanofibers, by the addition of phtalic anhydride (PA) as the cross-linking agent and tributlyamine (TBA) as the initiator. Despite the mixing of the cross-linker agents into the solution, cross-linking was successfully suppressed at room temperature, allowing continuous electrospinning without any adverse effect on the polymer solution viscosity. The cross-linking reaction was found to be initiated at around 60°C. Electrospun nanofibers with different PA amounts were cross-linked by the application of thermal cycle at intermediate temperatures of ~ 90°C (*i.e.*, just below T_g). Cross-linking at the highest capacity was sought, when the PA/epoxide ring (GMA) molar ratio was varied from 1 to 5. A proposed reaction route was validated by FTIR analyses, where the consumption of PA and available epoxide rings in GMA was observed. Swelling tests suggested that the gel fraction in cross-linked nanofibers maximized with the increasing PA amount up to molar ratio of 5. At the maximum cross-linking ratio, P(St-co-GMA)/PA-TBA nanofibers completely preserved their pristine nanofibrous morhology after 3 days of exposure to DMF solvent. The DSC analyses suggested that the T_g of the cross-linked nanofibers increased with the degree of cross-linking, by up to 30°C. Note that the glass transition temperature T_g may also be an important limit, as exceeding it may induce substantial changes in the nanofibrous structure/morphology. Un-crosslinked P(St-co-GMA) nanofibrous morphology and network degraded above their T_g, whereas

145

the cross-linked P(St-co-GMA)/PA-TBA nanofibers, especially the ones with R=5, were able to maintain their nanofibrous morphology intact. A similar outcome was observed when R=5 P(St-co-GMA)/PA-TBA nanofibers were processed in-situ at 150C accommodating the cure of the epoxy matrix. The fibrous morphology was contained and the P(St-co-GMA)/PA-TBA nanofibers were effectively embedded into the epoxy matrix. Lastly, the form-loose effect of an above-the-T_g process on the P(St-co-GMA) fibers was proposed as a strategy in the manufacturing of what we call the self-same nanocomposites. Un-crosslinked (R=0) and stabilized cross-linkable (R=5) nanofibers of P(St-co-GMA) backbone polymer were electrospun together by dual electrospinning. An intermingled nanofibrous structure were formed. The two types of fibers interacted upon a subsequent processing above the T_g reforming into a nanocomposite fibrous network, where the un-cross-linked P(St-co-GMA) appears to wrap/fuse around the self-cross-linkable P(St-co-GMA)/PA-TBA nanofibers .

.

4.1.6 References

[1]Ozden, E.; Menceloglu, Y.Z.; Papila, M. Engineering Chemistry of Electrospun Nanofibers and Interfaces in Nanocomposites for Superior Mechanical Properties ACS Appl. Mater. Interfaces 2010, 2, 1788-1793

[2] Kim, J.S. ; Reneker, D.H. Mechanical Properties of Composites Using Ultrafine Electrospun Fibers Polym. Compos. 1999, 20, 124-131.

[3] Bergshoef, M.M. ; Vansco, G.J. Transparent Nanocomposites with Ultrathin Electrospun Nylon-4, 6 Fiber Reinforcement Adv. Mater. 1999, 11, 1362-1365.

[4] Romo-Uribe, A.; Arizmendi, L.; Romero-Guzman, M.E.; Sepulveda-Guzman S.; Cruz-Silva R. Electrospun Nylon Nanofibers as Effective Reinforcement to Polyaniline Membranes ACS Appl. Mater. Interfaces. 2009,1, 2502-2508.

[5] Chen, L.S.; Huang, Z.M.; Dong, G.H.; He, C.L.; Liu, L.; Hu, Y.Y. Development of a Transparent PMMA Composite Reinforced With Nanofibers Polym. Compos. 2009, 30, 239-247.

[6] Nepalli, R.; Marega, C.; Marigo, A.; Bajgaj, M.P.; Kim, H.Y.; Causin, V. Poly (E-Caprolactone) Filled with Electrospun Nylon Fibres: A Model For a Facile Composite Fabrication Eur. Polym. J. 2010, 46, 968-976.

[7] Lee, J-R.; Park, S-J.; Seo, M-K.; Park, J-M. Preparation and Characterization of Electrospun Poly (Ethylene Oxide) (PEO) Nanofibers-Reinforced Epoxy Matrix Composites Mater. Res. Soc. Symp. Proc., 2004, NN5.11.

[8] Bilge, K.; Ozden-Yenigun, E.; Simsek, E.; Menceloglu, Y.Z.; Papila M. Structural Composites Hybridized with Epoxy Compatible Polymer/MWCNT Nanofibrous Interlayers Compos. Sci. Technol. 2012, 72, 1639-1645.

[9] Dzenis, Y. Structural Nanocomposites Science, 2008, 319, 419-420

[10] Dzenis, Y.; Reneker, D.H. Delamination Resistant Composites Prepared by Small Diameter Fiber Reinforcement At-Ply Interfaces 2001 US PATENT 626533

[11] Sihn, S.; Kim, R.Y.; Huh, W.; Lee, K-H.; Roy, A.K. Improvement of Damage Resistance in Laminated Composites with Electrospun Nano-Interlayers Compos. Sci. Technol. 2008, 68, 673-683

[12] Liu, L., Huang, Z-M.; He, C.; Han, X. Mechanical Performance of Laminated Composites Incorporated with Nanofibrous Membranes Mater. Sci. Eng., A 2006, 435, 309-317

[13] Liu, L.; Huang, Z.M.; Xu, G.Y.; Liang, Y.M.; Dong ,G.H. Mode II Interlaminar Delamination of Composite Laminates Incorporating with Polymer Ultrathin Fibers Polym. Compos. 2008, 29, 285-292.

[14] Lee, S-H.; Lee, J-H.; Cheong, S-K.; Noguchi, H.A. A Toughening And Strengthening Technique of Hybrid Composites with Non-Woven Tissue J. Mater. Process. Technol. 2008, 207, 21-29.

[15] Lee, S-H.; Noguchi, H.; Kim, Y-B.; Cheong, S-K. Effect of Interleaved Non-Woven Carbon Tissue on Interlaminar Fracture Toughness of Laminated Composites: Part I– Mode II J. Compos. Mater. 2002, 36, 2153-2168.

[16] Palazetti, R.; Zuchelli, A.; Gualandi, C.; Focarete, M.; Donati, L.; Minak, G. Influence of Electrospun Nylon 6, 6 Nanofibrous Mats on the Interlaminar Properties of Gr–Epoxy Composite Laminates Compos. Struct. 2012, 94, 571-579.

[17] Magniez, K.; Chaffraix, T.; Fox, B. Toughening of A Carbon-Fibre Composite Using Electrospun Poly (Hydroxyether of Bisphenol A) Nanofibrous Membranes through Inverse Phase Separation and Inter-Domain Etherification Materials 2011, 4, 1967-1984.

[18] Zhang, J.; Lin, T.; Wang, X. Electrospun Nanofibre Toughened Carbon/Epoxy Composites: Effects of Polyetherketone Cardo (PEK-C) Nanofibre Diameter and Interlayer Thickness Compos. Sci. Technol. 2010, 70, 1660-1666.

[19] Zhang, J.; Lin, T.; Wang, C.H. Phase Morphology of Nanofibre Interlayers: Critical Factor for Toughening Carbon/Epoxy Composites Compos. Sci. Technol. 2012, 72, 256-262.

[20] Bortz, D.R.; Merino, C.; Martin-Gullon, I. Mechanical Characterization of Hierarchical Carbon Fiber/Nanofiber Composite Laminates Composites Part A 2011, 42, 1584-1591.

[21] Nash, N.H.; Young, T.M.; McGrail, P.T.; Stanley, W.F. Inclusion of a Thermoplastic Phase to Improve Impact and Post-Impact Performances of Carbon Fiber Reinforced Thermosetting Composites- A Review Mater.Des. 2015, 85, 582-597.

[22] Liu, L.; Zhang, H.; Zhou, Y. Quasi-Static Mechanical Response and Corresponding Analytical Model of Laminates Incorporating with Nanoweb Interlayers Compos. Struct. 2014, 111, 436-445.

[23] Li, P.; Liu, D.; Zhu, B.; Li, B.; Jia, X.; Wang, L.; Li, G.; Yang, X. Synchronous Effects of Multiscale Reinforced and Toughened CFRP Composites by Mwnts-EP/PSF Hybrid Nanofibers with Preferred Orientation Composites Part A 2015, 68, 72-80

[24] Ary Subagia, I.D.G.; Jiang, Z.; Tijing, L.D.; Kim, Y.; Kim, C.S.; Lim, J.K. Hybrid Multi-Scale Basalt Fiber-Epoxy Composite Laminate Reinforced with Electrospun Polyurethane Nanofibers Containing Carbon Nanotubes Fibers Polym. 2014, 15, 1295-1302.

[25] Daelemans, L.; Van Der Heijden, S.; De Baere, I.; Rahier, H.; Van Paepegem, W.; De Clerck, K. Nanofibre Bridging As A Toughening Mechanism in Carbon/Epoxy Composite Laminates Interleaved with Electrospun Polyamide Nanofibrous Veils Compos. Sci. Technol. 2015,117, 244-256

[26] Van Der Heijden, S.; Daelemans, L.; Schoenmaker, B.D.; De Baere, I.; Rahier, H.; Van Paepegem, W.; De Clerck, K. Interlaminar Toughening of Resin Transfer Moulded Glass Fibre Epoxy Laminates by Polycaprolactone Electrospun Nanofibres Compos. Sci. Technol. 2014, 104, 66-73.

27] Saghafi, H.; Palazetti, R.; Zuchelli, A.; Minak, G. Influence of Electrospun Nanofibers on the Interlaminar Properties of Unidirectional Epoxy/Resin/Glass Fiber Composite Laminates J. Reinf. Plast. Compos. 2015, 34. 907-914.

[28] Beckermann, G.W.; Pickering, K.L. Mode I And Mode II Interlaminar Fracture Toughness of Composite Laminates Interleaved with Electrospun Nanofibre Veils Composites Part A 2015, 72, 11-21.

[29] Palazetti, R. Flexural Behavior of Carbon and Glass Fiber Composite Laminates Reinforced with Nylon 6,6 Electrospun Nanofibers. J. Compos. Mater. 2014, 0021998314565410.

[30] Zheng, J.; He, A.; Li, j.; Xu, J.; Han, C.C. Studies On The Controlled Morphology and Wettability of Polystyrene Surfaces by Electrospinning or Electrospraying Polymer 2006, 47, 7095-7102.

[31] Yordem, O.; Papila, M.; Menceloglu, Y.Z. Effects of Electrospinning Parameters on Polyacrylonitrile Nanofiber Diameter: An Investigation by Response Surface Methodology Mater. Des. 2008, 29, 34-44

[32] Ozden-Yenigun, E.; Menceloglu, Y.Z.; Papila, M. MWCNTS/P (St-Co-GMA) Composite Nanofibers of Engineered Interface Chemistry For Epoxy Matrix Nanocomposites ACS Appl. Mater. Interfaces 2012, 4, 777-784.

[33] Bilge, K. ; Venkataraman, S.; Menceloglu, Y.Z.; Papila, M. Global and Local Nanofibrous Interlayer Toughened Composites for Higher In-Plane Strength Composites Part A 2014, 58, 73-76.

[34] Huang, Z-M.; Zhang, Y-Z.; Koataki, M.; Ramakrishna, S. A Review on Polymer Nanofibers by Electrospinning and Their Applications in Nanocomposites Compos. Sci. Technol. 2003, 63. 2223-2253

[35] Dai, T.; Ebert, K. Electrospinning of Solvent-Resistant Nanofibers Based on Poly(Acrylonitrile-Co-Glycidyl Methacrylate) J. Appl. Polym. Sci. 2012, 126, 136-142

[36] Peresin, M.S.; Vesterinen, A.H.; Habibi, Y.; Johansson, L.S.; Pawlak, J.J.; Nevzorov, A.A. Crosslinked PVA Nanofibers Reinforced with Cellulose Nanocrystals: Water Interactions and Thermomechanical Properties J. Appl. Polym. Sci. 2014, 131, 40334

[37] Gupta, P.; Trenor, S.R.; Long, T.E.; Wilkes, G.L. In Situ Photo-Cross-Linking of Cinnamate Functionalized Poly (Methyl Methacrylate-Co-2-Hydroxyethyl Acrylate) Fibers During Electrospinning Macromolecules 2004, 37, 9211-9218.

[38] Kim, S.H., Kim, S-H.; Nair, S.; Moore, E. Reactive Electrospinning of Cross-Linked Poly (2-Hydroxyethyl Methacrylate) Nanofibers and Elastic Properties of Individual Hydrogel Nanofibers in Aqueous Solutions. Macromolecules 2005, 38, 3719-3723.

[39] Ji, Y. Ghosh, K.; Li, B.; Sokolov, J.C.; Clark, R.A.; Rafailovich M.H. Dual-Syringe Reactive Electrospinning of Cross-Linked Hyaluronic Acid Hydrogel Nanofibers for Tissue Engineering Applications Macromol. Biosci. 2006, 6, 811-817.

[40] Stone, S.A.; Gosavi, P.; Athauda, T.J.; Ozer, R.R. In Situ Citric Acid Cross-Linking of Alginate/Polyvinyl Alcohol Electrospun Nanofibers Mater. Lett. 2013, 112, 32-35.

[41] Liu, H.; Zhen, M.; Wu, R. Macromol. Ionic-Strength-and pH-Responsive Poly [acrylamide-co-(maleic acid)] Hydrogel Nanofibers Chem. Phys. 2007, 208, 874-880.

[42] Acatay, K.; Simsek, E.; Ow-Yang, C.; Menceloglu, Y.Z. Tunable, Superhydophobically Stable Polymeric Surfaces by Electrospinning Angew. Chem. Int. Edit.2004, 43, 5210-13

[43] Tang, C.; Saquing, C.D.; Harding, J.R.; Khan, S. In Situ Cross-Linking of Electrospun Poly(vinyl alcohol) Nanofibers Macromolecules 2010, 43, 630-637.

[44] Kim, K-J.; Lee, S-B.; Han, N-W. Kinetics of Cross-Linking Reaction of PVA Membrane with Glutaraldehyde Korean J. Chem. Eng. 1994, 11, 41-47.

[45] Guerrero, P.; De La Caba, K.; Valea, A.; Corcuera, M.; Mondragon I. Influence of Cure Schedule and Stoichiometry On The Dynamic Mechanical Behaviour of Tetrafunctional Epoxy Resins Cured with Anhydrides Polymer 1996, 37, 2195-2200

[46] Papila, M. Patent Corporation Treaty (PCT) Applied Patent Ref No: PCT/TR2015/000227

[47] Luo, X.; Zheng, S.; Ma, D. Mechanical Relaxation and Intermolecular Interaction in Epoxy Resins/ (Poly Ethylene Oxide) Blends Cured with Phthalic Anhydride Chin. J. Polym. Sci. 1995, 13, 144-153.

[48] Romao, B.M.V.; Diniz, M.F.; Azevedo, M.F.P.; Lourenco, V.L.; Pardini, L.C.; Dutra, R.C.L. Characterization of the Curing Agents Used in Epoxy Resins with TG/FT-IR Technique *P*olímeros: Ciência e Tecnologia 2006, 13, 144-153.

[49] Antoon, M.K.; Koenig, J.L. Cross-Linking Mechanism of an Anhydride-Cured Epoxy Resin as Studied by Fourier Transform Infrared Spectroscopy J. Polym. Sci. Polym. Chem. Ed. 1981, 19, 549-570.

[50] Huan, S., Liu, G., Han, G., Cheng, W., Fu, Z., Wu, Q., Wang, Q. Effect of Experimental Parameters on Morphological,Mechanical and Hydrophobic Properties of Electrospun Polystyrene Fibers Materials **2015**, 8, 2718-2734.

[51] Yuan, X., Zhang, Y., Dong, C., Sheng, J. Morphology of ultrafine polysulfone fibersprepared by electrospinning Polym Int 2004, 53(11), 1704-10.

4.2 Synergistic role of In-Situ Crosslinkable Electrospun Nanofibrous Interlayers for Superior Laminated composites

4.2.1 Abstract

In a multi-scaled toughening approach, in-situ crosslinkable P(St-co-GMA)/TBA-PA nanofibers are electrospun both onto epoxy adhesive films and carbon/epoxy prepreg plies that have the same epoxy system. Nanofiber/epoxy nanocomposite specimens were manufactured via in-house developed, hot press associated film casting methodology. Nanofiber crosslinking is in-situ, that is triggered and advanced through the epoxy curing cycle. The in-situ crosslinking is monitored by DSC analyses where increased cure enthalpies (ΔH) are reported. Furthermore cure kinetics analysis following Ozawa-Flynn-Wall method shows that P(St-co-GMA)/TBA-PA nanofibers have a significant autocatalytic effect on the epoxy matrix curing. Mechanical behavior-crosslinking chemistry correlation is initially investigated by the tensile test of nanofiber/epoxy nanocomposite samples where tensile strength and elastic modulus are increased by 30% and 8% respectively with respect to un-reinforced specimens. Laminated composites with $(0)_{48}$ lay-up configuration are subjected to end notched flexure. Significant increase as high as 95% in G_{IIC} is also noted due to incorporation of P(St-co-GMA)/TBA-PA nanofiber interlayers. Results suggest the crosslinking

manupilated properties of the nanofibers themselves and surrounding epoxy matrix synergistically form mechanically enhanced nanocomposite interlayer zones. Fracture surface analysis is presented to elaborate significant role of the proposed in-situ crosslinked nanofibers on the notable improvements in mechanical behavior of laminated composites.

4.2.2. Introduction

Interlayer toughening strategy typically refers to incorporation of sub-phases into the interlaminar region. They aim to improve transverse crack and delamination resistance of laminated composites which are susceptible to these damage formations [1,2]. The integration of electrospun nanofibers [3-5] was introduced as appealing choice among these toughening strategies, thanks to their tailorability and mechanical efficiency with low structural weight penalty [6]. With the recognition of its potential, search for the optimal nanofibrous toughening agents has been at the focus of numerous inter-disciplinary research activities where chemical and morphological differences due to polymer choice [7-12] and nano-particle incorporation [13-15] were offered and evaluated Special attention has also been given to the working mechanisms [16-18] and performance under various mechanical loading conditions applied to different composite laminates [19-26]. The basis of interlayer toughening strategy is a multi-scaled approach by itself and demands appropriate sub-phase design (namely epoxy/interlayer nanocomposite) that is also being investigated by several works in literature [6] A key in proposing coherent nanofiber and matrix system either in Nano or structural composites, is to establish a comprehensive process to evaluate potential choices of material, limits, and their adaptation within conventional engineering processes [27]. In-line with state of the art, our recent work [28] showed that appraisal of thermoplastic nanofibrous interlayer material limits is of importance in the processes of integrating them to composite

processing conditions. Addressing the issue, an in-situ crosslinking mechanism was seeded into the novel P(St-co-GMA)/PA-TBA nanofibers. They are able to crosslink as the epoxy matrix cures during associated nanocomposite processing as such the nanofibers could overcome the temperature limit, namely the glass transition temperature (T_g).

Sharing the apparent multi-scaled toughening objective, this work initially focuses on the effect of in-situ crosslinkable P(St-co-GMA)/TBA-PA nanofibers on the cure kinetics ofcarbon/epoxy prepregs. Synergistic curing behavior with increased cure enthalpy and an apparent catalytic effect achieved by nanofiber chemistry are discussed via non-isothermal DSC analysis and Ozawa-Flynn-Wall cure kinetics model. The effect of in-situ crosslinking on the mechanical behavior is then discussed in two separate examples. Initial examination was done on nanofiber/epoxy nanocomposites With an in-house developed hot press assisted film casting method nanocomposite specimens having 0.8% nanofiber weight fraction were efficiently manufactured. This methodology enabled a conventional laying-up (epoxy/epoxy/nanofiber/epoxy/epoxy) strategy in nano-scale. A significant increase in tensile strength and elastic modulus up to 30% and 8% respectively is achieved. Morphological changes and contributions to fracture pattern are investigated by fracture surface analaysis. With proven synergistic curing and toughening ability in nanocomposite form , P(St-co-GMA)/TBA-PA nanofibers are then incorporated to carbon/epoxy prepregs having the same resin system with adhesive films. End notched flexure test results performed to laminated composites with $(0)_{48}$ lay-up configuration showed that interlayered laminates have 95% increase in mode II strain energy release rate(G_{IIc}) values. Fracture surface analysis done on failed ENF specimens suggested that in-situ crosslinkable P(St-co-GMA)/TBA-PA nanofibers have multi-scaled toughening effect when applied to structural composites.

4.2.3 Experimental Procedure

4.2.3.1 Copolymer Synthesis, Crosslinking Agents and Electrospinning

Details of P(St-co-GMA) synthesis and crosslinking methodology were reported in our Chapter 4.1 [28]. Briefly, the crosslinker agents are Phtalic Anhydride (PA) (crosslinker) and tributyl amine (initiator). It was shown that the methodology led to the heat stimuli crosslinkable nanofibers and with GMA to PA molar ratio (R=5) 98% crosslinking ratio was achieved. The crosslinking reaction was also reported to begin around 60^0C and finish around 90^0C which makes proposed P(St-co-GMA)/TBA-PA nanofibers completely adaptable to elevated temperature epoxy curing processes. In the scope of this work P(St-co-GMA)/TBA-PA nanofibers with R=5 were used. The applied voltage, solution flow rate, and tip to collector distance were set at 15 kV, 0.4 mL/h, and 10 cm, respectively, during the electrospinning.

4.2.3.2 Specimen Manufacturing and Mechanical Testing

For the manufacturing nanocomposite specimens P(St-co-GMA)/TBA-PA nanofibers were firstly electrospun over aluminum foils and then transferred to adhesive epoxy films made out from AR2527 (same epoxy material used in prepreg plies) Fig.1. shows the whole process of the casting. Two aluminum plates 15×25 cm covered with release agent has been used as moulds. Nano-composites by the lay-up configuration of epoxy/epoxy/nanofiber/epoxy/epoxy were initially heated up to 90^0C with a heating rate of 2^0C/min and hold iso-thermally for 1 hour for in-situ crosslinking to take place [27]. A second heating step with heating rate of 2^0C/min was applied till 150^0C and hold isothermally for another 1 hour. Neat and nanofiber reinforced specimens were subjected to the same thermal processing for proper mechanical property comparisons. A uniform

compression of 4 tons was maintained throughout the process. To degas and remove bubbles during heat exposure, vacuum trap has been employed. Teflon straps have been located all around the cast to prevent any damage undoing the cast. In order to prevent resin loss due to initial decreasing viscosity of resin system before gelation, the sides of the aluminum plates were covered with a temperature resistant vacuum sealent.
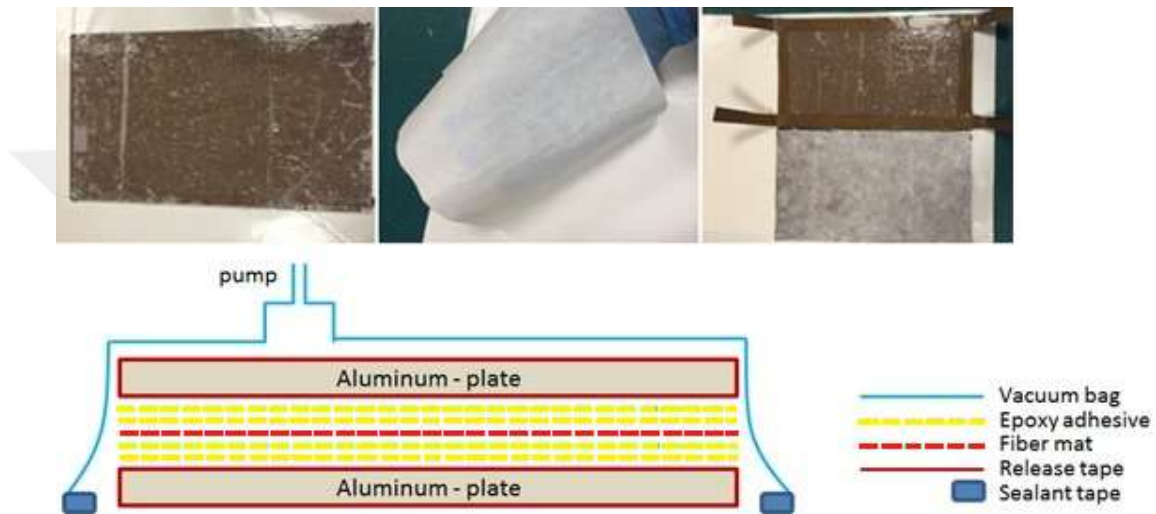
Figure 1: A view from adhesive film casting process

Specific attention was given during the removal of the cured (glassy) nanofiber/epoxy systems from the aluminum plates in order to prevented unwanted damages in the specimens. Obtained nanocomposites films were cut into specimens (length: 200mm, width: 15mm, average thickness: 0.4±0.1mm) with a well sharpened razor blade. Obtained nanofiber weight fraction was approximately 0.8 %. Tensile tests were done with a constant displacement rate of 2mm/min and strain was measured by a micro-extensiometer attached to the middle of the specimen.

For the manufacturing of laminated composite specimens, prepreg layers with and without incorporation of nanofibrous interlayers were stacked together. Electrospinning was done directly over the prepreg plies. Suggested curing cycle for 34–700 (24k)-AR2527 prepreg system was to ramp up to 150^0C at heating rate of 2^0C/min and to hold

at 150^{0}C for 2 hours. This cycle has been slightly altered due to .[28] by an additional isothermal dwell at 90^{0}C (crosslinking reaction peak temperature) for 2 hours to achieve complete nanofiber crosslinking.

End notched flexure tests were in accordance with ASTM D7905. The nanofibrous interleaf placement was only at the mid-plane where pre-crack front is typically formed. The lamination sequence was $(0)_{48}$ Mode II strain energy release rates were calculated using simple beam theory [29].

4.2.3.3 Thermal Analysis and Cure Kinetics

The thermal properties of interlayered and non-interlayered specimens were probed by the differential scanning calorimeter Q2000 (TA instruments) under the standard (non-isothermal) mode. The temperature was ramped from 25℃ to 300℃ at five different heating rates (β), $1, 2, 5, 10$ and 20℃ min^{-1} in the first cycle. After cooling down to RT, a second heating cycle at a rate of 10℃ min^{-1} was followed to remove any prior thermal history.. The first cycles of dynamic temperature scans are used to measure reaction enthalpies (ΔH) and reaction peak temperatures (T_{peak}).

For the study of cure kinetics Ozawa-Flynn-Wall analysis was done as described in [30]. The reaction peak temperatures at different degrees of conversion (α) were monitored and the activation energies for epoxy curing reactions were calculated by the slope of the least squared curve fitted trendline of log(β) vs. $(1/T_{peak})$ curves.

4.2.3.4 Fracture Surface Analysis

Fracture surface analysis of the composite laminates were carried out with a LEO Supra VP35 field emission scanning electron microscope after sputter deposition of a thin conductive carbon coating onto the samples.

4.2.4 RESULTS AND DISCUSSION

4.2.4.1 Effect of in-situ crosslinking on the cure kinetics of carbon/epoxy prepreg systems

In order to investigate the effect of in-situ crosslinking on the cure kinetics of epoxy system, P(St-co-GMA)/TBA-PA nanofibers of R=5 were chosen (i.e. the highest crosslinking capability which resulted in notable flexural stiffness increase when used as interlayers). Nanofibers were electrospun and collected directly on the carbon/epoxy prepreg layers. Five DSC scans on cured specimens were then carried out, each using different heating rates specifically at 1, 2, 5,10 and 20^0C/min. Reaction enthalpies (ΔH) and reaction peak temperatures (T_{peak}) are presented in Table 1. The crosslinking of epoxy matrix and P(St-co-GMA)/TBA-PA nanofibers result from the opening of functional epoxide rings. Moreover, the formulators TBA (an amine initiator) and PA (crosslinker) are both present within the nanofiber structure as such nanofiber crosslinking process is quite similar to anhydride curing of epoxy resins [31-34]. Specifically, for this case after around 60^0C, C-O-C bonds of PA get broken and react with the GMA epoxide groups already activated by TBA. In other words, both the initiator and the crosslinker in the nanofibers can also react with the epoxy matrix during composite making. The first associated observation from figure 2 is the presence of a single exothermic peak corresponding to epoxy curing.

An intermediate step corresponding to independent nanofiber based crosslinking reaction did not stand out. Furthermore, when reaction enthalpies at different heating rates are concerned it is vital to underline that for the heating rates of 10^0C/min and 20^0C/min the total reaction enthalpy of nanofiber containing samples were lower than the neat samples. However, as the heating rate drops (for 5^0C, 2^0C and 1^0C/min) curing enthalpy values for nanofiber added specimens begin to increase drastically. This observation underlined that

159

with enough time given (as applied in structural composite manufacturing) nanofiber related epoxide groups began to contribute to the composite matrix curing mechanism forming a cooperative curing reaction which is believed to be important for fiber/epoxy interface.
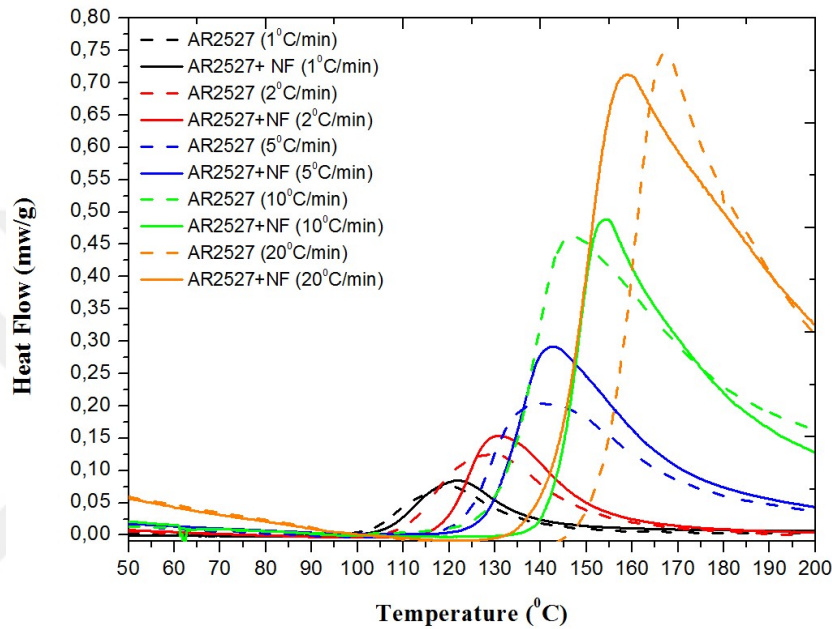
Figure 2: Non-isothermal DSC scans for un-cured PSt-co-GMA)/TBA-PA interlayered laminates

The effect of P(St-co-GMA)/TBA-PA nanofibers to the curing activation energy (E_a) was further addressed by using model free iso-conversional Ozawa-Flynn-Wall Analysis where E_a is assumed to change throughout the reaction. Temperature profiles associated with several degrees of cure have been extracted and plotted for five selected heating rates. (Figure 3a for neat epoxy, Figure 3b for P(St-co-GMA)/TBA-PA reinforced epoxy). Results suggest that the presence of in-situ crosslinkable nanofibers initially decreases the reaction activation energy which is attributed to their immediate role as reaction catalysts inside the epoxy matrix [30]

Table 1: Curing enthalpies and reaction peak temperatures from non-isothermal DSC scans

Specimen	Heating Rate (^{0}C/min)	Curing Enthalpy (Joules/gram)	Peak Temperature
Un-reinforced Carbon/Epoxy	1	95.9	120.2
	2	112.2	129.5
	5	87.6	138.5
	10	97.6	145.4
	20	89.8	158.6
P(St-co-GMA)/TBA-PA Reinfiorced Carbon/Epoxy	1	109.8	122.4
	2	126.4	130.1
	5	91.2	142.1
	10	99.8	154.2
	20	88.5	166.2

As the cure progresses however the difference between E_a values for epoxy-alone system and nanofiber incorporated epoxy system decreases (figure 3c). This observation supports the presumed curing characteristics, that is the nanofiber and epoxy system curing was initiated together, but beyond a degree of cure nanofiber effect diminishes and remaining epoxide groups of epoxy matrix continued to crosslink.
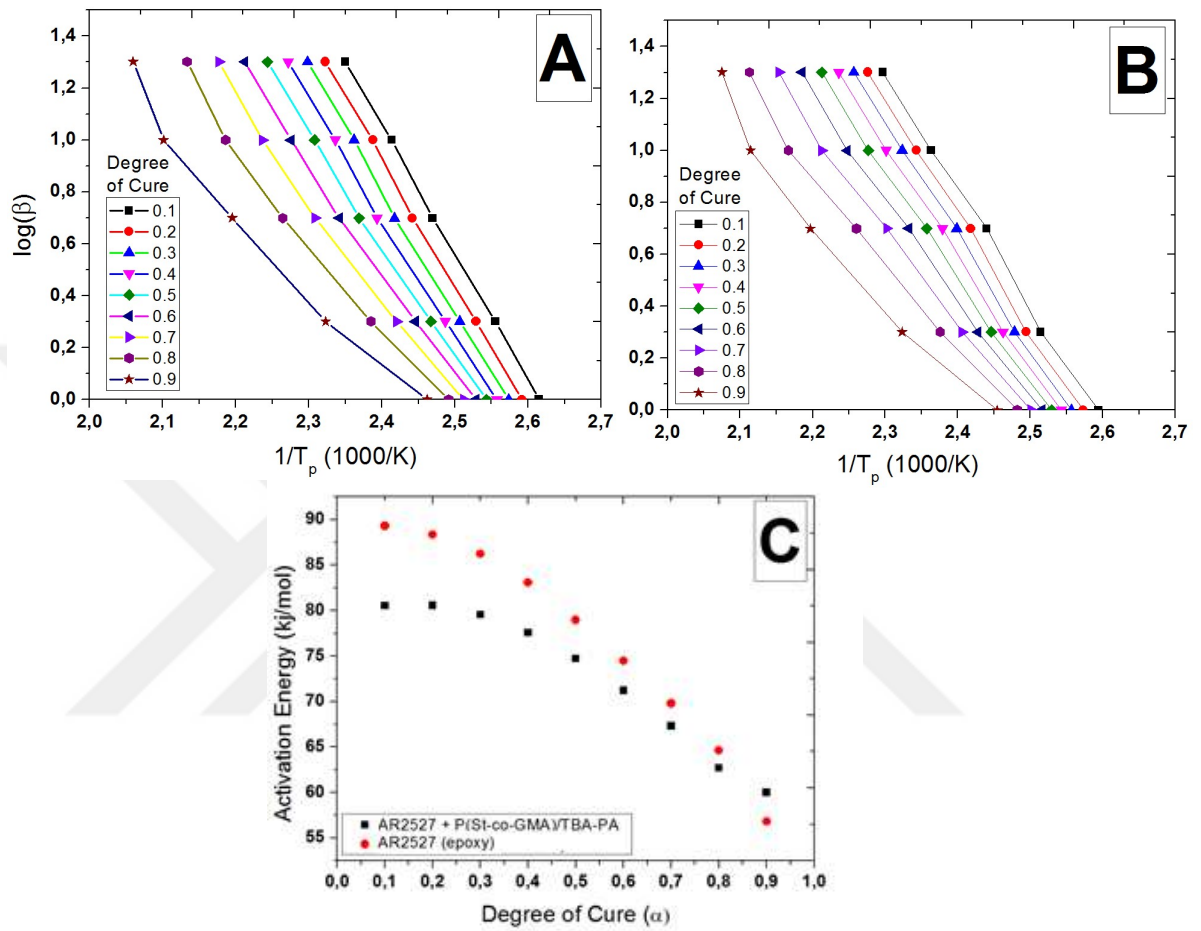
Figure 3: a) log (β) vs 1/Tp curves for a) Un-reinforced b) Nanofiber reinforced

laminates c) Activation energies for cure reaction at each cure degrees.

4.2.4.2 Tensile Performance of AR2527/P(St-co-GMA)/TBA-PA nanocomposite films

Prior to their applications to structural composites, synergistic effect and effective nanofibrous reinforcement capability of in situ crosslinkable P(St-co-GMA)/TBA-PA nanofibers is firstly evaluated in the form of nanocomposites. For this case P(St-co-GMA)/TBA-PA nanofibers were introduced to thin epoxy (AR2527) adhesive films which were then cast into tensile test specimens. Figure 4 shows the tensile test results for un-reinforced and P(St-co-GMA)/TBA-PA reinforced epoxy nanocomposites. The tensile strength and elastic modulus of nanofiber reinforced specimens were increased up to 33% and 8% respectively with the addition of 0.8 wt.% P(St-co-GMA)/TBA-PA nanofibers. The behavior of both type of specimens was brittle and the failure occurred due to sudden crack formation from the middle of the test specimens. Significant contribution of nanofibers to the mechanical behavior have been further supported by fracture surface analysis.
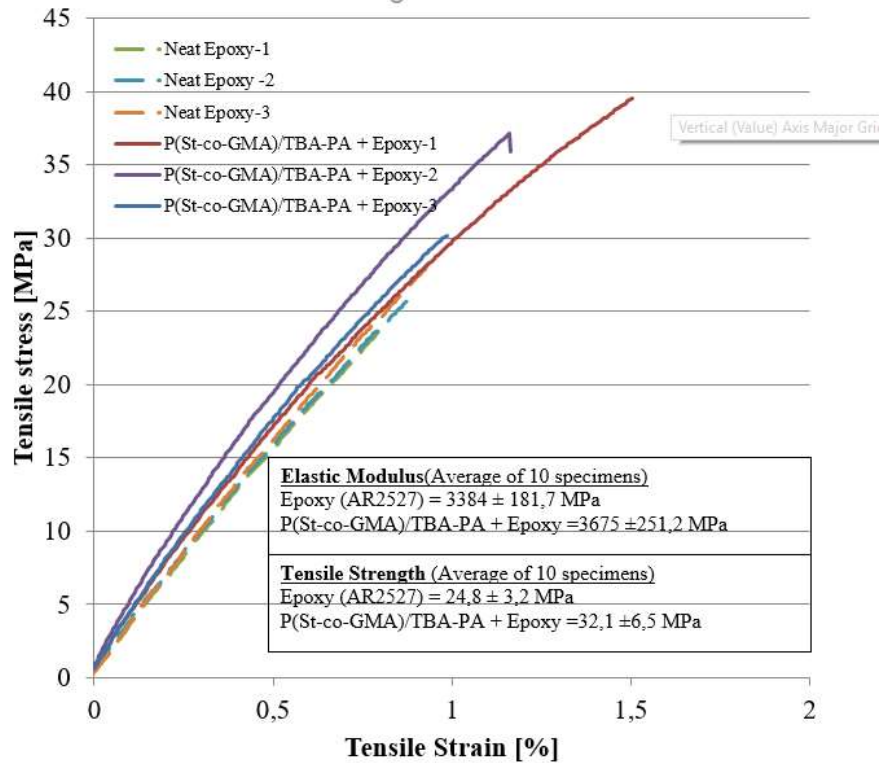
Figure 4: Tensile test result for nanocomposite samples

Figure 5a shows the fracture surface of an unsupported epoxy specimen with ridge formation (R1-R5) (with clear riverline formations underneath), and relatively smooth areas in between which also suggest a brittle failure pattern [35]. The formation of riverlines is attributed to the crack front progressing along the edge of the ridges [36,37] The directions of the formed riverlines suggests that minor crack propagation forming R1, R2, R3, R4 have occurred during the specimen failure. Ultimate failure of the specimens on the other hand occurred due to a severe crack formation propagating towards the end of the specimen and leaving a relatively bigger ridge formation (R1). Nanofiber reinforced specimens clearly separated into two distinct regions (Figure 5b). Nanofiber/epoxy nanocomposite embedded between two subsequent epoxy dominated regions had a significantly different fracture surface morphology. For epoxy dominated regions the propagation paths for internal cracks were again visible thanks to riverlines

and corresponding ridge formations. Nanocomposite region on the other hand, is formed of numereous nanofiber debonding marks embedded inside a substantially rough surface (Figure 5c). When analyzed more closely (figure 5d), some contact nanofibers as well as fractured nano-fibers became apparent. Parallel to the synergistic curing effect the epoxy morphology was also altered significantly without causing any related defect formation. Nanofiber/epoxy interfaces were nearly un-distinguishable. In terms of mechanical performance, the nanofiber addition seemed to significantly alter the failure mode of epoxy nad granted a superior tensile strength. As far as elastic modulus is concerned, 8% increase can be attributed to synergistic curing of P(St-co-GMA)/TBA-PA nanofibers with epoxy resin along with the moderate (with 0.8 wt%) modulus contribution of cross-linked (stiffened) nanofibers.
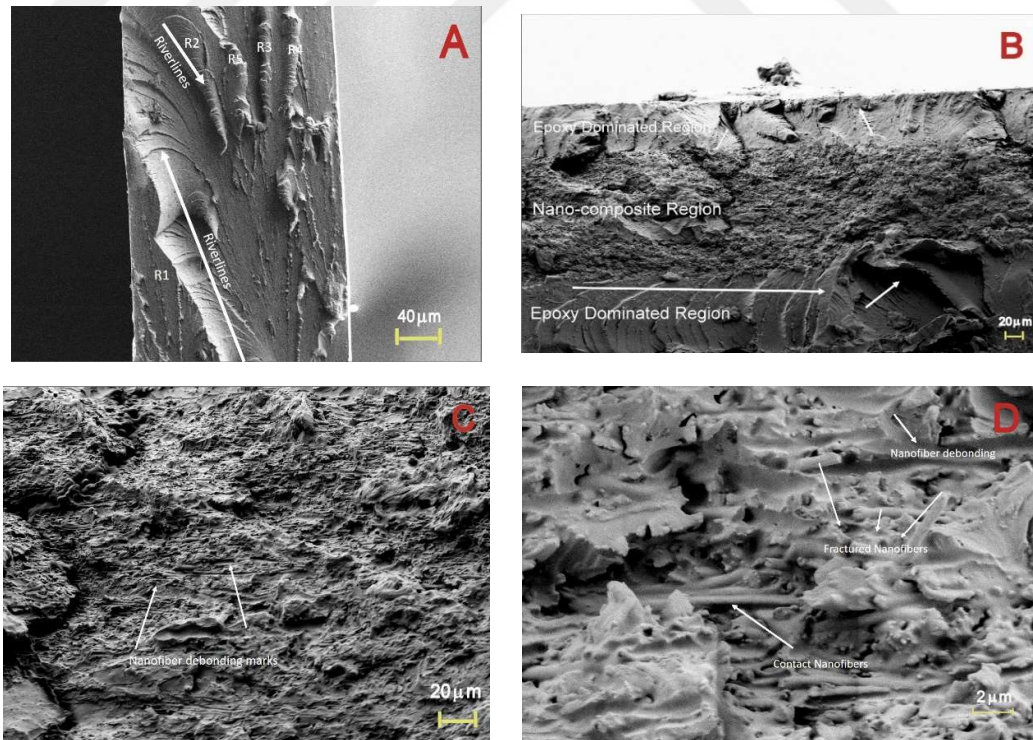
Figure 5: Fracture surfaces of tensile test specimens a) neat b,c,d) P(St-co-GMA)/TBA-PA reinforced

4.2.4.3 End Notched Flexure Tests

Representative force vs. displacement curves and corresponding G_{IIc} values calculated from direct beam theory are reported in figure 6. In line with the nanocomposite tension results, the presence of P(St-co-GMA)/PA-TBA nanofibers along with their cooperative interaction with the epoxy matrix curing process increased the G_{IIC} values as high as 95% (see table 2). Signature of this substantial increase in the strain energy release rate can also be tracked at the fracture surfaces. In figure 7a the pre-crack front of the standard reference specimen is presented. The hackle patterns, typical characteristics for a regular epoxy rich mode II failure, are clearly identifiable.

Figure 6: a) A representative force vs. displacement curve for ENF tests (G_{IIC} values are compared in the box

For P(St-co-GMA)/TBA-PA nanofiber reinforced laminates the fracture surface was formed two different formations. In first case (as dep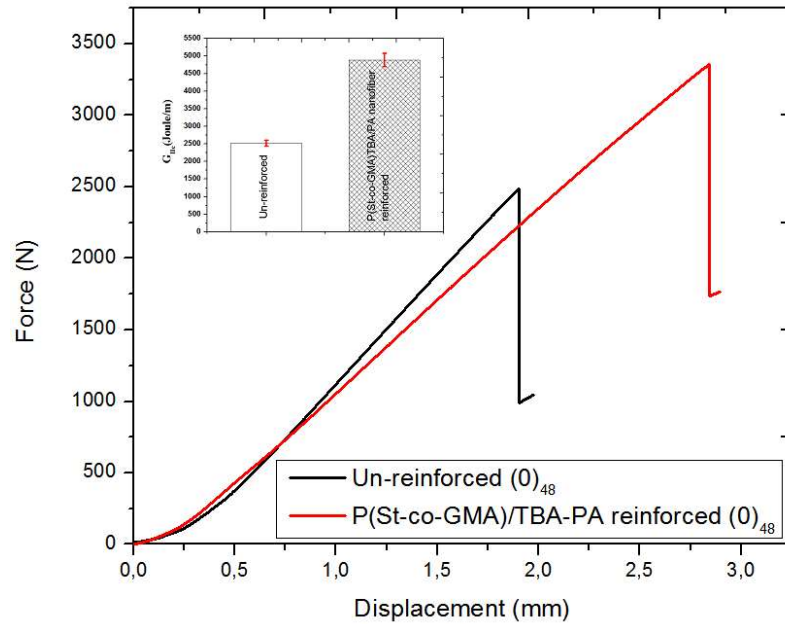icted in figure 7b) mode II crack propagation have occured directly through the interlayered region betwen carbon fibers by leaving (approximately as large as three carbon fibers) contact resin blocks containing relatively large hackles and clearly visualized contact/debonded/fractured nanofiber marks on it. In second case, the carbon fibers were not even visible (figure 7c) signaling the fact that resin propagated through a very large resin block leaving larger hackles along with nanofiber related failure marks. Higher magnification analysis revealed a more sophisticated fracture pattern achieved with nanofiber toughening. In figure 5d, inisde of a matrix hackle is depicted. Hackle boundary was clearly visible at up-right corner of the micrograph. Fracture marks associated with nanofiber debonding and nanofiber breakage were clearly distingusihable. Furthermore hackle formations having sub-micron to nano scale were observed. This observation suggested that a multi-scaled reinforcing effect was achieved due to P(St-co-GMA)/TBA-PA nanofibers which further increased the energy released during the ultimate specimen failure.
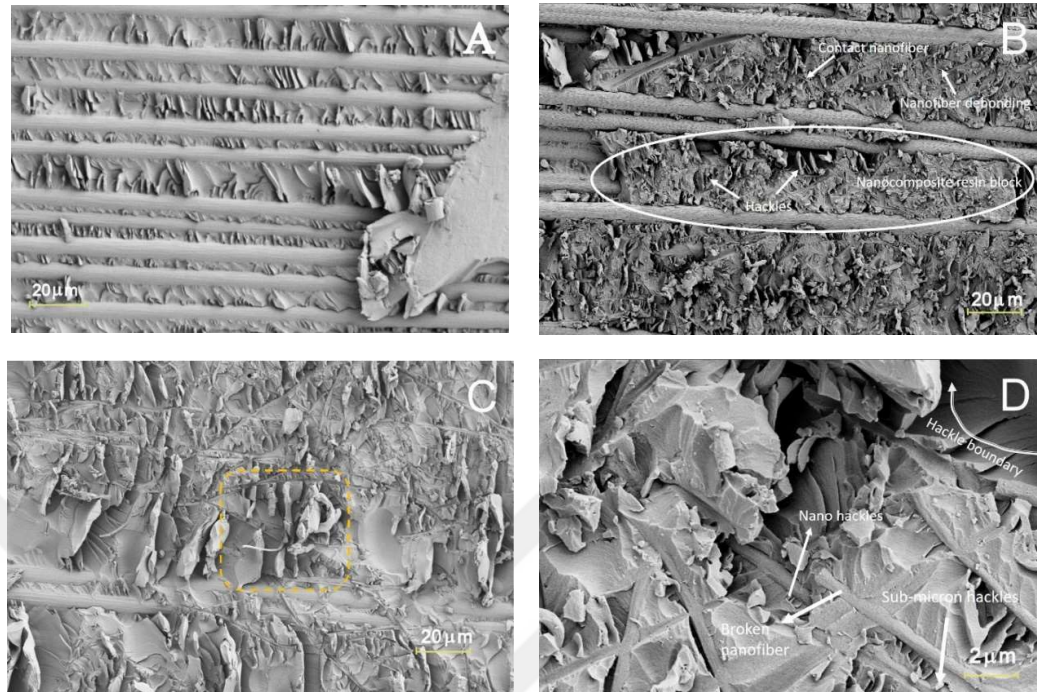
Figure 7 End notched flexure test specimens a) Un-interlayered b,c,d) interlayered

4.2.5 Conclusions

In-situ crosslinkable P(St-co-GMA)/TBA-PA nanofibers were integrated into structural carbon/epoxy composite laminates as interlayers. The nature of the in-situ crosslinking reaction during epoxy curing was also revealed by DSC analysis. Nanofiber integrated and as-is epoxy prepreg systems were heated from 20^0 C to 300^0C with 5 different heating rates (1,2,5,10,20^0C/min). Changes in the reaction enthalpies and reaction profile suggested that nanofiber and epoxy system were able to cure together, forming an enhanced nanocomposite structure. Associated synergistic or catalytic effect of P(St-co-GMA)/TBA-PA nanofibers was discovered by the use of Ozawa-Flynn-Wall kinetic model where reaction activation energies associated with in-situ curing was significantly lower than the as-is epoxy systems. Improved curing profile was backed-up by the tensile tests of nanofiber/epoxy nanocomposites manufactured by an in-house developed adhesive film casting methodology, where tensile strength and elastic

modulus improvements up to 39%and 8% respectively are noted. Mode II strain energy release rate, G_{IIC} values of P(St-co-GMA)/TBA-PA reinforced laminates increased by 95%. Fracture surface analysiss done on both nanocomposite and laminated composite samples revealed that with their unique in-situ crosslinkablity P(St-co-GMA)/TBA-PA nanofibers significantly altered the resin morphology and played a multi-scaled reinforcement role against crack propagation.

4.2.6 References

[1] T.K.Tsotsis, Interlayer Toughening of Composite Materials, Polymer Composites. 30(2010) 70-86.

[2] K. Bilge, M. Papila, Interlayer Toughening Mechanisms fo Composite Materials, Toughening Mechanisms in Composite Materials. Woodhead Publishing, Elsevier, 2015, pp. 263-294.

[3] N.H. Nash, T.M. Young, P.T McGrail, W.F. Stanley, Inclusion of a Thermoplastic Phase to Improve Impact and Post-Impact Performances of Carbon Fiber Reinforced Thermosetting Composites- A Review, Mater.Des. 85 (2015) 582-597.

[4] Y. Dzenis, Structural Nanocomposites Science, 319 (2008) 419-420.

[5] Y. Dzenis , D.H Reneker, Delamination Resistant Composites Prepared by Small Diameter Fiber Reinforcement At-Ply Interfaces, US PATENT 626533, 2001

[6] A. Zucchelli et.al., Electrospun nanofibers for enhancing structural performance of composite materials, Polymers for Advanced Technologies. 22 (2011) 339-349.

[7] K.Bilge, S. Venkataraman, Y.Z. Menceloglu, M. Papila, Global and Local Nanofibrous Interlayer Toughened Composites for Higher In-Plane Strength, Composites Part A. 58 (2014) 73-76.

[8] K.Bilge, E. Ozden-Yenigun, E. Simsek, Y.Z. Menceloglu, M. Papila, Structural Composites Hybridized with Epoxy Compatible Polymer/MWCNT Nanofibrous Interlayers, Compos. Sci. Technol. 72(2012) 1639-1645.

[9] G. Cicala et.al., Novel polymeric systems for high performance liquid molding Technologies, Recent Res. Dev. Polym. Sci. 11 (2012): 77-97.

[10] S. Mohammadzadehmoghadam, J. Davies, Recent progress in electrospun nanofibers: Reinforcement effect and mechanical performance, Journal of Polymer Science Part B: Polymer Physics 53(2015) 1171-1212.

[11] S. Van der Heijden et al., Novel composite materials with tunable delamination resistance using functionalizable electrospun SBS fibers, Composite Structures 159 (2017) 12-20.

[12] S. Van der Heijden et al., Interlaminar toughening of resin transfer molded laminates by electrospun polycaprolactone structures: Effect of the interleave morphology. Composites Science and Technology 136 (2016) 10-17.

[13] P. Li et. al., Synchronous effects of multiscale reinforced and toughened CFRP composites by MWNTs-EP/PSF hybrid nanofibers with preferred orientation, Composites Part A: Applied Science and Manufacturing 68 (2015) 72-80.

[14] I.D.G, Subagia et. al., Hybrid multi-scale basalt fiber-epoxy composite laminate reinforced with Electrospun polyurethane nanofibers containing carbon nanotubes, Fibers and Polymers, 15(2014) 1295-1302.

[15] L. Liu, H.Zhang, Y.Zhou, Quasi-static mechanical response and corresponding analytical model of laminates incorporating with nanoweb interlayers, Composite Structures, 11 (2014) 436-445.

[16] L. Daelemans, et. al., Nanofibre bridging as a toughening mechanism in carbon/epoxy composite laminates interleaved with electrospun polyamide nanofibrous veils, Composites Science and Technology, 117 (2015) 244-256.

[17] N.H. Nash, T.M Young, W.F. Stanley, An investigation of the damage tolerance of carbon/Benzoxazine composites with a thermoplastic toughening interlayer, Composite Structures, 147 (2016) 25-32.

[18] L. Daelemans, et.al., Damage-Resistant Composites Using Electrospun Nanofibers: A Multiscale Analysis of the Toughening Mechanisms, ACS applied materials & interfaces 8 (2016) 11806-11818.

[19] L. Daelemans, et.al., Improved fatigue delamination behaviour of composite laminates with electrospun thermoplastic nanofibrous interleaves using the Central Cut-Ply method, Composites Part A: Applied Science and Manufacturing 94 (2017) 10-20.

[20] N.H. Nash, et al. "The influence of hydrothermal conditioning on the Mode-I, thermal and flexural properties of Carbon/Benzoxazine composites with a thermoplastic toughening interlayer." Composites Part A: Applied Science and Manufacturing 76 (2015): 135-144.

[21] T. Brugo, R. Palazetti, The effect of thickness of Nylon 6, 6 nanofibrous mat on Modes I–II fracture mechanics of UD and woven composite laminates, *Composite Structures,* 154 (2016) 172-178.

[22] S.V.D Heijden, L.Daelemans, B.D.Schoenmaker, I.D. Baere, H.Rahier, W.V. Paepegem, K. de Clerck, Interlaminar toughening of resin transfer moulded glass fibre epoxy laminates by polycaprolactone electrospun nanofibres", Composites Science and Technology, 10 (2014) 66-73.

[23] K. Magniez, T.Chaffraix, B. Fox, Toughening of a Carbon-Fibre Composite Using Electrospun Poly(Hydroxyether of Bisphenol A) Nanofibrous Membranes Through

Inverse Phasen Separation and Inter-Domain Etherification, Materials, 4 (2011) 1967-1984.

[24] J.Zhang, T.Lin, X.Wang, Electrospun nanofibre toughened carbon/epoxy composites, Effects of polyetherketone cardo (PEK-C) nanofibre diameter and interlayer thickness, Composites Science and Technology, 70 (2010) 1660-1666.

[25] Zhang, J., Yang, T., Lin, C., Wang, C.H. (2012) "Phase morphology of nanofibre interlayers, Critical factor for toughening carbon/epoxy composites" , Composites Science and Technology, 72,256-262.

[26] A. Zuchelli, C. Gualandi, M.L. Focarete, L. Donati, G. Minak, S. Ramakrishna, Influence of electrospun Nylon 6,6 nanofibrous mats on the interlaminar properties of Gr-epoxy composite laminates", Composite Structures, 94 (2012) 571-79.

[27] Z.-M. Huang, Y.-Z. Zhang, M. Kotaki, S. Ramakrishna, A review on polymer nanofibers by electrospinning and their applications in nanocomposites, Compos. Sci. Technol. 63 (2003) 2223–2253.

[28] K.Bilge et. al., Stabilized electrospinning of heat stimuli/in situ crosslinkable nanofibers and their self-same nanocomposites, Journal of Applied Polymer Science, 133(2016) 44090.

[29] A.T Seyhan, M. Tanoglu, K. Schulte, Mode I and mode II fracture toughness of E-glass non-crimp fabric/carbon nanotube (CNT) modified polymer based composites." Engineering Fracture Mechanics 75(2008) 5151-5162.

[30] R. Hardis, "Cure kinetics characterization and monitoring of an epoxy resin for thick composite structures" Graduate Theses and Dissertations. Paper, (2012) 12608.

[31] P. Guerrero, K. De La Caba, A. Valea, M. Corcuera, I. Mondragon, Influence of Cure Schedule and Stoichiometry On The Dynamic Mechanical Behaviour of Tetrafunctional Epoxy Resins Cured with Anhydrides, Polymer 37 (1996) 2195-2200.

172

[32] X. Luo, S. Zheng, D. Ma, Mechanical Relaxation and Intermolecular Interaction in Epoxy Resins/ (Poly Ethylene Oxide) Blends Cured with Phthalic Anhydride, Chin. J. Polym. Sci. 13 (1995), 144-153.

[33] B.M.V. Romao, M.F Diniz, M.F.P Azevedo, V.L. Lourenco, L.C. Pardini, R.C.L Dutra, Characterization of the Curing Agents Used in Epoxy Resins with TG/FT-IR Technique *, P*olímeros: Ciência e Tecnologia 13 (2006) 144-153.

[34] M.K Antoon, J.L Koenig, Cross-Linking Mechanism of an Anhydride-Cured Epoxy Resin as Studied by Fourier Transform Infrared Spectroscopy, J. Polym. Sci. Polym. Chem. Ed. 19 (1981) 549-570.

[35] S. Ganguli , H. Aglan, P.Dennig, G.Irvin , Effect of Loading and Surface Modification of MWCNTs on the Fracture Behavior of Epoxy Nanocomposites, Journal of Reinforced Plastics and Composites 25(2005) 175-188.

[36] S. Samajdar, Kishore, Fracture Surface Characterization Of Epoxy-Based GFRP Laminates, Journal Of Materıals Scıence 26 (1991) 977 984

[37] E. Greenhalgh, Failure Analysis and Fractography of Polymer Composites, Woodhead Publishing, 2009.

CHAPTER 5 : GENERAL CONCLUSIONS

Parallel to the flow of thesis work conclusions achieved can ben listed as below:

- The progressive failure of $(0_m/90_n)_s$ laminates were effectively captured by a microphone assisted sound-tracking approach. Simultaneous video capturing of the polished specimen edges confirmed that the present simplified method is capable of capturing minor, intermediate, major and ultimate failure events as they produce sound fingerprints of their own. Audio and video assisted mechanical testing of $(0/90_5)_s$, $(0_3/90_3)_s$, $(0_5/90)_s$,$(0/90)_{3s}$, $(90/0)_{3s}$ and $(90_3/0_3)_s$ also demonstrated that the occurrence of the potent failure events and the corresponding sound outputs were significantly dependent on the lay-up sequence. This affordable, easy to set-up and quick method was found to be quite feasible and practical. The results presented herein suggest the proposed methodology provides valuable information by using the inherent acoustic signatures in testing/assessments rather than loosing completely when an acoustic emission toolset/software and associated expertise are not readily available.

- Electrospinning process was used to obtain nanofibrous P(St-co-GMA) interlayers on UD and woven fabric carbon/epoxy prepreg surfaces. Progressive wetting of P(St-co-GMA) nanofibers with the epoxy matrix were assessed. Uni-axial tensile tests of $(0)_6$ and $(0/90)_{6woven}$ laminates showed increase in tensile strength by 12% and 18%, respectively, with almost no weight penalty associated with the nanofibrous interlayers. Moreover, the local toughening effect assessed by open hole tension (OHT) tests showed that interlayer addition just in the vicinity of the highly stressed regions was also effective increasing the maximum failure stress by 9%. Reported test results underlined that electrospun P(St-co-GMA) nanofibrous mat is a promising interlayer candidate thanks to their ability to work also under in-plane loads which makes them integrable to conventional composite design.

- High strain rate response of the carbon fiber reinforced composite laminate of $(0/90)_{25s}$ stacking sequence and its toughened counterpart by P(St-*co*-GMA) nanofibrous interlayers were investigated both for in-plane and through the thickness loadings via SHPB. The compressive stress–strain behavior of the laminates was shown to be strain rate sensitive. Nanofibrous interlayered laminate was superior in regard to the through-the-thickness compressive characteristics at all high rates of strain tested in this study. Through-the-thickness, reference $(0/90)_{25s}$ composite specimens broke into individual ply pieces caused by extensive matrix failure leading to delamination and fiber fracture. Whereas block-of-plies fragmentation was observed in nanointerlayered specimens due to stronger and tougher interlaminar bonding, resulting in suppression of matrix cracking and subsequent failure events. At the in-plane loading, the effect of nanofibers on ultimate compressive strength, failure strain and failure mechanism was much more remarkable, enhancement in the energy dissipation due to the nanofibrous interlayers is as high as 80% whereas 40% improvement was also recorded through thickness directions. Interlayer nanofibers are concluded to be resistive against crack formation between the plies, resulting in increased ultimate compressive strength and failure strain.

- Heat-stimulated cross-linking capability was introduced into amorphous P(St-co-GMA) nanofibers, by the addition of phtalic anhydride (PA) as the cross-linking agent and tributlyamine (TBA) as the initiator. Despite the mixing of the cross-linker agents into the solution, cross-linking was successfully suppressed at room temperature, allowing continuous electrospinning without any adverse effect on the polymer solution viscosity. The cross-linking reaction was found to be initiated at around 60°C. Electrospun nanofibers with different PA amounts were cross-linked by the application of thermal cycle at intermediate temperatures of $\sim$ 90°C (*i.e.*, just below T_g). Cross-linking at the highest capacity was sought, when the PA/epoxide ring (GMA) molar ratio was varied from 1 to 5. A proposed reaction route was validated by FTIR analyses, where the consumption of PA and available epoxide rings in GMA was observed. Swelling tests suggested that the gel fraction in cross-linked nanofibers maximized with the increasing

175

PA amount up to molar ratio of 5. At the maximum cross-linking ratio, P(St-co-GMA)/PA-TBA nanofibers completely preserved their pristine nanofibrous morhology after 3 days of exposure to DMF solvent. The DSC analyses suggested that the T_g of the cross-linked nanofibers increased with the degree of cross-linking, by up to 30°C. Note that the glass transition temperature T_g may also be an important limit, as exceeding it may induce substantial changes in the nanofibrous structure/morphology. Un-crosslinked P(St-co-GMA) nanofibrous morphology and network degraded above their T_g, whereas the cross-linked P(St-co-GMA)/PA-TBA nanofibers, especially the ones with R=5, were able to maintain their nanofibrous morphology intact. A similar outcome was observed when R=5 P(St-co-GMA)/PA-TBA nanofibers were processed in-situ at 150C accommodating the cure of the epoxy matrix. The fibrous morphology was contained and the P(St-co-GMA)/PA-TBA nanofibers were effectively embedded into the epoxy matrix. Lastly, the form-loose effect of an above-the-T_g process on the P(St-co-GMA) fibers was proposed as a strategy in the manufacturing of what we call the self-same nanocomposites. Un-crosslinked (R=0) and stabilized cross-linkable (R=5) nanofibers of P(St-co-GMA) backbone polymer were electrospun together by dual electrospinning. An intermingled nanofibrous structure were formed. The two types of fibers interacted upon a subsequent processing above the T_g reforming into a nanocomposite fibrous network, where the un-cross-linked P(St-co-GMA) appears to wrap/fuse around the self-cross-linkable P(St-co-GMA)/PA-TBA nanofibers.

- In-situ crosslinkable P(St-co-GMA)/TBA-PA nanofibers were integrated into structural carbon/epoxy composite laminates as interlayers. The nature of the in-situ crosslinking reaction during epoxy curing was also revealed by DSC analysis. Nanofiber integrated and as-is epoxy prepreg systems were heated from 20^0 C to 300^0C with 5 different heating rates (1,2,5,10,20^0C/min). Changes in the reaction enthalpies and reaction profile suggested that nanofiber and epoxy system were able to cure together, forming an enhanced nanocomposite structure. Associated synergistic or catalytic effect of P(St-co-GMA)/TBA-PA nanofibers were discovered by the use of Ozawa-Flynn-Wall kinetic

model where reaction activation energies associated with in-situ curing was significantly lower than the as-is epoxy systems. Improved curing profile was backed-up by the tensile tests of nanofiber/epoxy nanocomposites manufactured by an in-house developed adhesive film casting methodology, where tensile strength and elastic modulus improvements up to 39%and 8% respectively are noted. Mode II strain energy release rate, G_{IIC} values of P(St-co-GMA)/TBA-PA reinforced laminates increased by 95%. Fracture surface analysiss done on both nanocomposite and laminated composite samples revealed that with their unique in-situ crosslinkablitt P(St-co-GMA)/TBA-PA nanofibers significantly altered the resin morphology and played a multi-scaled reinforcement role against crack propagation.